Technical Note N-1079

THE TURBULENT FREE CONVECTION FLOW ABOVE A HEATED
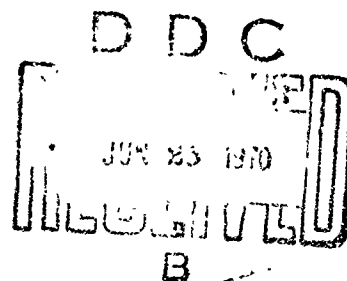HORIZONTAL CIRCULAR PLATE

By

T. T. Fu

May 1970

This document has been approved for public release and
sale; its distribution is unlimited.

NAVAL CIVIL ENGINEERING LABORATORY
Port Hueneme, California 93041

D D C

JUN 23 1970

B

199

THE TURBULENT FREE CONVECTION FLOW ABOVE A
HEATED HORIZONTAL CIRCULAR PLATE

Technical Note N-1079

ZF 38.512.001.014

by

T. T. Fu

ABSTRACT

The turbulent free convection of air above a 2-foot diameter,
heated horizontal plate has been studied experimentally and numerically.
The mean temperature fields and the indraft profiles for two mean plate
temperatures were measured using a thermocouple and a constant tempera-
ture hot-wire anemometer. Also, the turbulence and mean velocity were
measured for the higher plate temperature using the hot-wire method.
The flow field was visualized by shadow photograph technique. From
visualization and measurements, it was found that the region of signi-
ficant deviation from ambient temperature and velocity was restricted
to a region near the plate centerline (the primary flow region). The
indraft velocity was found to be relatively large near the ground level
(within approximately 1" of the ground).

The major temperature drop took place in the region very near the
plate. Within 0.02" of the plate the temperature distribution in the
air could be calculated based on conduction only. This region was
therefore, called the "conduction layer." At a given mean plate tempera-
ture, the temperature gradient was found to increase with the radius.
Data obtained from heat-transfer measurements were consistent with the
one-third power correlation reported in the literature.

The turbulence in the flow field was found to consist of low
frequency and high amplitude fluctuations (on the order of 10 Hz and
1 ft/sec). Because of the limitation of the hot-wire technique for
large turbulence measurements, flow velocities could not be deduced
directly from hot-wire data. To remove this difficulty, a numerical
data simulation scheme has been developed in which the parameters
describing the turbulent flow (r.m.s. fluctuations and correlation
coefficients) were used as input. By inferring from the simulated data
of know parameters, experimental hot-wire data reduction was then
possible. Data reduction model was validated by numerical experiments.

The eddy diffusivity in the region away from the conduction layer
was estimated based on temperature, velocity and turbulence data using
two independent methods. The agreement was good. The spatial varia-
tions of the eddy diffusivity in most of the primary flow region was

found to be gradual with rapid drops occurring in the region between the primary flow and the cold ambient.

A numerical flow calculation was made. The mathematical formulation was based on Boussinesq approximations using a constant eddy diffusivity model. A turbulent Grashof number Gr_T (the governing parameter) was defined through the definition of a characteristic plate temperature rise $\Delta\theta_T$, the plate mean heat flux and the eddy diffusivity. Gr_T and $\Delta\theta_T$ were obtained based on the best fit of experimental and numerical centerline temperatures.

By the specification of $\Delta\theta_T$ at the plate surface, the effect of the intense variation of eddy diffusivity in the conduction layer region could be avoided in the numerical calculations. Numerical results based on a constant eddy diffusivity model were obtained and compared with the experimental data. Due apparently to the non-constancy of the eddy diffusivity, the calculated temperature and velocity profiles exhibit less constriction than the experimental data. Therefore a more general turbulent transport model will be required to provide a good theoretical description of the phenomena.

TABLE OF CONTENTS

LIST OF FIGURES

LIST OF TABLES

LIST OF SYMBOLS

a, b_1, b_2, c_1, c_2, c_3	constants, Equation (E-4)
A	area
A, B, A'	constants, Equation (3-2)
b, d, e	coefficients, Equation (6-17)
C_1, C_2	constants in coordinate transformation, Equation (6-15)
C	constant
C_p	specific heat at constant pressure
d, D	diameter
E	voltage
E_1, E_2, E_3	component of u, $V_m + v$, w in the direction of hot-wire, Equation (5-5)
g	acceleration of gravity
G	a function, Equation (E-6)
Gr, Gr_T	Grashof number, $Gr = \dfrac{g\beta\Delta\theta\ D^3}{\nu^2}$; turbulent Grashof number, $Gr_T = \dfrac{g\beta\Delta\theta_T D^3}{\epsilon_M^2}$
h	average heat transfer coefficient
I	current
(i, j), (i_{max}, j_{max})	indices representing x, y locations in numerical grid, maximum value of (i, j)
k	thermal conductivity, constant in Equation (5-1)
K	correlation coefficient, Equation (5-9)
l, L	length
m	values of the index i at the edge of the plate

n	exponent in heat transfer correlation
Nu	Nusselt number, $Nu = hd/k$
p, P	pressure coefficient, pressure
Pr	Prandtl number, $Pr = \dfrac{\mu C_p}{k}$, $Pr = \dfrac{\epsilon_M}{\epsilon_H}$
q	mean heat flux
Q	heat transfer rate; dimensionless heat flux, Equation (6-16)
r, R	dimensionless radius, dimensional radius
R_1, R_2, R_3, R_4	random numbers
$\mathbb{R}$	gas constant
$\mathbb{R}_0$, $\mathbb{R}_1$, $\mathbb{R}_2$	shape parameters, Equation (5-3)
Ra	Rayleigh number, $Ra = GrPr$
Re	Reynolds number, $Re = VD/\nu$
S	dimensionless stream function, Equation (6-5)
t	dimensionless time, $t = \tau U_c/D$
T	dimensionless temperature, $T = (\theta - \theta_\infty)/\Delta\theta_T$
T_y	dimensionless mean plate surface temperature gradient
(u,v), (U,V)	dimensionless, dimensional velocities in (X,Y) directions
(u,v,w)	fluctuating velocity components
$\widetilde{u}, \widetilde{v}, \widetilde{w}, \widetilde{\theta}$	normalized velocity, temperature fluctuations, Equation (5-7)
U_c	characteristics velocity, $U_c^2 = g\beta\Delta\theta_T D$
V_m	magnitude of mean flow velocity

W	effective velocity sensed by hot-wire, over-relaxation parameter
$W_\perp$, W_k	effective velocity component perpendicular, parallel to hot-wire, Equation (5-6)
(x,y)	dimensionless radial, axial coordinates
(X,Y)	dimensional radial, axial coordinates
Z	dimensionless vorticity function, Equation (6-7)

Greek Letters

α, γ	coefficient specifying temperature fluctuations, Equation (5-10)
β	coefficient of volumetric expansion
Δ	increment
ϵ	emisivity
ϵ_H, ϵ_M	turbulent thermal diffusivity, momentum diffusivity
θ	angle, temperature
θ'	temperature fluctuation
$\Delta\theta_T$	characteristic temperature difference for the turbulent flow
λ	spectral radius
μ, ν	dynamic viscosity, kinematic viscosity
ξ, η	transformed (x,y) coordinates, Equation (6-15)
ρ	density
σ	standard deviation, r.m.s. value of fluctuations (Equation 5-8), Stefan-Boltzmann constant
τ	time

ϕ	angle
ϕ_i, ψ_i	random numbers, Equation (E-1)

Subscripts

a	air, asbestos
c	conductive, convective
f	floor
h, v	horizontal, vertical
p	plate
r, rad	radiative
t, T	thermocouple, turbulent
u, v, w	in the direction of u, v, w
v	velocity
w	wire
∞	ambient

Superscripts

'	at an advanced time
n	the n-th iteration
$\overline{(\ )}$	time average

ACKNOWLEDGMENT

I. INTRODUCTION

The research described in this thesis is an investigation of the turbulent flow field above a heated circular plate mounted flush with a large horizontal surface, hereafter called the ground. The motivation for this work was provided by the hypothesis that the heated flat plate is a proper model for some of the interesting features of large area fires. The relationship between this model and fire problems is discussed in detail in Appendix A.

The flow field above a heated surface is generated by the upward motion of the heated air adjacent to the plate. The temperature field is determined by the interaction between heat transfer from the plate and ingestion of ambient air. Features of primary interest are the updraft above the plate, the indraft near the ground, and the temperature field. For mathematical simplicity, this problem may be modeled by a circular, heat source of finite radius R at elevation $Y = 0$, in the semi-infinite region $Y \geq 0$. The updraft is the result of the buoyancy of the heated air above the plate. To replace the upward moving hot air, there is induced an indraft of the cold ambient air moving toward the plate in a more or less horizontal direction. There are no significant thermal effects in this induced flow. Complex interactions between these two distinctively different types of flow take place in the region near the plate. This fact precludes the applicability of the familiar boundary layer approximations.

Theoretical investigations of free convection problems have been concerned primarily with problems of simple geometry such as a fluid layer above a large, horizontal, heated surface, or one located between two large, horizontal, parallel surfaces. These geometries allow one-dimensional formulations. Using Boussinesq approximations (1),[*] Howard (2) obtained a solution for the one-dimensional turbulent convection above a heated horizontal surface. He has demonstrated agreement between his solution and the experimental data of Townsend (3).

At some distance above the surface where the updraft is a dominant feature, the flow resembles a free jet. This flow region is called the convection plume. The boundary layer approximations are then applicable (4). Similarity solutions have been obtained for problems such as convection above a line heat source or a linear heat source of finite width. The results are in reasonable agreement with experimental measurements (e.g., reference 5, 6 and 7). Because of the conditions of zero average shear stress and heat flux along the plume axis and at infinity, the shear stress and heat flux terms appearing in the governing differential equations may be eliminated by integration in the transverse direction from the plume axis to infinity. The solution to the problem may be obtained by use of either assumed or measured profile functions of mean temperature and velocity in the transverse direction.

---

[*]Numbers in parentheses indicate references listed in
the Bibliography.

Since no explicit knowledge of the turbulence structure is necessary for obtaining the plume solutions, the study of turbulence structure even in the plume region has been only in the infant stage (8).

For multi-dimensional flows of the type studied in this investigation, the highly non-linear nature of the governing equations effectively precludes analytical solutions. Recent development in numerical methods utilizing large digital computers has made possible the treatment of some of the non-linear features in the equations of motion, for such problems as convection in an enclosed cavity (9), and wake flow behind an obstacle (10). Reasonably successful solutions can usually be obtained for problems of this nature. An additional uncertainty in the problem formulation for the work described here derives from the fact that an infinite domain must be approximated by a finite one and it is not clear how to specify boundary conditions at the artificial boundaries. Beyond this, it is in general not easy to demonstrate that the results of numerical calculations of complex non-linear phenomena actually constitute a valid solution of the problem as formulated.

In view of these multiple uncertainties, the proper initial approach is to build understanding on the basis of a simple numerical calculation model which is easily interpreted in the light of experimental evidence and which can be reduced to analytically tractable limiting cases for validating the calculations. This approach has, to varying degrees, been followed for several free convection problems

(e.g., references 11, 12, 13). Among these, only one (13) describes numerical flow field calculations directly relevant to the present problem. Unfortunately, no correlation with experimental data was reported.

Although there exists a large body of experimental literature concerning free convection in general, very little is reported which is directly applicable to the present study. The particularly difficult experimental feature of this problem is the accurate measurement of the flow velocity vector. For any reasonable experimental dimensions, velocities near the heater plate are small, i.e., on the order of a fraction of a foot per second. Moreover, turbulent fluctuation velocities in some regions of the flow field are of the same order of magnitude as the mean. In the experimental portion of this investigation, a hot-wire anemometer was used to obtain flow field data. Toward the low end of the velocity range of interest, hot-wire techniques suffer from orientation effects due to local perturbation of the flow by the hot-wire itself. Recently, laser doppler techniques (14,15) have been developed which may obviate most of the difficulties associated with hot-wire techniques. However, these techniques appeared after the hot-wire measurements reported in this thesis were well underway, and were not used for the present work.

SCOPE OF THIS WORK

This thesis consists of two major parts: experimental measurements and numerical flow and temperature field calculations. A constant

temperature hot-wire anemometer together with a thermocouple was used for obtaining the velocity and temperature data. The numerical calculation was intended for exploring the qualitative features of the flow field. Therefore, calculations were made based on the Boussinesq approximations (1) incorporating a constant eddy diffusivity model. With the mesh spacing (0.75 inch) used in the study, the flow between the ground and the nodel points next to it cannot be predicted. Since the indraft at the ground level is one of the most interesting features in the flow field, the numerical results must be supplemented to make possible the indraft prediction very near the ground. This was accomplished by an integral method.

II. LITERATURE SURVEY

The quantitative investigation of a fluid layer heated from below
may be traced back to the late 1800's when Thomson (16) and later
Benard (17) observed the flow patterns following the onset of thermal
instability. Lord Rayleigh (18) used a linearized stability theory and
established the criterion (a critical Rayleigh Number) at which convective
motion commences. Since then the linear instability properties for
fluid layers of infinite horizontal extent have been studied by a
number of investigators. A comprehensive account of this type of
problem appears in Chandrasekhar's book (19).

The convection which develops due to a heated surface of finite
size is the subject of concern in this investigation. Due to the three-
dimensionality of the flow configuration, this problem is quite different
from that due to an infinite surface. Linearization has not been
possible, and no analytical approach to this problem has been reported
in literature.

Examination of the available literature reveals that knowledge of
the turbulent flow field above a heated horizontal plate of finite
extent exists only in a primitive state. This may be attributed to the
intrinsic non-linearity of the basic governing equations. It is
complicated further by the lack of an adequate description of the
turbulent transport mechanism. Relevant experimental, mathematical
and numerical studies are discussed below.

EXPERIMENTAL STUDIES

The measurement of free convection above a heated horizontal surface was apparently first reported by Ramdas (20,21). He measured temperature variations above heated land surface (e.g., during the day) and concluded that the variation of temperature was most rapid nearest to the surface, and was linear. Information of this type is important to the understanding of mass movement of the atmospheric air (wind formation) and many early investigations were made by meteorologists (e.g., references 22, 23, 24).

Heat transfer data of an engineering nature were presented by Schmidt (25), who photographed the boundary layer formed in the neighborhood of a heated horizontal plate. Later, Fishenden and Saunders (26) measured the heat transfer from horizontal, rectangular plates of sizes up to 2-foot square and at temperature up to 1000°F above the ambient. They presented data for both the cases of a heated surface facing up and facing down but gave no detailed description of the experimental configuration. The data were correlated in the familiar fashion of Nusselt Number (Nu) versus Rayleigh Number (Ra). For the turbulent range, the data gave the correlation:

$$Nu = constant\ (Ra)^{1/3}$$

Since Nu contains a length scale and the heat flux to the first power and Ra contains a length scale to the third power, the above correlation implies that the heat flux is independent of length scale in the turbulent regime. A comprehensive summary of the heat transfer

data from horizontal plate was compiled by Jakob (27), however, little in the way of experimental detail and measurement technique were discussed.

Townsend (3) measured the temperature fluctuations above the middle of the uniformly heated bottom of an open-topped box (30cm x 40cm x 56cm high). All the measurements were made within 8 cm of the bottom surface. The mean temperature distribution near the surface was reasonably linear. From the implied temperature gradient and the overall heat transfer, he obtained the same correlation as did Fishenden and Saunders (26). The data showed relatively large scatter when the surface temperature was high. The largest temperature fluctuations occurred within 0.5 cm of the surface and were about 20% of the temperature difference between the plate and the ambient. The rate of spatial temperature decay was found to decrease with plate temperature.

Tritton (28) investigated the turbulent free convection above a heated plate inclined at a small angle to the horizontal. He used a resistance wire thermometer to measure the temperature and a quartz fiber anemometer to measure the velocity parallel to the plate in the boundary layer region. He found that the temperature field was not greatly altered due to plate inclination (no systematic variations were observed) and that the mean temperature field was largely controlled by the turbulence. He succeeded in measuring the velocity in the boundary layer region by observing the deflection of a cantilevered quartz fiber in the flow field. This method, however, was apparently handicapped by the lack of a continuous recording technique.

Project FLAMBEAU (29) is a program of research on large area fires. During recent years, a large amount of experimental data (e.g., fuel consumption rate, flow and temperature field information, radiation effects, etc.) has been collected from large size experimental fires of horizontal length scale up to 1000 feet. Little systematic analysis of these data has been reported.

Recently, Parker, Corlett and Lee (30) attempted to test the hypothesis that Grashof number is unimportant in determining such flow field characteristics as inflow velocities. Using a hot-wire anemometer, they measured the inflow velocity at the edge of a square array (24" x 24") of horizontally arranged electric heater elements which, according to the hypothesis, should scale the September 1967 FLAMBEAU test fire. Insofar as the severely limited prototype data permitted comparison, the hypothesis was found correct. More data of the same work in improved form may be found in reference 31.

MATHEMATICAL STUDIES

Boussinesq (1) in 1903 introduced his well-known approximations for calculating thermal convection problems. The Boussinesq approximations are: (1) Density variation due to pressure (as opposed to temperature) variation is legligible; (2) Density variation in the governing differential equations is negligible except in the buoyancy term in the momentum equation.

The mathematical formulation of the problem of free convection from a horizontal plate was discussed by Stewartson (32). He demonstrated

that boundary layer approximations were no longer applicable. Thus, purely mathematical treatments of this problem have so far been restricted to the one-dimensional case. Howard (2) formulated a one-dimensional problem using the Boussinesq approximations. He was able to predict Townsend's experimental data (3) from his calculations.

Recently, Morton (8) has discussed the turbulent transport in a convection plume and formulated the plume problem afresh. His calculations are in preparation.

NUMERICAL METHOD

Numerical methods are a very powerful tool for solving non-linear and multi-dimensional flow problems. Several numerical flow calculations for free convection problems appear in the literature. These calculations have all been based on the formulation using Boussinesq approximations incorporating the assumption of constant fluid properties or constant eddy diffusivities, and have dealt with problems with well defined boundaries (within a rectangular cavity, e.g.). In most procedures a time advancing (transient) scheme has been used to obtain eventually steady state solutions. Typical of these are work by Wilkes (9), Deardorff (33), and Fromm (34). Torrance (43), in a recent paper, has made detailed comparisons of five transient type finite-difference computation schemes (9,34,43) for laminar free convection in a vertical axisymmetric enclosure with a small heated spot centrally located on the floor. He concluded that the calculated flows for all methods were similar and the required computer times were also of comparable magnitudes.

The work by Nielsen (13) is probably the most directly relevant to this thesis. He calculated the flow field due to free convection over a heated, horizontal, circular surface. The calculation was intended for the modeling of the flow fields generated by a mass fire. A steady state formulation including possible rotation about the axis of symmetry was chosen. The use of Boussinesq approximations and constant eddy diffusivity assumption in his calculations reduced the governing differential equations to the form of a laminar flow problem in which Grashof number is the governing parameter. Because of the rather large equivalent laminar Grashof number implied in his calculations ($\sim 10^{10}$) through the choice of eddy diffusivity (20 ft^2/sec), diameter (4340 ft) and surface temperature rise ($200^\circ F$ - $800^\circ F$), the validity of his results is uncertain. His results showed that earth rotation has little effect on the overall behavior of the flow field. No interpretation or experimental correlation was reported in reference (13).

Laminar free convection due to a heated horizontal plate (35) and a horizontal disk (36) in a full space for small Grashof numbers (<300) have been reported in the recent literature. These studies were carried out using the Boussinesq approximations, constant fluid properties and a steady state formulation. At the conclusions of their report, Kane and Yang (36) recommended the study of cases for higher Grashof numbers using a transient type formulation such as that reported in references (9), (34) and (43). This particular work incorporating a Gr_T defined

explicity in terms of an equivalent surface temperature rise was carried out in the numerical calculation part of this thesis. The details are discussed in Chapter VI.

III. DESCRIPTION OF EXPERIMENTAL WORK

The objective of the experimental program was to investigate the turbulent flow and temperature fields above a heated, circular, horizontal plate which was mounted flush with the ground surface. Both flow visualization and flow and temperature field measurements were conducted in this program.

EXPERIMENTAL APPARATUS

The experimental apparatus for this study consisted of three major items: the heater assembly, the traversing mechanism, and the platform assembly. The size of the experimental apparatus was designed so that fully turbulent flow could always be obtained. Since any laboratory size free convection flow field is very weak, any side wind would easily break the flow symmetry. Therefore, the experimentation was conducted indoors. The overall arrangement of the apparatus is shown in Figure 1a.

Flow visualization is a useful means of gaining understanding of a flow field. Shadow observation and photography are well suited to this problem. The required collimated light was approximated by a high intensity mercury arc lamp placed at a large distance from the heated plate. Therefore, a basement laboratory adjacent to a long hallway was chosen as the site of the experiment. This location was also desirable because it was free from air currents that would disturb the light path.

Heater Assembly

The heater assembly used in the apparatus is shown in Figure 2. A one-half inch thick by 24 inch diameter aluminum plate was heated by radiation from an electrical heating unit located directly below it. The heater assembly was mounted in the center of an 8' x 8' horizontal, wooden platform such that the aluminum plate surface was flush with the floor of the platform which simulated the ground surface. Electricity was supplied to the heater unit by a variable voltage power transformer (0 - 110 volt). By this means the power input to the heater unit could easily be set for each experimental run.

Number 14 Nichrome V wire was used for heating. It was placed in equally spaced (0.4" apart) parallel slots cut in a 1/2" thick by 24" diameter transite board. This arrangement permitted free lengthwise movement due to thermal expansion. The wire was held in place by a 1/8" thick by 24" diameter copper plate. A 1/16" thick asbestos sheet was sandwiched between the copper and the transite plates for electrical insulation. The heating unit was placed in an aluminum pan which was insulated on the inside wall with a high temperature insulation.[*] The aluminum plate was supported freely by the heads of four equally spaced bolts protruding from the aluminum pan. The outside surface of the copper plate in the heating unit and the underside surface of the aluminum

---

[*]INSULAG, $k = 0.7$ But-in/hr-ft^2-$^{\circ}$F at 1000°F and lower for lower temperatures. Detailed information may be found in Bulletin No. 332-A, Quigley Co., 415 Madison Avenue, New York 17, New York.

plate were painted with matte black high temperature paint.[*] A 1/2" air

gap was maintained between these two painted surfaces. Due to the high

thermal conductivity of copper and the closely spaced heating wire, the

temperature of the copper plate was very uniform.[**] This arrangement

permitted indirect heating by radiation which insured a uniform heat

flux to the aluminum plate. The aluminum pan was supported at its

periphery by the platform. An insulation jacket[***] was placed outside

the aluminum pan for the purpose of low temperature insulation. The

heat loss through this insulation was about 25% of the total electrical

power input to the heater assembly. With temperature measurements at

various locations in the insulation jacket, an energy balance calculation

could be made for the heater assembly.

Traversing Mechanism

The traversing mechanism is shown in Figure 1a and 1b. It was

designed to provide for translation of a hot-wire probe in three mutually

perpendicular directions (translation parallel to the vertical axis of

the plate, and horizontal translations in the radial and the tangential

directions) plus rotation about the probe axis.

---

[*]Fuller paint - flat black primer. Ordinarily used for painting
fireplace walls. Satisfactory for temperatures up to 1000°F.

[**]Based on the lateral surface area, 20% of the heat loss from the
side wall of the insulation jacket was assumed to be from the
copper plate. The radial temperature gradient thus calculated
was less than 1°F/ft.

[***]No. 4 vermiculite (a water-repellent masonry fill insulation)
was used in the jacket (k = 0.55 Btu-in/hr-ft^2-°F at 200°F,
tabulated values of k may be found in Special Report No. 256,
Research Laboratory, Zonolite Company, 1827 Benson Avenue,
Evanston, Illinois.

A traversing head supported by an 8-foot long horizontal bar was used to permit the radial movement. The ends of this horizontal bar were guided by two vertical supports fastened to the wooden platform for the vertical movement.

The method of mounting the hot-wire probe is shown in Figure 3. The hot-wire probe could be rotated by rotating either the probe holder or the probe support. Tangential motion of the probe was achieved simply by sliding motion of either the probe holder or the probe support. Small ball bearings were used for guiding all translational movements except in the tangential direction. A counterweight was used to balance the weight of the horizontal bar so that it could easily be moved vertically.

Platform Assembly

The platform assembly consisted of two main parts: the wooden platform and the screens. The platform supported both the heater assembly and the traversing mechanism. The floor of the platform was made of two sheets of 3/4" x 4' x 8' plywood placed side by side. A circular opening large enough for the heater assembly was made at the center of the floor. A small concentric circular opening was cut in a piece of 3/4" x 4' x 4' plywood board bolted below the floor. The step thus formed served as a support for the heater assembly (see Figure 2). Four pieces of 8-foot long angle iron were bolted to the bottom of the floor for reinforcement. The floor was raised to a level approximately 10 inches above the floor of the laboratory and was firmly supported by twelve wooden legs.

To minimize the effects of air currents inside the room, the region above the platform was enclosed on all four sides by vertical sections of ordinary window screen (14 x 18 mesh galvanized iron) and by a horizontal section of screen positioned 7 feet above the platform. The screens were made such that the traversing mechanism could be operated from outside of the screen. Since the turbulent flow field was generated from the hot plate which was far from the screens, and since the turbulence generated by free convection must greatly exceed that in a calm ambient atmosphere, the presence of the screens would have very little effect on the turbulnece level in the flow field.

FLOW VISUALIZATION

General Discussion

Due to the large size of the apparatus, many of the well-established flow visualization techniques, such as interferometry or the Schlieren method, were ruled out for this study. Two basically different flow visualization methods were investigated: smoke tracing* and shadow-graph. The latter method was finally chosen for this study because of

---

*A dense smoke is generated by pouring FOG JUICE (a petroleum derivative, available in theatrical supply stores) on the hot surface. The fluid is evaporated upon contact with the hot surface thus forming a smoke which is indicative of the pattern of the flow field. The heat flux available from the plate was small (~ 0.25 Btu/sec-ft^2). Due to heat removal, the plate temperature would drop so that shortly after the application of the fluid, it was evaporated in an erratic manner. This limited the possible observation period to only a few minutes at a time. The difficulty of uniform application on the plate without disturbing the flow was another undesirable feature of this method.

the capability of wide coverage and unobstructed continuous observations. The basic requirements for the shadow method are a collimated light beam and a projecting screen. A General Electric B-H6 mercury vapor arc lamp was used for the light source. This was a quartz-capollary enclosed arc 1.5 mm x 25 mm with a total flux of 60,000 lumens. The lamp dissipated 900 watts and was cooled by a 30 psig air supply. In order to approximate a collimated light beam, this light source was placed at the far end of a hallway in the basement laboratory ($\sim$165 feet from the hot plate). A translucent viewing screen made of a sheet of ordinary tracing vellum was placed normal to the light path about 20 feet on the other side of the hot plate. Due to the light transmission of the screen, it was found quite satisfactory to view the shadow from hehind the screen.

For photography, a piece of household curtain material (aluminum coated lining) was hung on the wall normal to the light path about 27 feet on the other side of the hot plate. Photographs were taken in front of the screen at an angle just large enough not to block the light path (Negative Tri X Pan 35 mm film was exposed f2 at 1/30 second and developed in Acufine for an ASA rating of 1200).

Flow Field Description

The flow field about the heated plate was viewed using the shadow method. Figure 4 shows the shadow pictures taken at two plate mean temperatures by photographing the reflection of the shadows from the aluminum coated lining screen. These pictures show that the overall flow field consists of two major regions which are separated by a fairly

well defined boundary. Above the plate and inside this boundary is a
region here called the primary flow region in which there is a dominant
upward moving stream of eddies. The upward flowing column is fully
turbulent and is constricted about the axis of symmetry (the centerline)
of the plate. It may be seen from Figure 4 that the flow boundary is
more sharply defined for higher plate temperature (or equivalently higher
heat flux). This phenomenon has been repeatedly observed.

Outside the boundary is the region of secondary flow which moves
across the boundary into the primary flow region to replace the upward
moving hot air. The temperature in the secondary flow is substantially
uniform. Because of this, it is impossible to visualize in the shadow
picture. The shape of the flow region boundary together with knowledge
of the velocities from direct observation suggest that the secondary
flow (the indraft) velocity is largest within a few inches above the
ground.

It was observed that the flow field could be upset by even a small
ambient disturbance. This is to be expected, in view of the very weak
velocity field. Careful observation of the shadow revealed an interesting
feature of the disturbed flow field. In a closed room of still air, the
flow field remains symmetric. If a small disturbance is introduced,
e.g., by placing a small piece of curled paper near the edge of the plate,
the flow field sometimes is disturbed. A clearly defined continuous
whirling column of finite width may be seen, as illustrated in Figure 5.
This whirl starts from the plate surface and eventually penetrates upward

for several heater plate radii. In shape this whirl may be straight or
curved, wide or narrow. It may stand still or wander. Its life may
vary from a fraction of a second to a few seconds. For large disturbances
such as bulk motion of the room air, the occurrence of this whirl
becomes much more frequent and the whirl width may be as wide as 2 inches.
Further studies of this phenomenon will certainly be of interest.

For the purpose of this experimental study, flow field symmetry is
essential. In order to minimize any room disturbances which might
break the flow symmetry, the screens described in the previous section
were installed. Shadow observations showed that these screens did
indeed stabilize the flow field.

The turbulence in the primary flow region is of course another
interesting feature of the flow field. It is more appropriate to describe
the turbulence in conjunction with the hot-wire data so the discussion
of the turbulence will be postponed until Chapter V.

HEATER PERFORMANCE

In free convection flows, the plate temperature and the heat transfer
are related. The performance of the heater can be characterized by
either the mean temperature difference between the plate and its ambient
or the mean heat flux.

Plate Temperature

The surface temperature distribution of the heated aluminum plate
was measured by thirteen thermocouples installed in the four radially

milled slots on the underside of the plate (Figure 6). These thermo-
couples were made from Number 24 "high accuracy" copper-constantan wire
(L & N Wire No. 24-55-11, error $= \pm 1/4^{\circ}F$ at $175^{\circ}F$ with reference junction
at $32^{\circ}F$), and were connected to a 24 channel switching box which was
directly connected to a potentiometer. Only time mean temperatures were
measured. Figure 7 shows the measured plate surface temperature distri-
butions for two mean plate temperatures. It is noticed that the plate
temperature is quite uniform in the central region and drops off slightly
toward the edge of the plate. This fact is expected, and attributed to
the more effective cooling by the cold air near the edge of the plate
(considering the fact of uniform heat flux input to the plate). Assuming
that the heat flux is proportional to the 4/3 power of the plate tempera-
ture rise above the ambient (27), this temperature non-uniformity repre-
sents a maximum of 3% local heat flux variation. As far as concerns the
boundary condition for the overall free convection flow field, this
slight temperature non-uniformity is insignificant.

Energy Balance

Twenty No. 24 iron-constantan thermocouples (L & N Wire No. 24-50-39)
were installed in the insulation jacket of heater assembly for energy
balance measurements (Installation details are given in Figure 2). These
thermocouples were also connected to a 24 channel switching box through
which any one of them could be connected to a potentiometer for reading.

The total energy loss from the heater assembly is the sum of energy
lost to the surrounding air by radiation from the aluminum plate (Q_p),

by convection and radiation from the asbestos ring (Q_a), by convection
and radiation from the floor of the platform (Q_f), and by conduction
through the insulation jacket (Q_j).

The net convective heat transfer from the heated plate to the air
above (Q_c) is computed as follows:

$$Q_c = Q_{in} - Q_{loss} = 3.413 \ EI - (Q_p + Q_a + Q_f + Q_j)$$

where E = voltage drop across the heater, volt

I = current passing through the heater, ampere

Q = heat transfer rate, Btu/hr

Energy balances were made for two heater power settings. The detailed
calculations of these terms are given in Appendix B. A summary of all
the loss terms is tabulated below:

Table 1. Energy balance terms.

Run No.	E volt	I amp.	θ_p °F	θ_∞ °F	Q_{in} B/hr	Q_p B/hr	Q_a B/hr	Q_f B/hr	Q_j B/hr	Q_c B/hr
1	132	8.6	520	77	3880	229	525	241	347	2538
2	108	7.1	410	77	2615	133	359	114	240	1769

It is clear that the loss terms are all small relative to Q_c. Therefore,
the percent accuracy of Q_c is better than any of the heat losses. As a
check, a direct energy balance measurement was made by blocking off the
heat dissipation from the aluminum plate. In this manner, the energy
input to the heater assembly at any given plate temperature would
represent the net heat loss from the assembly (less the radiative heat
loss from the aluminum plate). The results of this direct measurement

and those calculated based on temperature measurements are shown in Figure 8.

Heat Transfer Correlation

An examination of the significant governing variables for the heat transfer phenomenon leads to the following relation:

$$Nu = f(Pr, Gr, \beta \Delta \theta)$$

where $Nu = hD/k$, Nusselt number,

$Pr = \mu C_p/k$, Prandtl number,

$Gr = g\beta\Delta\theta D^3 \rho^2/\mu^2$, Grashof number,

and h, D, k, μ, g, β, $\Delta\theta$, and ρ are, respectively, the average heat transfer coefficient, plate diameter, thermal conductivity, dynamic viscosity, gravitational acceleration, coefficient of volumetric expansion, temperature difference between the plate mean and the ambient, and density. For weakly buoyant flows (4,27,37,38) such as in free convection, the parameter $\beta\Delta\theta$ is not significant enough to affect the flow by itself and is absorbed in Gr. This can also be seen from the governing differential equations for small density variations (see Chapter VI).

For free convection, the flow becomes fully turbulent when the Grashof number is very large ($>10^6$). This can be achieved most effectively by making D sufficiently large. Since the heat flux of a very large surface can only be finite and cannot be affected by changing its size, we assume that the heat flux is independent of the size D, i.e.,

$$Nu \propto (Gr)^{1/3}$$

Furthermore, experimental correlations (26,27) indicate that the primary effect of Pr^* can be taken into account by grouping it with Gr to form a Rayleigh number Ra, i.e.,

$$Nu = constant \times Ra^{1/3}$$

where Ra = PrGr. Using the property values of air at the ambient temperature, and the definition of heat flux (q, Btu/hr-ft^2)

$$q = h\Delta\theta$$

Nu and Ra for the two runs in Table 1 may be calculated. The relevant values are given below:

Table 2. Dimensionless heat transfer parameters.

Run No.	q, Btu/hr-ft^2	h, Btu/hr-ft^2-^{o}F	Pr	Nu	Gr x 10^{-10}	Ra x 10^{-10}
1	800	1.81	0.72	244	0.772	0.556
2	560	1.68	0.72	226	0.573	0.413

The above data are plotted in Figure 9 and are found to be in good agreement with experimental results of Fishenden and Saunders (26). One may observe that the result Nu $\propto$ Ra$^{1/3}$ is consistent with the present data, as expected. The proportionality constant was calculated to be 0.141, so that:

$$Nu = 0.141 \times Ra^{1/3}. \tag{3-1}$$

---

*The Prandtl number for air is substantially a constant in the range of temperature in this investigation.

VELOCITY MEASUREMENT

General Discussion

We are concerne! with the velocity measurement in the turbulent
free convection regime. In a flow field of this type local mean velocity
varies up to 3 ft/sec, but the velocities over most of the flow field are
only on the order of a fraction of a foot per second. The turbulence in
the flow field is characterized by low frequency, high amplitude fluctua-
tions (see Chapter V for detailed discussions). Very little has been
reported in the literature concerning this type of velocity measurement.
Tritton (28,39) used a quartz fiber to measure the mean velocities in the
boundary layer region above an almost horizontal heated plate. He used
a telescope to observe the deflection of the cantilevered quartz fiber
in the flow field. Since there is no easily recorded signal, this method
is not considered suitable for large number of measurements. Very
recently, the laser doppler technique (14,15) has been successfully
applied to turbulent flow field measurement. Aside from the obvious
advantage of undisturbed measurement, it is possible to use this technique
to measure both the instantaneous and mean velocity component in a desired
direction. No attempt was made to use this technique for the present
studies since the measurements for this experiment were well underway
before the possibilities of using such a technique became apparent.

The hot-wire technique is very useful for turbulence measurements.
However, in slow velocity measurements, it suffers severely from
orientation effects due to the free convection field generated by the

wire itself. Nevertheless, the ease of meeting the time response requirement, ease of recording, and the immediate availability of the required electronic components prompted the decision to use the hot-wire method for this experiment. In order to minimize the effects due to heat generated in the wire, earlier attempts were centered at making the sensing wire as small as possible. The smallest wire used was 0.00012" diameter Pt-10% Rh wire. Unfortunately, wire of this size did not survive the vibration resulting from large probe traveling. Moreover, as long as the wire is at a higher temperature than the ambient, free convection effects are always present.

Collis (40,41) in his reports on forced convection of heat from cylinders at low Reynolds numbers ($Re = dV\rho/\mu$), gave the following criterion:

Free convection effects are negligible when: $Re > Gr^{1/3}$

This expression implies that free convection effects are unimportant when the local flow velocity undisturbed by the wire is larger than $(g\beta\Delta\theta\nu)^{1/3}$. It shows also that free convection effects are independent of the wire diameter and that they can be reduced by operating the wire at small values of $\Delta\theta$, the temperature difference between the wire and the ambient.

The resistance and, hence, the calibration of a thin wire tends to drift due to self-straining. This situation may be improved by choosing a large wire diameter and by properly soldering the wire to its supports. Large wire diameter is desirable for its strength but it reduces the wire

resistance and hence the output signal (the voltage drop across the wire) for fixed temperature operation. As a reasonable compromise, the hot-wire chosen was bare platinum wire 0.001" diameter by 0.5" long. This kind of wire was found to be quite satisfactory in terms of strength, repeatability of results, sensitivity, directional sensitivity, and fast time response (see Chapter V for more discussions on the choice of this wire length). The time constant for this wire was calculated to be less than one millisecond for constant temperature operations (42). In order to minimize the effects due to the free convection field induced by the hot-wire, a low wire operating temperature (i.e., a small overheat ratio) was used.

Hot-Wire Calibration

A TSI[*] model 1010 constant temperature anemometer was used for generating the hot-wire signals. In order to account for the free convection effects, extensive calibrations were made in which both the wire orientation and the velocity vector were taken into consideration.

A calibration tunnel was designed to meet the requirements of variable flow velocity, orientation, and air temperature. Figure 10 shows a schematic diagram of this tunnel. The tunnel test section was an enclosed 4" I.D. aluminum can, the axis of which could be rotated through an angle of 180 degrees on a supporting bracket. An air jet issued from a 1" diameter orifice with a rounded inlet. Six sheets of

---

[*]Thermo-Systems, Inc., 2500 Cleveland Avenue North, St. Paul, Minnesota 55113.

spaced 100 x 100 mesh bronze wire strainer cloth were placed upstream of the orifice to straighten the flow. The hot-wire probe was inserted into the tunnel through a removable support plug, when the wire was in place it was about 1/2" downstream of the orifice exit plane. The probe is shown approximately to scale in Figure 3.

The uniformity of the velocity distribution in the jet was checked by traversing a 0.2" long hot-wire probe along the jet diameter. The velocity distribution in the center region of the jet was essentially uniform. A drop of approximately 1% of the hot-wire bridge voltage output was observed at 95% radius. With the hot-wire placed in the center of the jet during calibration, the total length of the hot-wire was exposed to a uniform velocity stream.

The velocity at the orifice could be varied from 0 to 3 ft/sec by a control valve which was located between the outlet of a pressure regulator and the inlet of a Manostat flow meter.* This meter was used for measuring velocities below 2 ft/sec. A water U-tube manometer was used for measuring higher velocities. Figure 11 shows the calibration curves for the flow meter and the U-tube expressed in terms of the orifice exit velocity at a standard condition (70°F and 30" Hga) versus the meter or U-tube readings. The temperature of the jet could be varied through the use of a 100 watt cartridge type electric heater which could heat the air up to 160°F at an orifice exit velocity of 2 ft/sec.

_____

*Manufactured by Manostat Corporation, New York.

The desired wire operating temperature was determined by comparing the calibration at several wire temperatures. It was found that operating the wire at approximately 300°F was quite satisfactory for the present applications. At this wire temperature, a reasonably good wire sensitivity could be obtained and the free convection effect was found negligible for velocities greater than 0.15 ft/sec.

Figure 12 shows a set of hot-wire calibration curves. This set of curves consists of the calibrations of a horizontal wire at constant wire operating temperature ($\sim$300°F or 4.50 Ω wire operating resistance) but at three different ambient air temperatures. The calibration data were fitted into the following functional form by the method of least squares:

$$E^2 = A + BW^{1/2} \tag{3-2}$$

where E is the hot-wire bridge voltage output, W the velocity, and A and B are constants depending on the ambient temperature through their dependence on fluid properties. Direct comparison of the data for air blowing upward and blowing downward shows that the free convection effect is indeed small for $W < 0.15$ ft/sec.

For small velocities on the order of 0.15 ft/sec, another set of calibration curves for the hot-wire was prepared (Figure 13). It is seen that the velocity vector of a laminar flow can be determined once a set of two hot-wire outputs (for wire horizontal and vertical) at the same location is obtained. This set of calibration curves was used only

for reducing the indraft velocity data for which the flow was essentially laminar and hence no non-linear averaging process was involved as would be the situation for turbulent flows.

It is remarked that for small velocity and laminar flow such as the indraft velocity measurements, wire orientation effects are important and therefore were considered in determining the velocity vector. For the turbulent flow regime of this study however, the wire output is substantially independent of orientation because of the relatively high fluctuating velocities.

Further details on hot-wire data taking and the response equation will be discussed where appropriate in Chapter V.

IV. TEMPERATURE FIELD AND ANALYSIS

The overall temperature field may be divided into two main regions:
the region very near the plate (within 1/2" of the plate" and the region
above. In the region near the plate, a large temperature gradient
exists. The major portion of the overall temperature drop takes place
in this region. In the region above, both the air temperature and the
temperature gradient are much smaller than those in the near-plate-region.
For this reason, the measurements for these regions were taken at separate
times with different thermocouple mounting methods. They will be discussed
under separate headings.

Air temperatures in both of these regions were measured with a No. 34
gage copper-constantan thermocouple. This thermocouple was calibrated
against a pair of certified Pt and Pt-Rd thermocouples in an oil bath
(see calibration curve in Figure 14). The thermocouple data output was
displayed on a BRUSH continuous chart recorder via the amplifier output
circuit of a Hewlett Packard Type 413A DC null voltmeter. The time
average of the thermocouple output (time constant ~ 1 sec) was obtained
by use of a large time constant (~ 1 minute) integrating circuit similar
to those shown in Figure 15. The temperature at each measured location
was recorded on the chart for a period of two to five minutes and the
steady state thermocouple output was used.

MEAN TEMPERATURE FIELD ABOVE THE PLATE

The mean temperature field was measured simultaneously with the velocity field. The thermocouple was mounted on the hot-wire probe (Figure 16) and traversed with it. Since temperature is a scalar quantity and the response of a thermocouple is nearly linear with temperature in the range of interest, the temperature field measurement is a relatively simple task compared with that of the velocity field. Several runs were made for each of the two mean plate temperatures investigated.

In order to determine the symmetry of the temperature field, measurements were made at three locations (on the same radius but spaced at 90° apart). Data showed that discrepancies among these three readings were generally very small. The largest (observed only occasionally) were less than 3% of the average reading. The discrepancy was believed to be mainly due to the large period variation of the air temperature in the laboratory room and to a less extent due to plume leaning. Shadow viewing showed that the plume was almost always straight up even when the laboratory door was wide open, and that the duration of occasional plume leaning was too short to affect the mean temperature readings significantly. In view of the data scatter ($> \pm 3^{\circ}F$) shown in Figures 17, 18 and 19, asymmetry of the data was considered to be relatively insignificant.

For each plate temperature the centerline temperature profile and three horizontal temperature profiles were obtained ($Y = 3''$, $6''$, $12''$ above the plate). Figure 17 shows the centerline temperature profiles for both plate temperatures investigated. Figures 18 and 19 show the

horizontal temperature profiles measured for the two plate temperatures.
In these figures, each point represents the average of six to ten mean
temperature readings. A line is drawn through each average temperature
to indicate the error of ± one standard deviation. It is interesting to
note that the temperature drops off almost linearly with radius in the
region near the centerline.

Figures 18 and 19 show that lower average air temperature and
relatively flat horizontal temperature profiles are associated with lower
plate temperature. These flat average temperature profiles imply a
larger plume width in agreement with Morton's analysis (38) that the
width of a weakly buoyant plume is larger than that of a strongly buoyant
plume. Because of the limited amount of data, quantitative determination
of plume width was not practical.

MEAN TEMPERATURE NEAR THE PLATE

The temperatures near the plate surface were measured with the same
thermocouple (34 gauge Cu-constantan wire) as was used for the tempera-
ture field probing; however, a different mounting method was employed
(Figure 20). Temperatures were measured at three radial locations (X =
0", 6", 12") for each vertical position Y. Because of the large tempera-
ture gradient existing near the plate, a small increment in elevation Y
was necessary. This small increment was obtained through the use of a
micrometer attached to one end of the horizontal bar of the traversing
mechanism. By advancing the micrometer screw against a hard stationary

surface, the whole traversing mechanism could be raised to any desired
height with respect to the plate in increments of 0.001".

Figures 21 and 22 show the temperature distribution in the region
near the plate surface for the two plate temperatures investigated
(t_p = 520°F and 410°F). These temperatures were obtained by correcting
the raw data for losses due to radiation and conduction (see Appendix C
for details of calculations). One may observe two interesting facts from
these temperature data. The major portion of the overall temperature
drop takes place within approximately 0.1" of the plate. This region is
thicker for the higher plate temperature.

The surface temperature gradient is larger for the higher plate
temperature and, because of the more effective cooling near the plate
edge, this temperature gradient increases with the radius. This cooling
effect is also reflected in the plate radial temperature distribution as
shown in Figure 7.

The temperatures within 0.1" of the plate were calculated based on
the average heat flux and molecular conduction only (solid lines in
Figures 21 and 22). These calculations show that, very close to the
plate surface, the measured temperatures are nearly the same as those
based on conduction calculations. This region is within approximately
0.02" of the plate surface. We will follow Townsend (3) and call this
region the conduction layer.

THERMAL DIFFUSIVITY

Some estimates on the turbulent transport coefficient based on the
available temperature data are made here. Adopting the thermal diffusivity
concept, the steady state energy equation may be written as follows:

$$\vec{V} \cdot \nabla \theta = \epsilon_H \nabla^2 \theta + \nabla \epsilon_H \cdot \nabla \theta$$

or,

$$\epsilon_H = \frac{\vec{V} \cdot \nabla \theta - \nabla \epsilon_H \cdot \nabla \theta}{\nabla^2 \theta}$$

where $\vec{V}$, θ, ϵ_H, and ∇ are, respectively, the velocity vector, mean
temperature, thermal diffusivity and gradient operator. ϵ_H is calculated
using the following procedure: We proceed arbitrarily to neglect the
spatial variation of $\nabla \epsilon_H \cdot \nabla \theta$. This gives:

$$\epsilon_H = \frac{\vec{V} \cdot \nabla \theta}{\nabla^2 \theta} \tag{4-1}$$

The value of ϵ_H calculated from Equation (4-1) are then used to estimate
the magnitude of the neglected term $\nabla \epsilon_H \cdot \nabla \theta$ to see if the procedure is
justified.

Based on the mean temperature data (Figure 18) the values of $\nabla \theta$
and $\nabla^2 \theta$ were obtained graphically. Using the data of $\vec{V}$ from Chapter V,
the values of ϵ_H were calculated from Equation (4-1) for the case $\theta_p =$
520°F. The values of $\nabla^2 \theta$ and ϵ_H for several locations in the flow field
are given in Table 3.

The estimates in Table 3 show that the values of ϵ_H are nearly
constant in the major portion of the primary flow region. ϵ_H is large
near the plate and is relatively small at the location (6,3) which is

near tne boundary of the primary flow region. The magnitudes of the neglected term $\nabla\epsilon_H \cdot \nabla\theta$ are estimated and are also give in Table 3. It is seen chat they are much smaller than the typical values of the term $\vec{V}\cdot\nabla\theta$. Neglecting of $\nabla\epsilon_H \cdot \nabla\theta$ makes the values of ϵ_H somewhat too high.

Table 3. Thermal diffusivity estimates ($\theta_p = 520^oF$).

Location in.		Velocity fps		θ	$-\nabla^2\theta$	$-\vec{V}\cdot\nabla\theta$	$\nabla\epsilon_H\cdot\nabla\theta$	ϵ_H
X	Y	-U	V	^oF	$^oF/ft^2$	$^oF/sec$	$^oF/sec$	ft^2/sec
0	1.5	0	.93	162.5	1400	93	11	.066
0	3	0	1.35	152	1673	88	5	.053
0	6	0	1.90	140	1700	68	.7	.04
0	12	0	2.22	125.5	1424	52	.1	.037
3	3	.47	.78	137	504	26.2	2.8	.052
3	6	.13	1.06	120	656	28.4	1.4	.043
6	3	.41	.45	115.3	486	4.7	.1	.01
6	6	.26	.77	98.7	142	5.3	.3	.037

V. RESULTS AND ANALYSIS OF HOT-WIRE DATA

INTRODUCTION

The experimental measurements of the flow above a heated horizontal circular plate are described here. The mean velocities and turbulence kinetic energies are of primary interest. Using the turbulence measurements, the eddy diffusivity will be estimated.

As will be shown, the mean flow velocities are small (~ 1 ft/sec) and the turbulence velocities are on the same order of magnitude as the mean. Due to the large fluctuations, conventional experimental methods and attendant mathematical simplifications for turbulence measurements fail. No data directly relevant to the present investigation have been published.

In any particular geometric space, the desired flow properties are all determined by the probability density function over four-dimensional velocity-temperature space. The data reduction procedure is based on the idea that the essential features of this probability density function are determined by the one-point probability density distribution of hot-wire output voltage with wire orientation as a parameter. This information is approximated by a set of averages of hot-wire output repeated at several orientations.

A constant temperature hot-wire anemometer was used for this experiment. The one-point averaged values of the hot-wire output and selected low-order moments were obtained at selected wire orientations. The quantities of interest were then inferred from knowledge of these moments

and a set of numerically simulated hot-wire data. In the following

section, the hot-wire data from direct experimental measurements will

be summarized and a numerical simulation of the turbulence based on an

idealized computation model will be described. A data reduction proce-

dure using the above results is then discussed and the reduced data

presented. Finally, the justification of the numerical model and the

assumptions incorporated in it will be given.

HOT-WIRE DATA SUMMARY

Instrumentation

The complete instrumentation setup is shown in Figure 15. It

consists primarily of a constant temperature hot-wire anemometer, two

linearizers, the integrating circuits and the recording devices. One-

point time averages of the quantities shown in Figure 15 (i.e., E, $\overline{E}$,

$\overline{E^2}$, etc) are the basic data to be taken.

A 0.001" diameter x 0.5" long bare platinum wire was chosen as the

sensing element. Shadow observations showed that the eddy size was on

the order of 1", therefore, a 1/2" long wire would be a reasonable choice.

In order to determine the length effect on the resolution of turbulence

sensing, a 0.2" long wire was also made. These two wires were operated

at the same wire temperature (approximately $300^{\circ}F$) and were placed in

the flow field 6" above the plate. The hot-wire outputs were recorded

on an AMPEX Model FR-1200 tape recorder at a recording speed of 1-7/8

inches per second (ips). Comparisons were made by playing the tapes

back at 60 ips and analyzed with a Hewlett Packard Model 302A wave
analyzer. As shown in Figure 23, there was no significant difference
between the two wire outputs in either frequency or amplitude of the
fluctuations. It was therefore concluded that for this investigation
wire length within the range studied was not an important parameter.

The longer wire (0.5" long) was used for all measurements because
of the desired larger voltage output or better sensitivity.

Characteristic Quantities of the Turbulence

Figure 24[*] shows some typical hot-wire output traces for both
horizontal and vertical orientation of the wire at various distances
above the center of the plate. Figure 25[*] shows hot-wire output traces
for a horizontal wire at five radial locations 6" above the plate. This
figure shows that the turbulence degenerates with increasing radius.
At a radius of 9" the traces indicate intermittent turbulence. At 6"
radius, the large amplitude and the erratic excursion of the traces suggest
that the hot-wire is located approximately on the boundary of the primary
flow region. Both Figures 24 and 25 show that the amplitude of the
fluctuations are on the order of one volt. This corresponds to velocity
fluctuations on the order of 1 ft/sec (Figure 13), which is of the same
order of magnitude as the mean flow velocity.

---

[*]Since the zero velocity position of these traces depends on the
local temperatures which vary from location to location, it is
impractical to mark these traces with the corresponding velocities.
Therefore, by themselves these hot-wire traces (Figures 24 and 25)
demonstrate only the qualitative nature of the turbulence.

The use of a wave analyzer was originally intended to obtain the characteristic frequency of the turbulence. Analysis of the data showed that the main contribution of the frequency was in the range below 10 Hz. At frequencies below 25 Hz the amplitude dropped off rapidly to less than one percent of the value at 1 Hz and became negligibly small at higher frequencies (e.g., Figure 23). Due to the poor low frequency capability, the wave analyzer could not be used to obtain a meaningful time scale for the turbulence. Therefore, the autocorrelation function of the recorded turbulence data was obtained using a PAR Model 101 correlation function computer (manufactured by Princeton Applied Research Corporation).

The autocorrelation function of the hot-wire bridge voltage output E is defined as:

$$\varphi(\tau) = \lim_{T \to \infty} \int_{-T}^{T} E(t) \; E(t + \tau) dt$$

where τ is a delay time. Figure 26 shows the autocorrelation function of the hot-wire bridge voltage output for a few centerline locations. Since $\varphi(\tau)$ is a pure function of delay time, the integral time scale of the turbulence can be defined as the area under the autocorrelation function curve (42). As shown in the tabulation in this figure, the integrated time is on the order of 0.1 second. In other words, the characteristic frequency of the turbulence in the flow field of the present experiment is low (on the order of 10 Hz) which is well within the capability of the electronic instruments used.

We conclude that the turbulence in the primary flow region is characterized by low frequency ($\sim$10 Hz) and large amplitude ($\sim$1 ft/sec) fluctuations.

Hot-Wire Response Equation

Since the cooling effect on a hot-wire depends primarily on the velocity component $W_\perp$ perpendicular to the wire and to much less extent on the parallel component $W_{\parallel}$, it is useful to define an effective instantaneous velocity W (44):

$$W^2 = W_\perp{}^2 + k^2 W_{\parallel}{}^2 \qquad (5\text{-}1)$$

where k^2 is an experimental constant. For a wire of length-to-diameter ratio greater than 600, k^2 is essentially zero (44). Equation (5-1) will be used to obtain the value of W in Equation (3-2). Rearranging Equation (3-2), the following relations are obtained:

$$\frac{E^2 - A}{B} = W^{1/2}$$

$$\left(\frac{E^2 - A}{B}\right)^2 = W \qquad (5\text{-}2)$$

$$\left(\frac{E^2 - A}{B}\right)^4 = W^2$$

In these equations the ambient tempterature dependent quantities A and B are lumped on the left hand side. We will assume and later verify on the basis of computer simulated output calculations that the following ratios are substantially independent of the fluctuations in A and B.

$$\mathcal{R}_0 = \overline{W^{1/2}}/(\overline{W^{1/2}})_{\phi_w=0}$$

$$\mathcal{R}_1 = \overline{W}/(\overline{W})_{\phi_w=0} \qquad \qquad (5\text{-}3)$$

$$\mathcal{R}_2 = \overline{W^2}/(\overline{W^2})_{\phi_w=0}$$

where an over bar refers to the corresponding time-averaged value. $\mathcal{R}_0$, $\mathcal{R}_1$, $\mathcal{R}_2$ are primarily functions of the normalized turbulence velocity and the wire orientation angle ϕ_w.

Data in Primary Flow Region

Eight locations in the primary flow region were probed. The data consisted of the time-averaged values (averaging time $\sim$2-5 minutes) of E, E^2, W and W^2 for ϕ_w from -90° to +90° at 15° intervals. To facilitate the data taking, the temperature dependent quantity A in Equations (5-2) was replaced by a fixed value A' nearly equal to A. The data thus obtained were used to compute the correct values of $\overline{W}$ and $\overline{W^2}$. The conversion formulas are given below (see Appendix L for details):

$$\overline{W} = C_1 \overline{W'} - 2C_2\overline{W^{1/2}} - C_2{}^2$$

$$\overline{W^2} = C_1{}^2\overline{W'^2} - 6C_2\overline{W}(C_2 + 2\overline{W^{1/2}}) + 4C_2\overline{W^{1/2}}(2\overline{W^{1/2}}{}^2 - C_2{}^2) - C_2{}^4 \qquad (5\text{-}4)$$

where $C_1 = B^{-2}$, $C_2 = (A-A')/B$, $\overline{W'} = \overline{(E^2-A')^2}$, $\overline{W'^2} = \overline{(E^2-A')^4}$.

For all the data taken, A' was set equal to 25. At this A' setting, the whole data taking system (Figure 15) was calibrated against a known d.c. plus a.c. voltage input. The calibrations of $\overline{E^2}$, $\overline{W'}$, $\overline{W'^2}$ were plotted versus their corresponding line outputs on the recorder and are shown in Figure 27.

Since A' was taken as a constant, we are essentially treating A

and B as constants evaluated at the average ambient temperature. The

maximum error introduced due to this assumption may be estimated from

the dependences of A and B on fluid properties (p. 79 , reference 42) and

can be shown to be on the order of 1%. As a check the effects of the

fluctuations of A and B due to temperature fluctuations is evaluated by

numerical simulations as will be described later.

The hot-wire data obtained are shown in Figure 28. The ratios

defined in Equations (5-3) at $\phi_w = 90^\circ$ may be used to describe the

shape of these curves in Figure 28. These "shape parameters" and the

relevant hot-wire data are summarized in Table 4. A comparison between

$\overline{W}$ and σ_W shows clearly that the turbulence intensity is indeed much

larger than that reported for typical low turbulence measurements (e.g.,

references 42, 45).

Indraft Data

Two indraft profiles at the edge of the plate were measured. These

measurements were all made in the secondary flow region, a laminar flow

region. Therefore, direct measurement using only the hot-wire bridge

voltage output E was possible. Since the velocity in this region was

small, a relatively high wire operating temperature was desirable. The

wire was operated at approximately 400°F. A set of calibration curves

was obtained for this purpose (Figure 13). Figure 13 shows that the

velocity vector at any location can be determined once the hot-wire bridge

voltage outputs for $\phi_w = 0^\circ$ and 90° (E_h and E_v respectively are obtained.

Table 4. Summary of hot-wire data in primary flow region ($\theta_p = 520°F$).

X in.	Y in.	ϕ_v deg.	$\mathcal{R}_0$	$\mathcal{R}_1$	$\bar{E}$ volt	$\overline{E^2}$ volt²	σ_E volt	$\bar{W}$ fps	$\overline{W^2}$ (fps)²	σ_W fps
0	1.5	0	.86	0.75	5.57	31.4	0.61	1.28	2.54	0.95
0	3	0	.78	0.61	6.08	37.3	0.58	1.58	3.64	1.07
0	6	0	.62	0.43	6.88	47.6	0.52	2.08	4.79	0.68
0	12	0	.50	0.29	7.43	56.0	0.89	2.30	6.19	0.95
3	3	31	.78	0.59	6.35	40.5	0.42	1.07	1.38	0.48
3	6	7	.61	0.42	6.98	49.0	0.53	1.16	1.54	0.44
6	3	42	.74	0.60	6.64	44.4	0.56	0.74	0.58	0.40
6	6	20	.61	0.40	7.11	51.2	0.80	0.85	0.92	0.44

The results are shown in Figure 29. Clearly, the largest indraft occurs near the ground level.

NUMERICAL SIMULATION OF HOT-WIRE DATA

Described here is an idealized numerical model to generate simulated hot-wire data for a given set of flow parameters. The results thus obtained will be used to interpret data from experimental measurements.

The Numerical Model

Consider the mean velocity vector V_m, the fluctuating velocities (u, v, w) and the hot-wire described in the following coordinate system:
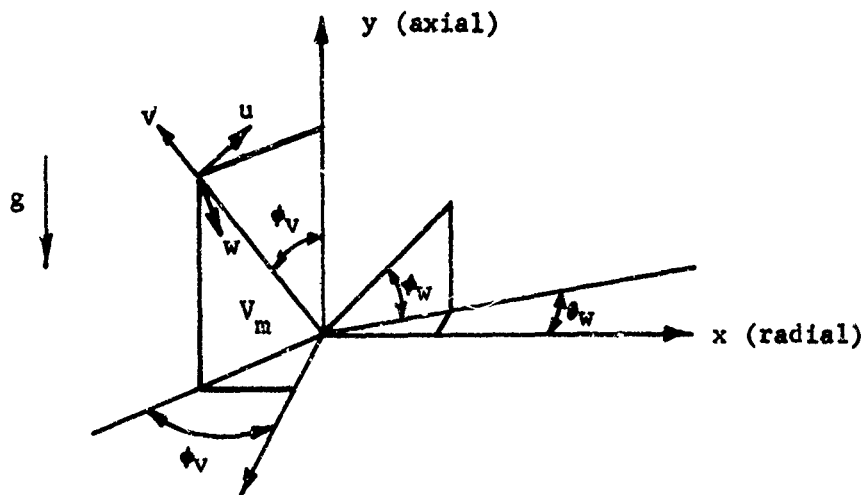
where v is the random fluctuating velocity component parallel to V_m, w is the random fluctuating velocity component in the horizontal direction normal to v, and u is the random fluctuating velocity component in the direction normal to both v and w such that (u, v, w) form a right-handed triad. The direction cosines of V_m, u, v, w and the wire in the (x, y, z) coordinate system are given below:

Direction	u	V_m+v	w	Wire
x	$\cos\phi_v \sin\theta_v$	$-\sin\phi_v \sin\theta_v$	$\cos\theta_v$	$\cos\phi_w \cos\theta_w$
y	$\sin\phi_v$	$\cos\phi_v$	0	$\sin\phi_w$
z	$-\cos\phi_v \cos\theta_v$	$\sin\phi_v \cos\theta_v$	$\sin\theta_v$	$-\cos\phi_w \sin\theta_w$

Denoting the component of u, V_m+v, and w in the direction of the wire, respectively, by E_1, E_2, and E_3 the above tabulation gives, after a little manipulation:

$$E_1 = \sin(\phi_w - \phi_v) + \sin\phi_v \cos\phi_w \left[1-\sin(\theta_w+\theta_v)\right]$$

$$E_2 = \cos\phi_w \cos(\theta_w+\theta_v) \tag{5-5}$$

$$E_3 = \cos(\phi_w - \phi_v) - \cos\phi_v \cos\phi_w \left[1-\sin(\theta_w+\theta_v)\right]$$

Finally, for given values of V_m, (u, v, w):

$$W_{\parallel}^2 = \left[uE_1 + (v + V_m)E_2 + wE_3\right]^2$$

$$W_{\perp}^2 = u^2 + (v + V_m)^2 + w^2 - W_{\parallel}^2 \tag{5-6}$$

These expressions will be used in Equations (5-1) and (5-2) to generate the desired hot-wire output.

For convenience of specification of the fluctuations, the following normalized variables are defined:

$$\tilde{u} = \frac{u}{\sigma_u} \, , \quad \tilde{v} = \frac{v}{\sigma_v} \, , \quad \tilde{w} = \frac{w}{\sigma_w} \, , \quad \tilde{\theta} = \frac{\theta'}{\sigma_\theta} \tag{5-7}$$

where

$$\sigma_u^2 = \overline{u^2} \, , \quad \sigma_v^2 = \overline{v^2} \, , \quad \sigma_w^2 = \overline{w^2} \, , \quad \sigma_\theta^2 = \overline{\theta'^2} \tag{5-8}$$

are the variance of the fluctuations. The correlation coefficients of turbulence may be written in terms of the above quantities:

$$K_{uv} = \frac{\overline{uv}}{\sigma_u \sigma_v} = \overline{\tilde{u}\tilde{v}} \quad , \quad K_{u\theta} = \frac{\overline{u\theta'}}{\sigma_u \sigma_\theta} = \overline{\tilde{u}\tilde{\theta}} \quad , \text{ etc.} \qquad (5-9)$$

The values of these correlation coefficients may be positive or negative but must not exceed unity in magnitude.

Substituting Equations (5-1), (5-6) and (5-7) into (3-2) and making modifications for studying the effects of temperature dependent fluctuations of A and B, we have:

$$E^2 = (1 + \alpha\sigma_\theta\tilde{\theta}) A + (1 + \gamma\alpha\sigma_\theta\tilde{\theta}) BV_m^{1/2} \left[\left(\frac{W_\perp}{V_m}\right)^2 + k^2 \left(\frac{W_{||}}{V_m}\right)^2 \right]^{1/4} \qquad (5-10)$$

For computations, we can without loss of generality take $\alpha = -1$ and $V_m = 1$. The factor γ accounts for the fact that A and B do not have the same dependence on temperature.

The results, with combinations of the σ's and K's as defined in Equations (5-8) and (5-9), will be used for this study. The flow variables characterizing the turbulence (u, v, w, θ') define actually random variables, sequences of which can be simulated with the numbers obtained from a random number generator (see details in Appendix E), given the values of σ's and K's. After making some idealizations described below, the desired hot-wire response and its moments can be readily computed as functions of the flow variables from the above equations.

Some Numerical Results

Calculations were made for four types of probability density distributions. Some typical results are presented in Tables 5 and 6. It is seen that fairly good results in both reproducing input data and errors can be obtained from calculations using 400 samples. The effects of the type of distribution function appear minor.

Figures 30 and 31 show some simulated hot-wire data corresponding to the experimental results given in Figure 28. Resemblance in basic shape of the data curves in Figures 28 and 30 and 31 is clearly shown.

For the hot-wire used in this experiment, the value of k^2 was found to be essentially equal to zero. For data reduction, the shape parameters and the effective flow velocity for the case: $k^2 = 0$, zero correlation and temperature fluctuations, Gaussian distribution, are presented in Figure 32.

DATA REDUCTION

Data reduction utilizes the results of simulated hot-wire data based on the following idealizations: $k^2 = 0$, no correlations, no temperature fluctuations, and Gaussian distribution of fluctuation of each velocity component. The justification of these assumptions will be discussed under the next heading.

The data reduction procedure is described below with an actual example.

Table 5. Comparison of simulated hot-wire data - basic output.

I. Input data:

$A = 7$, $B = 1$, $k^2 = 0$; $\phi_v = \theta_v = \phi_w = \theta_w = 0°$

$\sigma_u = \sigma_v = \sigma_w = 0.5$, $\sigma_\theta = 0.06$, $\gamma = 1$

II. Output data:

IC[#]	Number of Samples	$\overline{E}$ volts	Error %	$\overline{W^{1/2}}$ $(fps)^{1/2}$	Error %	$\overline{W}$ (fps)	Error %	$\overline{W^2}$ $(fps)^2$	Error %	$\mathscr{R}_0$	$\mathscr{R}_1$	$\mathscr{R}_2$
0	100	1.7363	0.46	1.0212	2.73	1.1205	5.08	1.5789	9.73	0.7268	0.5423	0.3079
	400	1.7402	0.25	1.0361	1.46	1.1652	2.74	1.7645	5.25	0.7343	0.5634	0.3546
	1000	1.7386	0.16	1.0302	0.91	1.1497	1.70	1.7025	3.33	0.7341	0.5656	0.3629
-1	400	1.7486	0.21	1.0628	1.18	1.1921	2.19	1.6935	4.23	0.7411	0.5675	0.3503
1	100	1.7467	0.52	1.0591	2.95	1.2192	5.29	1.9029	9.36	0.7790	0.6098	0.3712
	400	1.7361	0.25	1.0219	1.50	1.1378	2.82	1.7067	5.26	0.7738	0.6045	0.3713
	1000	1.7398	0.16	1.0345	0.91	1.1592	1.70	1.7312	3.16	0.7768	0.6044	0.3647
2	100	1.7474	0.46	1.0599	2.65	1.2021	5.05	1.8138	9.11	0.8063	0.6315	0.3627
	400	1.7387	0.22	1.0291	1.31	1.1314	2.53	1.6090	4.77	0.8080	0.6368	0.3735
	1000	1.7440	0.15	1.0481	0.85	1.1775	1.62	1.7517	2.94	0.7955	0.6150	0.3462
3	100	1.7523	0.57	1.0807	3.67	1.3249	13.53	4.9692	67.94	0.6153	0.4490	0.3461
	400	1.7455	0.24	1.0537	1.36	1.1920	2.60	1.8063	6.65	0.6360	0.4581	0.3131
	1000	1.7418	0.13	1.0393	0.77	1.1440	1.53	1.6165	3.74	0.6539	0.4732	0.3242

[#]IC refers to the type of random number probability distribution. IC = -1 (normal distribution scheme), IC = 0 (general scheme), IC = 1 (Eq. E-8), IC = 2 (Eq. E-9), IC = 3 (Eq. E-10).

Table 6. Comparisons of simulated hot-wire data - correlation coefficients.

I. Input data:

$A = 2.0$, $B = 1.0$, $k^2 = 0.1$, $V_m = 1.0$
$\sigma_v = 1.0$, $\sigma_u = \sigma_w = 0.5$, $\sigma_\beta = 0.12$, $\gamma = 1.0$; $K_{uv} = K_{u\beta} = 0.5$,
$K_{vw} = K_{wu} = K_{v\beta} = K_{w\beta} = 0$, $\phi_v = \theta_v = \phi_w = \theta_w = 0$

II. Output data:

IC#	Number of Samples	r.m.s. fluctuations				correlation coefficients						basic data			
		σ_v fps	σ_u fps	σ_w fps	σ_β F	K_{uv}	K_{vw}	K_{wu}	$K_{u\beta}$	$K_{v\beta}$	$K_{w\beta}$	$\bar{E}$ volt	$\overline{w^{1/2}}$ $(fps)^{1/2}$	$\bar{w}$ fps	$\overline{w^2}$ $(fps)^2$
0	100	1.054	.527	.534	.125	.584	.031	-.074	.400	.002	-.121	1.747	1.053	1.296	2.927
	400	1.070	.522	.504	.128	.586	-.015	-.052	.525	.105	-.109	1.757	1.100	1.392	3.358
	1000	1.011	.506	.501	.122	.528	-.016	-.040	.523	.044	-.099	1.754	1.090	1.347	3.124
1	100	0.990	.505	.482	.120	.481	-.113	-.048	.751	.225	.060	1.759	1.101	1.313	2.440
	400	1.016	.503	.487	.123	.500	-.014	-.024	.496	-.018	-.020	1.763	1.121	1.417	3.225
	1000	1.009	.506	.502	.121	.529	.011	-.027	.502	.040	-.005	1.758	1.101	1.354	2.836
2	100	1.000	.498	.494	.120	.562	-.013	-.041	.461	.025	-.051	1.753	1.083	1.320	2.612
	400	0.995	.498	.500	.120	.450	-.054	-.029	.512	-.037	-.039	1.761	1.112	1.372	2.751
	1000	0.999	.499	.500	.120	.511	-.100	-.060	.476	-.013	-.014	1.753	1.085	1.319	2.595
3	100	0.735	.399	.404	.091	.290	.041	-.016	.718	-.003	-.010	1.736	1.019	1.089	1.442
	400	1.192	.442	.426	.145	.256	.057	.025	.774	-.075	.011	1.743	1.055	1.303	5.282
	1000	1.041	.449	.479	.128	.351	-.023	.027	.696	-.031	.018	1.749	1.074	1.348	5.117

#See footnote of Table 5.

1. Center line Locations

On the centerline, symmetry requires that $\sigma_u = \sigma_w$ and $U = 0$, so the shape parameters plotted in Figure 32 are directly applicable. Consider the data for $X = 0$, $Y = 3"$:

	Shape Parameter of Actual Data	Range of σ_u/V_m from Figure 32	Common Range of σ_u/V_m
$\mathfrak{R}_0$	0.775	0.52-0.55	0.52-0.55
$\mathfrak{R}_1$	0.608	0.51-0.56	0.52-0.55

The value of σ_u will be chosen (within the above common range) such that the values of $(\sigma_u - \sigma_v)/V_m$ obtained from $(\sigma_u/V_m, \mathfrak{R}_0)$ and $(\sigma_u/V_m, \mathfrak{R}_1)$ are the same, this being a requirement. In this manner, the value of σ_u/V_m and $(\sigma_u - \sigma_v)/V_m$ are found equal to 0.52 and 0, respectively.

From Figure 32 for $\sigma_u/V_m = 0.52$ and $(\sigma_u - \sigma_v)/V_m = 0$.

$$\overline{W} = 1.18 \, V_m$$

The hot-wire data in Figure 28 shows that:

$$\overline{W} = 1.58 \, fps$$

Finally, $V_m = 1.35 \, fps$

$$\sigma_u = \sigma_v = \sigma_w = 0.7 \, fps$$

2. Off-Centerline Locations.

For off-centerline locations, V_m is making an angle ϕ_v with the centerline. This angle is set approximately equal to the phase

shift of the peak value of the hot-wire data. Using the peak values
as a basis, $\mathcal{Q}_0$, $\mathcal{Q}_1$, and $\overline{W}/V_m$ are then obtained. The rest of the
data reduction is carried out in the same manner as described in (1).

A summary of the reduced data is given in Table 7. It is seen
that the turbulence velocities are indeed large (of comparable magnitude
as the mean flow velocity), and that the turbulence decreases, as it
must, as the distance from the plate increases. It is remarked that in
the data reduction procedure described above the effects of local free
convection due to the hot-wire has been ignored, i.e., the hot-wire
output is assumed unaffected by the wire orientation with respect to
the mean flow. In view of the large turbulence velocities, this appears
to be justified (see Chapter III).

Table 7. Summary of hot-wire velocity results (t_p = 520°F).

X in.	Y in.	t_v deg.	-U fps	V fps	σ_u fps	σ_v fps	τ, sec. (Fig. 26)	$\sigma_u^2 \tau$ ft²/sec
0	1.5	0	0	0.93	0.7	0.7	0.114	0.056
0	3	0	0	1.35	0.7	0.7	0.092	0.045
0	6	0	0	1.9	0.57	0.57	0.181	0.059
0	12	0	0	2.22	0.47	0.47	0.270	0.06
3	3	31	0.47	0.78	0.52	0.76	---	---
3	6	7	0.13	1.06	0.34	0.34	---	---
6	3	42	0.45	0.50	0.34	0.17	---	---
6	6	20	0.26	0.77	0.25	0.33	---	---

If we assume that the turbulence is characterized by σ_u and the time
obtained from the autocorrelation function, then $\sigma_u^2 \tau$ can be used to
estimate the order of magnitude of the eddy diffusivity. Table 7 shows

that the values thus calculated are consistent with the estimates made based primarily on temperature data (Table 3).

JUSTIFICATIONS

Simulated hot-wire data have been obtained for a variety of cases based on different assumptions such as: type of random number distribution function, correlation coefficients, temperature fluctuations, and the values of A and B. The results show that the computed values of ϑ_0 and ϑ_1 are somewhat insensitive to the assumptions used and the values of ϑ_2 and $\overline{W}/V_m$ show more pronounced dependence on assumptions.

Figure 33 shows comparisons of some of the typical results with the largest differences (i.e., ϑ_2 and $\overline{W}/V_m$). Clearly, relatively large differences (although small by themselves) may be caused by the type of random number distribution functions used and the results are relatively insensitive to other assumptions. In the data reduction procedure, only the results of ϑ_0, ϑ_1 and $\overline{W}/V_m$ are used. In view of their insensitivity to the assumptions, this procedure is reasonably general and the expected error involved due to assumptions may be best shown by that of V_m.

In order to show quantitatively the effects of assumptions on the reduced data, the procedure for the actual data reduction was repeated for a number of cases using simulated hot-wire data based on different assumptions. Relative errors are defined as the percentage deviation of the calculated results from their corresponding values tabulated in Table 7. Results show that the relative errors of the reduced turbulence

velocities σ_u, σ_v and the mean flow velocity V_m are of comparable magnitudes. This is expected because of the dominant dependence of errors on $\overline{W}/V_m$ described above.

Table 8 shows the relative errors of V_m and one case of σ_u. It can be seen that the possible error in data reduction due to the various assumptions used is on the order of 10%. The mean flow direction is unaffected by the assumptions in any way because it is determined by the location of the peak value of the actual hot-wire data. The error of the mean flow direction is mechanical which is less than $\pm 2^{\circ}$.

Table 8. Relative errors of V_m^* - percent variations based on data in Table 7.

assumptions								
#IC =	-1	1	2	3	0	0	0	1
**σ_θ =	0	0	0	0	0.06	0.06	0	0
$K_{u\theta}$ =	0	0	0	0	0	0.05	0	0
K_{uv} =	0	0	0	0	0	0	0.5	0.5
Location (X, Y), inch								
(0, 1.5)	-2, 2	-8	-3.6	-0.6	-1.2	2.3	0	-2.2
(0, 3)	-3, 5	-7	-4.2	-2	-1.2	3.6	0.5	-2.8
(0, 6)	1, 8	-5.6	-4.3	-3	-1.5	1.4	0	-3
(0, 12)	-1, 4	-4	-3.8	-2.5	-1.7	1	0	-2.2
(3, 3)	0, 6	-6.5	-4	-2	-1.2	1.7	-1.4	-1
(3, 6)	-9, 9	-5.4	-4.2	-2.8	-1.8	1	2	0
(6, 3)	-2, 2	-6.2	-4.2	-2.6	-1.7	1.2	0	-1.4
(6, 6)	-1, 7	-5	-4.3	-2.8	-1.8	1	1	-1

*The numbers after comma for the case IC = -1 refer to the relative errors of σ_u. These errors are the largest for all the cases studied.
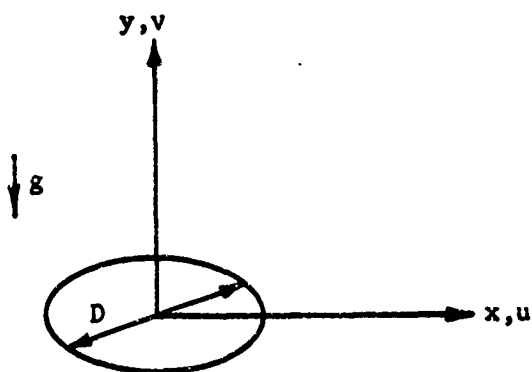#See footnote of Table 5.
**For $\sigma_\theta \neq 0$, the value of γ used is 0.15.

VI. NUMERICAL MODEL

The purpose of this chapter is to present a numerical method for predicting the flow field near the plate.

MATHEMATICAL FORMULATION

In the cylindrical coordinate system sketched below,

the flow field to be described is that generated in the half space $y \geq 0$ by a heat source of diameter D at $y = 0$. An order of magnitude analysis shows that the viscous dissipation (Eckert number $\sim 10^{-8}$ for our problem) and the flow work terms in the energy equation are negligible (Chapter 14, Reference 45). In the primary flow region, the region in which there is a dominant upward moving stream of eddies, the density (or absolute temperature) variations are small compared with the ambient density, therefore, the familiar Boussinesq approximations are used (1). At present, the physical behavior of the flow field is not well-understood, nor have there been any proposed turbulent transport formulations in the literature. The constant eddy diffusivity model is the simplest

plaus_ble turbulent transport model and is chosen for the calculations described below. After introducing these simplifications, and a characteristic velocity $U_c^2 = g\beta\Delta\theta_T D$, the resulting equations for the mean flow field become the same as those for laminar free convection (13, 36). These differential equations in dimensionless form are given below:

Continuity

$$\frac{\partial(xu)}{\partial x} + \frac{\partial(xv)}{\partial y} = 0 \tag{6-1}$$

Momentum

$$\frac{\partial u}{\partial t} + u\frac{\partial u}{\partial x} + v\frac{\partial u}{\partial y} = -\frac{\partial p}{\partial x} + \frac{1}{\sqrt{Gr_T}}\left(\frac{\partial^2 u}{\partial x^2} + \frac{1}{x}\frac{\partial u}{\partial x} - \frac{u}{x^2} + \frac{\partial^2 u}{\partial y^2}\right) \tag{6-2}$$

$$\frac{\partial v}{\partial t} + u\frac{\partial v}{\partial x} + v\frac{\partial v}{\partial y} = -\frac{\partial p}{\partial y} + \frac{1}{\sqrt{Gr_T}}\left(\frac{\partial^2 v}{\partial x^2} + \frac{1}{x}\frac{\partial v}{\partial x} + \frac{\partial^2 v}{\partial y^2}\right) + T \tag{6-3}$$

Energy

$$\frac{\partial T}{\partial t} + u\frac{\partial T}{\partial x} + v\frac{\partial T}{\partial y} = \frac{1}{Pr\sqrt{Gr_T}}\left(\frac{\partial^2 T}{\partial x^2} + \frac{1}{x}\frac{\partial T}{\partial x} + \frac{\partial^2 T}{\partial y^2}\right) \tag{6-4}$$

where x, y, u, v, p, T, Gr_T, Pr and t are, respectively, the dimensionless radial and axial coordinate (x = X/D, y = Y/D), dimensionless x and y component of the mean flow velocity (u = U/U_c, v = V/U_c), pressure coefficient (p = (p-p_∞)/$\rho_\infty U_c^2$), dimensionless temperature (T = (θ-θ_∞)/$\Delta\theta_T$), turbulent Grashof number ($Gr_T = g\beta\Delta\theta_T D^3/\epsilon_M^2$), turbulent Prandtl number ($P_r = \epsilon_M/\epsilon_H$), and dimensionless time (t = τU_c/D). $\Delta\theta_T$, ϵ_M and ϵ_H are, respectively, the equivalent temperature rise, momentum and thermal diffusivities for turbulent flow.

The physical boundary conditions are: Zero disturbance at large distance from the heat source and non-slip and thermally insulated

conditions at the ground surface $(y = 0)$, and $T = 1$ at the source.

METHOD OF SOLUTION

Defining a stream function S such that:

$$xu = \frac{\partial S}{\partial y},$$

$$-xv = \frac{\partial S}{\partial x} \tag{6-5}$$

automatically satisfies Equation (6-1). Subtracting the derivative of Equation (6-3) with respect to x from the derivative of Equation (6-2) with respect to y and making use of Equation (6-1) yields:

$$\frac{\partial Z}{\partial t} + u \frac{\partial Z}{\partial x} + v \frac{\partial Z}{\partial y} = \frac{1}{x} \frac{\partial T}{\partial x} + \frac{1}{\sqrt{Gr_T}} \left[\frac{\partial^2 Z}{\partial x^2} + \frac{3}{x} \frac{\partial Z}{\partial x} + \frac{\partial^2 Z}{\partial y^2} \right] \tag{6-6}$$

The new quantity Z, defined as:

$$-xZ = \frac{\partial u}{\partial y} - \frac{\partial v}{\partial x} \tag{6-7}$$

in Equation (6-6) is called the modified vorticity function. Substituting Equation (6-5) into Equation (6-7) a relation between the stream function and the modified vorticity function is obtained:

$$-x^2 Z = \frac{\partial^2 S}{\partial x^2} - \frac{1}{x} \frac{\partial S}{\partial x} + \frac{\partial^2 S}{\partial y^2} \tag{6-8}$$

The set of auxiliary conditions for the present problem becomes:

(a) $t < 0$: $u = v = T = S = Z = 0$ for $y \geq 0$.

(b) $t \geq 0$:

u, v, T, S, Z $\rightarrow 0$ at large distances from the source.

$y = 0$:

$T = 1 \qquad |x| \leq D/2$

$\frac{\partial T}{\partial y} = 0 \qquad |x| > D/2$

$$\tag{6-9}$$

$$u = v = S = 0$$

$$Z = -\frac{1}{x^2}\frac{\partial^2 S}{\partial y^2}$$

$$x = 0:$$

$$u = S = \frac{\partial v}{\partial x} = \frac{\partial T}{\partial x} = 0$$

$$Z = \frac{\partial^2 v}{\partial x^2} .$$

$$(6-9)$$

The set of equations to be solved consists of (6-4), (6-6), (6-8) and (6-5). These equations were solved numerically.

We seek steady state solutions for the problem posed above. In general, two basically different numerical approaches may be considered: the time-independent and the time-dependent formulations and solutions. The former approach requires the simultaneous solution of the steady state version of all the governing equations. This requires iterative procedure which may be complex and time-consuming (13, 35, 36). The latter approach is to introduce a disturbance (i.e., for our problem, temperature at the source) into the initially undisturbed region of interest at $t \geq 0$. The subsequent changes in the region of interest as the time increases will be described by the governing equations. The steady state solution, if any, will be that obtained at large time.

Various types of numberical flow calculations (for example, references 9, 34, 43, 46, 47, 48, 49, etc.) have shown that using a time-dependent numerical scheme to obtain a steady state solution is convenient. The time-dependent approach was used here.

FINITE DIFFERENCE SCHEME

Grid System

For an axially symmetric problem, calculations need be performed only over a radial plane containing the symmetry axis. The square mesh grid system for such numerical computation is described below:
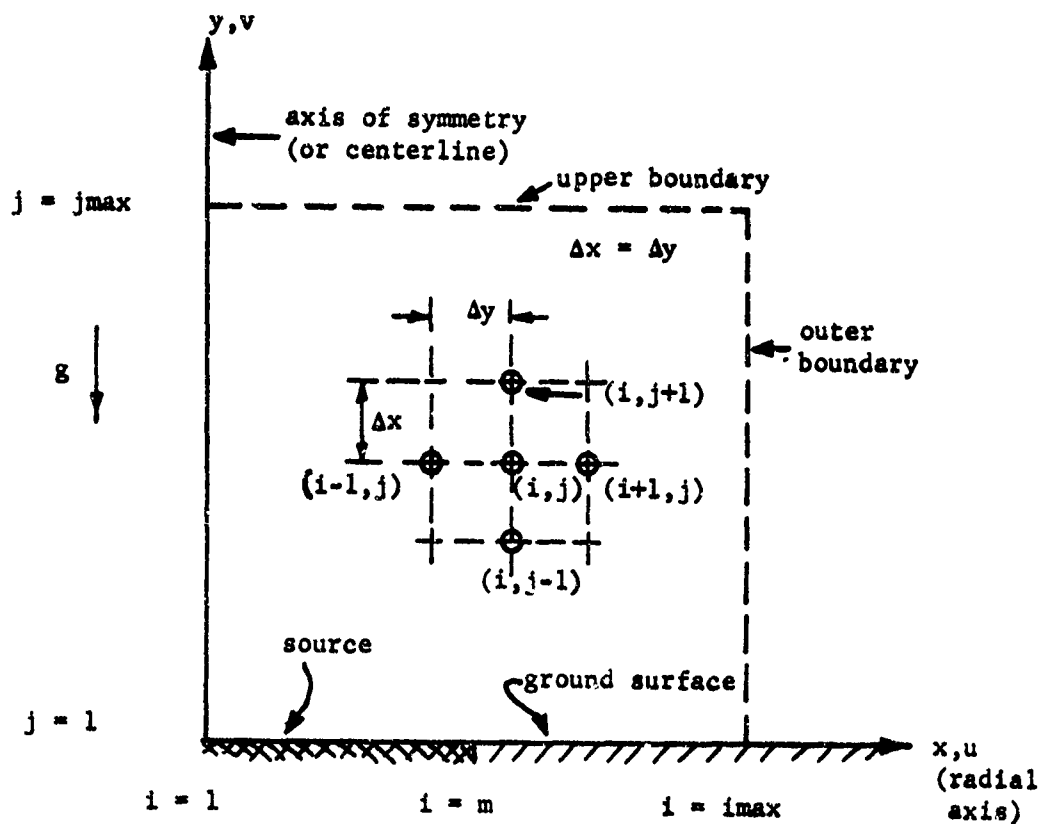
Henceforth, two subscripts (i,j) will be attached to each dependent variable (when necessary) for identification purposes. Thus $T_{1,j}$ refers to a dimensionless temperature on the line $x = 0$.

For identifying the particular size of array of nodal points and the relative size of the source, the following symbol will be used in the future discussions:

"imax x jmax, 1-m"

Here the first part specifies the array size and the second part means that the source occupies the region from i = 1 to i = m, or source size = (m-1)Δx.

Difference Forms

The derivatives in the differential equations to be solved will all be approximated by their difference analogs. Three difference forms (forward, backward, and central) will be used for the first derivatives and a single form will be used for the second derivatives. To illustrate, the space derivative for any function S(x, y, t) are given below:

(a) **First derivatives**

Forward difference

$$\left(\frac{\partial S}{\partial x}\right)_{i,j} = \frac{S_{i+1,j} - S_{i,j}}{\Delta x} \quad , \quad \left(\frac{\partial S}{\partial y}\right)_{i,j} = \frac{S_{i,j+1} - S_{i,j}}{\Delta y} \quad .$$

Backward difference

$$\left(\frac{\partial S}{\partial x}\right)_{i,j} = \frac{S_{i,j} - S_{i-1,j}}{\Delta x} \quad , \quad \left(\frac{\partial S}{\partial y}\right)_{i,j} = \frac{S_{i,j} - S_{i,j-1}}{\Delta y} \quad .$$

Central difference

$$\left(\frac{\partial S}{\partial x}\right)_{i,j} = \frac{S_{i+1,j} - S_{i-1,j}}{2\Delta x} \quad , \quad \left(\frac{\partial S}{\partial y}\right)_{i,j} = \frac{S_{i,j+1} - S_{i,j-1}}{2\Delta y} \quad .$$

(b) **Second derivatives**

$$\left(\frac{\partial^2 S}{\partial x^2}\right)_{i,j} = \frac{S_{i+1,j} - 2S_{i,j} + S_{i-1,j}}{\Delta x^2} \quad , \quad \left(\frac{\partial^2 S}{\partial y^2}\right)_{i,j} = \frac{S_{i,j+1} - 2S_{i,j} + S_{i,j-1}}{\Delta y^2} \quad .$$

Stability Criterion and the Difference Equations

Equations (6-4), (6-6), (6-8), and (6-5) are replaced by their difference analogs. Wilkes (9) has investigated this system of equations extensively for a free convection problem in a rectangular cavity with heated vertical walls. He used a differencing scheme (50) such that, for the convective terms on the left hand side of Equations (6-4) and (6-6), the forward difference form was used when the coefficient velocity was negative, and the backward difference form was used when the coefficient velocity was positive. The central difference form was used for all other terms. Based on a linear Fourier analysis the following stability criterion may be derived:

$$\Delta t \leq \left[\frac{|u_{max}|}{\Delta x} + \frac{|v_{max}|}{\Delta y} + \frac{2}{Pr\sqrt{Gr_T}} \left(\frac{1}{\Delta x^2} + \frac{1}{\Delta y^2} \right) \right]^{-1} \qquad (6-10)$$

Taking u as negative and v as positive, for illustrative purposes, the difference forms of Equations (6-4) and (6-6) are written as follows:

$$\left(\frac{\partial T}{\partial t} \right)_{i,j} = -u_{i,j} \frac{T_{i+1,j} - T_{i,j}}{\Delta x} - v_{i,j} \frac{T_{i,j} - T_{i,j-1}}{\Delta y}$$

$$+ \frac{1}{Pr\sqrt{Gr_T}} \left[\frac{T_{i+1,j} - 2T_{i,j} + T_{i-1,j}}{\Delta x^2} + \frac{T_{i+1,j} - T_{i-1,j}}{2x\Delta x} \right. \qquad (6-11)$$

$$\left. + \frac{T_{i,j+1} - 2T_{i,j} + T_{i,j-1}}{\Delta y^2} \right]$$

$$\left(\frac{\partial Z}{\partial t}\right)_{i,j} = - u_{i,j} \frac{Z_{i+1,j} - Z_{i,j}}{\Delta x} - v_{i,j} \frac{Z_{i,j} - Z_{i,j-1}}{\Delta y}$$

$$+ \frac{T_{i+1,j} - T_{i-1,j}}{2x\Delta x} + \frac{1}{\sqrt{Gr_T}} \left[\frac{Z_{i+1,j} - 2Z_{i,j} + Z_{i-1,j}}{\Delta x^2} \right. \qquad (6\text{-}12)$$

$$\left. + 3 \frac{Z_{i+1,j} - Z_{i-1,j}}{2x\Delta x} + \frac{Z_{i,j+1} - 2Z_{i,j} + Z_{i,j-1}}{\Delta y^2} \right]$$

Equation (6-8) may be written first as follows:

$$\frac{S_{i+1,j} - 2S_{i,j} + S_{i-1,j}}{\Delta x^2} - \frac{S_{i+1,j} - S_{i-1,j}}{2x\Delta x}$$

$$+ \frac{S_{i,j+1} - 2S_{i,j} + S_{i,j-1}}{\Delta y^2} = - x^2 Z_{i,j}$$

In the above equation, $S_{i,j}$ was solved by an iterative procedure using an over-relaxation scheme (51). Rearranging and introducing the over-relaxation parameter W, and $x = (i-1)\Delta x$, we have:

$$S_{i,j}^{n+1} = \frac{W}{2\left(1 + \frac{\Delta x^2}{\Delta y^2}\right)} \left[(x\Delta x)^2 Z_{i,j}' + \left(1 - \frac{1}{2(i-1)}\right) S_{i+1,j}^n \right.$$

$$\left. + \left(1 + \frac{1}{2(i-1)}\right) S_{i-1,j}^n + \frac{\Delta x^2}{\Delta y^2} \left(S_{i,j+1}^n + S_{i,j-1}^n\right) \right] + (1-W) S_{i,j}^n \qquad (6\text{-}13)$$

Here, the left hand side is the value of $S_{i,j}$ from the most recent iteration based on the established values of $S_{i,j}^n$, etc. from the previous iteration on the right hand side. Finally, from equation (6-5):

$$u_{i,j} = \frac{S_{i,j+1} - S_{i,j-1}}{2x\Delta y}$$

$$v_{i,j} = \frac{S_{i+1,j} - S_{i-1,j}}{2x\Delta x}$$

(6-14)

Boundary Conditions

The governing differential equations for this problem are of the elliptic type; the specification of conditions on all the boundaries is required. We define a natural boundary as one at which appropriate boundary conditions are obvious. The only natural and finite boundaries in this problem are the ground surface and the axis of symmetry. The others are at infinity. For numerical calculations, one is restricted to perform calculations in a finite domain of a feasible number of nodal points. To meet this restriction one may either map the semi-infinite space $y \geqq 0$, into a region defined between 0 and 1 or assume some approximate artificial boundaries. Mathematically it is possible to map the infinite domain into a finite one by a transformation such as the following pair:

$$\xi = \frac{C_1 x}{1 + C_1 x} , \quad x = \frac{1}{C_1} \frac{\xi}{1 - \xi}; \quad 0 \leqq x \leqq \infty, \quad 0 \leqq \xi \leqq 1.$$

(6-15)

$$\eta = \frac{C_2 y}{1 + C_2 y} , \quad y = \frac{1}{C_2} \frac{\eta}{1 - \eta} ; \quad 0 \leqq y \leqq \infty, \quad 0 \leqq \eta \leqq 1.$$

where C_1 and C_2 are constants which determine respectively the manner in which the x- and y-coordinate are to be shrunk.

Some attempts were made to use the transformed coordinate system as
described above. It was found that although the calculation seemed to
converge reasonably well and produce stationary results near the source,
it exhibited large oscillations at large distances from the source.
This is because of the singular behavior near $\xi = 1$ and $\eta = 1$ and the
associated unusually large truncation error due to the transformation
in these regions. Figure 34 is a plot of some numerical results using
the mapped coordinates for the case of $Gr_T = 7.4 \times 10^9$ for the different
stages of calculations. Although the Grashof number used in this
example is too large to be realistic in the physical sense, the plotted
results do show the large oscillations near infinity. Furthermore, it
took about 50% more computing time than when an ordinary physical
coordinate system was used. For these reasons the physical coordinate
system was used and non-natural boundaries defined where necessary.

Some reasonable boundary conditions on these non-natural boundaries
are constructed. Boundary conditions, with discussions where appropriate
are given below:

(a) <u>Source Plane</u> (j=1, y=0)

$$T_{i,1} = 1 \quad \text{for } x \leq D/2$$

$\left.\left(\frac{\partial T}{\partial y}\right)\right|_{i,1} = 0$ for $x > D/2$. Due to the inflow of air at ambient
temperature, this condition is nearly equivalent to $T = 0$.

$$u_{i,1} = v_{i,1} = 0$$

Since no flow is crossing the source plane, $y = 0$ is a stream surface. Thus we can set:

$$S_{i,1} = 0 .$$

By Equation (6-8):

$$Z_{i,1} = - \left(\frac{1}{x^2} \frac{\partial^2 S}{\partial y^2} \right)_{i,1}$$

Expand S near $y = 0$,

$$S_{i,2} \simeq S_{i,1} + \Delta y \left(\frac{\partial S}{\partial y} \right)_{i,1} + \frac{\Delta y^2}{2} \left(\frac{\partial^2 S}{\partial y^2} \right)_{i,1} + \frac{\Delta y^3}{6} \left(\frac{\partial^3 S}{\partial y^3} \right)_{i,1}$$

$$S_{i,3} \simeq S_{i,1} + 2\Delta y \left(\frac{\partial S}{\partial y} \right)_{i,1} + \frac{4\Delta y^2}{2} \left(\frac{\partial^2 S}{\partial y^2} \right)_{i,1} + \frac{8\Delta y^3}{6} \left(\frac{\partial^3 S}{\partial y^3} \right)_{i,1}$$

Noting that:

$$S_{i,1} = 0 \text{ and } (xu)_{i,1} = \left(\frac{\partial S}{\partial y} \right)_{i,1} = 0,$$

and eliminating $\left(\frac{\partial^3 S}{\partial y^3} \right)_{i,1}$ from the above two expansions, we get:

$$\left(\frac{\partial^2 S}{\partial y^2} \right)_{i,1} = \frac{8S_{i,2} - S_{i,3}}{2\Delta y^2}$$

Finally,

$$Z_{i,1} = - \frac{8S_{i,2} - S_{i,3}}{2x^2 \Delta y^2}$$

This expression (9) is accurate to the second order of Δy. This high accuracy is desirable in order to minimize the inaccuracy in u and v as calculated through Equation (6-5).

(b) <u>Axis of Symmetry</u> ($i=1$, $x=0$)

Based on the symmetry of the flow field and the requirement that field variables and their gradients be everywhere continuous,

the following conditions prevail:

$$u_{1,j} = S_{1,j} = \left(\frac{\partial v}{\partial x}\right)_{1,j} = \left(\frac{\partial T}{\partial x}\right)_{1,j} = 0.$$

From Equation (6-7):

$$z_{1,j} = \left(\frac{1}{x}\frac{\partial v}{\partial x}\right)_{1,j} = \left(\frac{\partial^2 v}{\partial x^2}\right)_{1,j} \quad \text{by l'Hospital's rule.}$$

(c) <u>Upper Boundary</u> ($j=j_{max}$, $y=y_{max}$)

Above the source, the variation of the flow variables decreases as the distance increases. Therefore, at some distance y_{max} above the source, we choose:

$$(T,\ S,\ Z)_{i,jmax} = (T,\ S,\ Z)_{i,jmax-1} \ .$$

As y increases, the flow enters into the convection plume region where the governing differential equations are of the parabolic type (4,7,38,52). Since the downstream conditions in a parabolic system only weakly affect the upstream region where the flow is described by elliptic type differential equations, we assume that this specification is satisfactory for the present problem. The validity of these conditions as indicated by numerical experiments will be discussed at a later time.

(d) <u>Outer Boundary</u> ($i=imax$, $x=x_{max}$)

Experience and analysis show that the influence of a heat source on the ambient region diminishes rapidly in an upstream direction. Therefore, for some suitably chosen value of imax, the location of the outer boundary across which the cold ambient air flows in, one may assign:

$$T_{imax,j} = 0 .$$

This condition simply means that the temperature reaches the ambient value on the outer boundary.

We have so far specified zero temperature gradients on the other three boundaries (except at the source). In a steady flow problem, the velocity field is established and the energy equation becomes linear. The specification of zero temperature gradient on this boundary would result in a trivial solution of $T = 1$ everywhere inside the boundaries. Furthermore, the temperature on the outer boundary can be higher than that of the ambient only by heat diffusion in an upstream direction. The characteristic diffusion length is proportional to $\left(\dfrac{\epsilon_H D}{U_c}\right)^{1/2}$. For our problem, this diffusion length is on the order of 10^{-1} foot. Therefore, at a distance not far from the plate, the air temperature would be very near the ambient value. Thus the choice of $T_{imax,j} = 0$ at sufficiently large value of imax (e.g., 1.5D) is well justified.

For velocity conditions at this boundary, we choose:

$$S_{imax,j} = S_{imax-1,j}$$

$$Z_{imax,j} = 0, \quad (j \neq 0).$$

The first of these implies $v = 0$ and $xu = $ constant from Equations (6-5) and (6-1). Since the largest velocity change takes place within the boundary layer near the ground surface, the remaining portion of the secondary flow region at this boundary may be considered approximately irrotational. Experience in numerical calculations shows that the

specification of $Z_{imax,j}$ is insensitive to the solution.

Following the basic scheme discussed in (a) above, the boundary values for the condition of vanishing first derivative were established by 3-point extrapolation scheme (53). Considering $T_{1,j}$ for example, a Taylor series expansion gives:

$$T_{2,j} \simeq T_{1,j} + \Delta x \left.\left(\frac{\partial T}{\partial x}\right)\right|_{1,j} + \frac{\Delta x^2}{2} \left.\left(\frac{\partial^2 T}{\partial x^2}\right)\right|_{1,j} + \frac{\Delta x^3}{6} \left.\left(\frac{\partial^3 T}{\partial x^3}\right)\right|_{1,j}$$

$$T_{3,j} \simeq T_{1,j} + 2\Delta x \left.\left(\frac{\partial T}{\partial x}\right)\right|_{1,j} + \frac{4\Delta x^2}{2} \left.\left(\frac{\partial^2 T}{\partial x^2}\right)\right|_{1,j} + \frac{8\Delta x^3}{6} \left.\left(\frac{\partial^3 T}{\partial x^3}\right)\right|_{1,j}$$

$$T_{4,j} \simeq T_{1,j} + 3\Delta x \left.\left(\frac{\partial T}{\partial x}\right)\right|_{1,j} + \frac{9\Delta x^2}{2} \left.\left(\frac{\partial^2 T}{\partial x^2}\right)\right|_{1,j} + \frac{27\Delta x^3}{6} \left.\left(\frac{\partial^3 T}{\partial x^3}\right)\right|_{1,j}$$

Since $\left.\left(\frac{\partial T}{\partial x}\right)\right|_{1,j} = 0$, the above equations may be solved simultaneously to give:

$$T_{1,j} = (18T_{2,j} - 9T_{3,j} + 2T_{4,j})/11.$$

Since the profiles of interest have no rapid changes in slope along $(1,j)$, this method was found to be very satisfactory. Similarly, $\left.\left(\frac{\partial^2 v}{\partial x^2}\right)\right|_{1,j}$ may be obtained for specifying $Z_{1,j}$. Since v is a quantity derived from the stream function S which in turn is obtained by solving Equation (6-8) from the known values of Z, it is more accurate to compute $Z_{1,j}$ directly by extrapolation from $Z_{2,j}$, $Z_{3,j}$, and $Z_{4,j}$. This scheme was used and was found to be both convenient and satisfactory.

It is realized that the conditions imposed on the outer and upper boundaries are somewhat artificial. Further justifications will be given when the domain of calculations is discussed.

Calculation Procedure

The governing equations were programmed in FORTRAN IV computer language and the calculations were done on an IBM 7094 digital computer. A block diagram describing the calculation procedure with discussions where necessary is given in Appendix F. The computer program listing is given in Appendix G.

VALIDATING OF NUMERICAL METHOD

The Diffusion Equation Limit

We attempt to validate the numerical results by going through a limiting procedure. As a preliminary test, the velocity field in the computer program was suppressed so that the numerical results would correspond to the solution for a diffusion problem with the same boundary conditions. This procedure was used also by Kane and Yang (36) in a similar calculation. An exact solution for this problem in closed form is given below (54):

$$T = \frac{2}{\pi} \sin^{-1}\left[\frac{2}{\sqrt{(x-1)^2 + y^2} + \sqrt{(x+1)^2 + y^2}}\right].$$

Three numerical results are presented in Figure 35. It is seen that the numerical results tend toward the exact solution as the domain of calculation is extended. The discrepancy between numerical and exact results is apparently due to the artificial boundary condition on the outer boundary. This is further illustrated for a case in which the lower portion of the outer boundary is insulated. The results are also shown in Figure 35. With respect to the thermal boundary condition,

the non-flow example is a severe test. An inflow of air at ambient

temperature tends to make the condition $T_{imax,j} = 0$ much more realistic.

As an additional test of the computer program, solutions were

obtained for various specified degrees of flow activity. As discussed

earlier, Gr_T is the governing parameter in this problem. The flow

velocities are large for large Gr_T. The numerical results for two

Grashof numbers (10^2 and 10^3) are presented in Figure 36. As must be

the case, the solution of the diffusion equation (the case of $Gr \rightarrow 0$)

is again approached as the Grashof number decreases.[*] At large Gr_T, the

region where the temperature differs significantly from the ambient

value is squeezed toward the centerline. This fact is in agreement

with experimental evidence (Chapter IV) and theory (5,38). It is also

indicative of the unimportance of the temperature specification on the

outer boundary as the Grashof number increases. We are interested in

the Grashof number in the range around 10^5.

Effects of the Domain of Calculation

The required computing time for obtaining a converged solution for

a given problem depends on the size of the array of mesh points.

Numerical experiments were carried out to test the minimum array size

---

[*]Kane and Yang (36) studied the laminar free convection problem
due to a heated horizontal disk in a full space for very small
Gr (<100) and found that their solutions tend to coincide with
the diffusion equation solution as Gr decreases, as is true
with the present solution. Direct comparison of these results
was not made due to difference in geometrical configurations.

which would produce reasonable results for the region of interest.
Calculations were made for the case of $Gr_T = 10^4$ with a source radius
of $4\Delta x$. Figures 37 and 38 show, respectively, the effects of vertical
extent and horizontal extent of calculation on the numerical results.
It only the region defined by $x \leq 1$, $y \leq 1$ is of concern, these figures
show no appreciable difference on the numerical results when the source
radius is $4\Delta x$ and array size is increased beyond 15×17. For this
reason the "15×17, 1-5" (see p. 61 for explanation of this identification)
array was used for further calculations.

Effect of Mesh Spacing

The truncation error for the present system of equations is on the
order of $K_1 \Delta t + K_2 \Delta x$ where K_1 and K_2 are positive constants depending
on the dependent variables T and Z. By making either Δt or Δx or both
small the accuracy of the computed results may be improved. Since we
are interested in the steady state solution, the above dependence shows
that reducing Δx is an effective method of improving accuracy. A brief
investigation of the effects of Δx on the numerical results is described
below.

Calculations were made for $Gr_T = 10^4$ and 10^5 by subdividing the
mesh spacing in steps; the converged solution for the "15×17, 1-5"
grid system was obtained first. This first solution was then used as
the input for a new system with a mesh spacing equal to one-half that
of the first one, etc. In this fashion, the mesh spacing could be

reduced to a reasonably small value with a reasonable amount of computing time. A summary of the computing time for various grid systems is given in Appendix F.

Figure 39 shows the centerline temperature distribution for $Gr_T = 10^5$ for three values of Δx (3", 1.5", 0.75"). A nearly linear variation for T with respect to Δx is shown in this figure. The line for $\Delta x = 0$ was obtained by constructing a smooth curve for T(y) versus Δx on a sheet of graph paper and reading the intersecting point of this curve and the line $\Delta x = 0$.

Heat Transfer

The mathematical formulation for our numerical calculations is essentially that for a laminar flow case. Therefore, it is well to use selected laminar flow results to further check the correctness of our numerical scheme. Letting $\Delta\theta$ be the difference between the mean plate temperature and that of the ambient, we have:

$$h\Delta\theta = -k \frac{\partial\theta}{\partial Y}$$

where h, k, θ and Y are, respectively, the average heat transfer coefficient, thermal conductivity, temperature and distance from the source surface. If we define, as before, $T = (\theta - \theta_\infty)/\Delta\theta$, $y = Y/D$ and substituting in the above expression, we get:

$$h\Delta\theta = -k \frac{\Delta\theta}{D} \frac{\partial T}{\partial y} = -k \frac{\Delta\theta}{D} T_y$$

or,

$$\frac{hD}{k} = Nu = -T_y$$

where T_y is the dimensionless mean temperature gradient at the source surface. Thus, the magnitude of the dimensionless mean temperature gradient is actually the Nusselt number. Free convection heat transfer is usually correlated in the following form:

$$Nu = C \cdot Gr^n \qquad \text{or} \qquad -T_y = C \cdot Gr^B$$

For laminar flow n = 0.25 (e.g., reference 27). This will be used as our basis for comparison.

Calculations were made for a range of Gr_T using the "15 x 17, 1-5" grid system. The variation of T_y with Gr_T is shown in Figure 40. Since large Gr_T also means large heat transfer, the value of T_y as shown in Figure 40 increases with Gr_T as expected but the value of n was found to be 0.11. The effect of mesh spacing on T_y is shown in Figure 41. It is clear that there is an almost linear variation of T_y with respect to Δx. If the values of $(T_y)_{\Delta x = 0}$ (see Figure 41) are used, n = 0.24, C = 0.51 may be calculated. This value of n agrees well with values reported in the literature. No value of C for a horizontal plate (C = 0.36 for vertical plate) has been reported in the literature, but the present result appears to be good to within a proportionality constant. For turbulent free convection n = 1/3, therefore, some discrepancy between numerical results and experimental data would be expected.

NUMERICAL RESULTS

Velocity and Temperature Profiles

Based on the numerical results for three mesh spacings and the graphical extrapolation method described above, the temperature and velocity fields for $Gr_T = 10^4$ and 10^5 extrapolated to $\Delta x = 0$ were obtained. These results are shown in Figures 42 and 43. As expected, the indraft velocity is large near the ground level and the maximum value of $-u$ occurs always within the plate radius. The outer edges of the velocity and temperature profiles are more constricted toward the centerline for large Gr_T than small Gr_T.

Indraft Calculations in the Region near the Ground $(1 < j < 2)$

The indraft velocity near the ground is one of the most important features of the flow field. Measurements show that the indraft is largest near the ground and decreases rapidly as the distance from the ground increases (Figure 29). Due to this boundary layer behavior[*] near the ground, no feasible mesh spacing for numerical calculations (e.g., D/16) is fine enough for predicting the detail in this region. In order to obtain a complete flow field description, the present method must be supplemented by appropriate auxiliary calculations.

If we use the numerical results obtained with a reasonably coarse mesh spacing as an indication of the outer flow field, this indraft velocity may be calculated approximately by an integral method.

---

[*]Here we refer to the condition that only the velocity gradient normal to the plate is significant.

Consider the control volume described below:
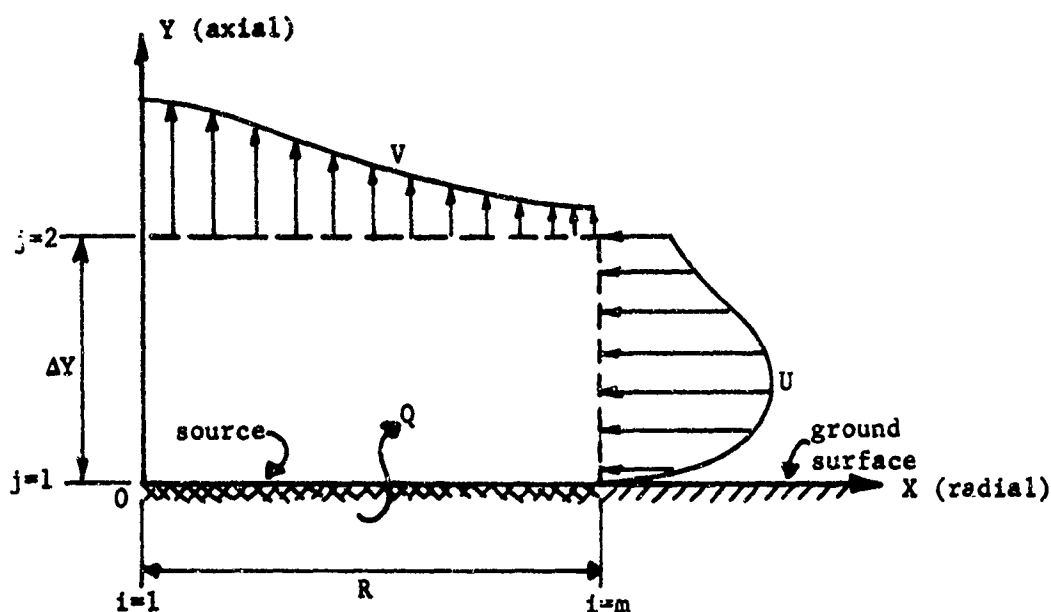
By the principle of conservation of energy and using the perfect gas law $\rho\theta = \frac{P}{\mathcal{R}} =$ constant, the following relation in dimensionless form may be obtained for the control volume:[*]

$$\int_0^{\Delta y} u\,dy = Q \qquad (6\text{-}16)$$

where

$$Q = \frac{1}{r}\int_0^r v x\,dx - \frac{q\mathcal{R}}{8rC_pU_cP}$$

and q, r, C_p, P and $\mathcal{R}$ are, respectively, the average heat flux, dimensionless radius (r = R/D), specific heat at constant pressure, pressure and gas constant. In this equation Q may be regarded as a known quantity

---

[*]The conductive heat transfer term is neglected due to the small local temperature gradients. The kinetic and potential energy terms are very small and are also neglected.

in which the integral term may be evaluated from numerical results and the last term may be obtained from experimental heat transfer data. The function u(y) is found to be such that the equality of Equation (6-16) holds.

The numerical results obtained with Δx extrapolated to zero will be used in the calculations. The function u(y) for the interval $0 \leq y \leq \Delta y$ will be determined based on as much known information as possible. From numerical results, the end values $u_{m,1}$ and $u_{m,2}$ are fixed. For a better approximation, $\left(\dfrac{\partial u}{\partial y}\right)_{m,2}$ is also to be satisfied. This may be computed from $u_{m,j}$ in a fashion similar to that given in the discussion of boundary conditions. The resulting equation is:

$$\left(\frac{\partial u}{\partial y}\right)_{m,2} = -\frac{1}{6\Delta y} (11u_{m,2} - 18u_{m,3} + 9u_{m,4} - 2u_{m,5})$$

In the secondary flow region, because the velocities are small and the flow is in a direction more or less parallel to the plate surface, we assume that the boundary layer equation for flows with negligible pressure gradient is applicable in the neighborhood of (m,1). This leads to the requirement of vanishing $\left(\dfrac{\partial^2 u}{\partial y^2}\right)_{m,1}$ (reference 45). Considering a fourth order polynomial in y with vanishing u and its second derivative at $y = 0$, the general form of the polynomial may be written as:

$$u(y) = by + dy^3 + ey^4 . \tag{6-17}$$

The coefficients b, d, and e may be determined from the known values of $u_{m,2}$, $\left(\dfrac{\partial u}{\partial y}\right)_{m,2}$, and Q. An equation similar to (6-16) may be obtained from the principle of conservation of mass. This may be used to chec' the results of Equation (6-16).

The calculated results for the case of θ_p = 520°F is shown in
Figure 44. A discussion will be given at the end of Chapter VII.

Equations (7-1) and (7-2) may then be used to solve for $\Delta\theta_T$ and ϵ_M in terms of Gr_T, T_y and q. The following relations are obtained:

$$\Delta\theta_T = \left[\frac{q \, Pr}{(\rho C_p)_\infty (-T_y)}\right]^{2/3} \left[\frac{Gr_T}{g\beta D}\right]^{1/3} \tag{7-3}$$

$$\epsilon_M = \left[\frac{g\beta \, Pr \, q \, D^4}{(\rho C_p)_\infty (-T_y) Gr_T}\right]^{1/3} \tag{7-4}$$

In the numerical calculations, T_y was obtained as a function of Gr_T (Figure 40). Equations (7-3) and (7-4) show that if q is given, $\Delta\theta_T$ and ϵ_M become functions only of Gr_T.

COMPARISONS

Substituting the experimental value of q into Equation (7-3), the values of $\Delta\theta_T$, and hence U_c may be calculated for a number of Gr_T's. The $\Delta\theta_T$ and U_c thus obtained will be used for converting the dimensionless numerical results into physical quantities. In this manner, the experimental and numerical centerline temperatures were first compared to obtain the suitable values of Gr_T. Figure 17 shows that the numberical results for $Gr_T = 40000$ and 25000 could fit the experimental data reasonably well for $\theta_p = 520^\circ F$ and $410^\circ F$, respectively. The values of T_y, $\Delta\theta_T$, U_c and ϵ_M corresponding to these Gr_T's are tabulated in Table 9. It is seen that the experimental and numerical values of ϵ_M are in good agreement.

VII. COMPARISON OF NUMERICAL AND EXPERIMENTAL RESULTS

GENERAL DISCUSSIONS

In the discussion in the early chapters, we have shown that, in
the region sufficiently close to the plate surface ($< 0.02"$, say), the
local air temperature can be calculated based on molecular conduction
(Figures 21 and 22). Away from this thin region, the flow is quite
turbulent (Figure 4) and the flow field, therefore, cannot be suitably
described by the molecular properties (i.e., Gr). It is not a simple
task to attempt to describe the detailed flow behavior in the neighbor-
hood of the source by a single overall transport formulation.

In order to gain some insight to the basic features of the
numerical results using the turbulent Grashof number as the governing
parameter, a comparison is made between the experimental data and the
numerical results presented in Chapters IV, V and VI, respectively.

The turbulent Grashof number is defined as:

$$Gr_T = \frac{g\beta\Delta\theta_T D^3}{\epsilon_M^2} \tag{7-1}$$

where $\Delta\theta_T$ and ϵ_M are, respectively, the temperature difference and eddy
diffusivity characterizing the flow field. The mean heat flux may be
expressed in terms of a mean temperature gradient T_y through the
definition of a thermal diffusivity as follows:

$$q = (\rho C_p)_\infty \, \epsilon_H \, \overline{\frac{\partial\theta}{\partial Y}} = -(\rho C_p)_\infty \, \frac{\epsilon_M}{Pr} \frac{\Delta\theta_T}{D} T_y \tag{7-2}$$

Table 9. Comparisons of experimental & numerical results.

Experimental Data			Numerical Results ($\Delta x \rightarrow 0$)				
θ_p °F	q B/hr-ft^2	ϵ_M ft^2/sec	Gr_T	$-T_y$	$\Delta\theta_T$ °F	U_c fps	ϵ_M ft^2/sec
520	800	.031*	40000	6.27	86	3.2	.0324
410	560	---	25000	5.64	61	2.8	.0348

*Average value of $\epsilon_H P_r$ in Table 3.

Having established the values of $\Delta\theta_T$, the comparisons between the horizontal temperature profiles and updraft velocities are then compared. These are shown in Figures 18, 19 and 45. The numerical results show, in general, more gradual profiles than do the experimental data. Only qualitative agreement is seen. This is due to the non-realistic constant eddy diffusivity model used in the numerical calculations. Numerical results given in Figures 18 and 19 show that the flow and temperature fields are more constricted about the centerline for larger Gr_T.

In reality, the turbulence level decreases as the radius and the distance from the plate increases. At some distance outside the primary flow region, the flow field (the secondary flow due to entrainment) is laminar, and the description of the flow behavior in this region would be determined by the molecular properties (i.e., by Gr). There must exist some sort of transition of the governing transport mechanisms. It appears possible to improve the numerical results by incorporating a spatial variation of Gr_T (i.e., the eddy diffusivity) in the numerical

82

formulation such that Gr_T would increase with the radius and the elevation until it is approached to the ambient value Gr. This, however, would require an extensive numerical experimentation. Because of the large amount of computer time which would be required, this procedure was not pursued.

Figure 44 shows the calculated indraft profile for the case $\theta_p = 520^oF$. The results show that the calculated indraft velocity is consistently larger than the experimental data. The percentage discrepancy is large especially at large elevations ($\sim 90\%$). Since all measurements of indraft velocity were in the laminar, secondary flow region, it is conceivable that this discrepancy was due to the use of too large a value of U_c for nondimensionalization, or it may have been due to the inability of describing the whole flow field by means of a single transport mechanism.

VIII. CONCLUSIONS

Based on the findings of this research the following conclusions are drawn for the turbulent free convection field above a heated, horizontal, circular flat plate:

EXPERIMENTAL

1. The turbulence in the primary flow region (Figure 4) is characterized by low frequency ($\sim$10 cps) and large amplitude ($\sim$1 fps) turbulent fluctuations. The fluctuating velocities are the largest on the centerline and decay as the radius increases.

2. Because of this large turbulence, the conventional hot-wire technique for turbulence measurements on linearized theory was impossible to apply.

3. There exists a thermal boundary layer, within approximately 0.02" of the plate surface, in which the major part of the overall temperature drop takes place. The temperature distribution in this region may be calculated based on molecular conduction.

4. The vertical temperature gradient and hence the local heat flux at the plate surface increases significantly with the radius. Data show that the temperature gradient at plate edge is approximately twice the value at centerline.

5. The region of significant deviation from ambient temperature and velocity is constricted toward the centerline.

6. The induced indraft is large at low elevation (~0.5 fps) and is largest within an inch of the ground. This indraft is on the same order of magnitude as U_c (a characteristic velocity directly obtainable from a dynamic force balance).

7. Hot-wire method has been developed which is suitable for this type of velocity and turbulence measurements when the information contained in the various moments of the hot-wire voltage output is used. Details of the data can be more clearly shown as the order of the moment increases, being a more sensitive measure of the phenomena. However, due to the amplification and accumulation of errors during the process of taking higher moments, the proper interpretation of the high moment data may be a difficult task (e.g., the problem of separating signal voltage and background noise may be an analogy).

8. Numerical simulation of the the hot-wire voltage output is shown to be a useful tool for the actual hot-wire data reduction.

9. The eddy diffusivity can be estimated either from the energy equation using basically temperature data or from the product $\sigma_u^2 \tau$ of the turbulence velocity and the characteristic time data. The agreement of available data is within 15% for low elevation points and up to 60% for higher elevations.

NUMERICAL CALCULATIONS

1. A numerical calculation method using a time advancing, explicit differencing scheme for computing essentially the laminar free convection

field above a heated, horizontal disk has been developed and validated. The calculated temperature gradient at the plate surface increases with the radius (also an observed experimental fact). The numerical heat transfer results obtained agree with experimental heat transfer correlation ($Nu \propto Ra^{1/4}$) to within 4% of the value of the exponent.

2. The centerline temperature data were compared with numerical results and the best fit was used to establish the appropriate values of Gr_T and $\Delta\phi_T$, the turbulent Grashof number and temperature rise characterizing the flow. The match between calculation and experimental data is most successful when Gr_T is on the order of 10^5 (Grashof number Gr based on molecular viscosity is on the order of 10^{10} for this work).

3. For describing the gross behavior of the flow field, the intense variation of eddy diffusivity in the boundary layer region is neglected by the specification of a characteristic temperature rise $\Delta\phi_T$ at the plate surface. This temperature rise is determined also on the basis of plate heat flux and eddy diffusivity. Only qualitative agreement can be obtained between the numerical and the experimental data. Clearly, the constant eddy diffusivity model is not suitable for describing the complete flow field.
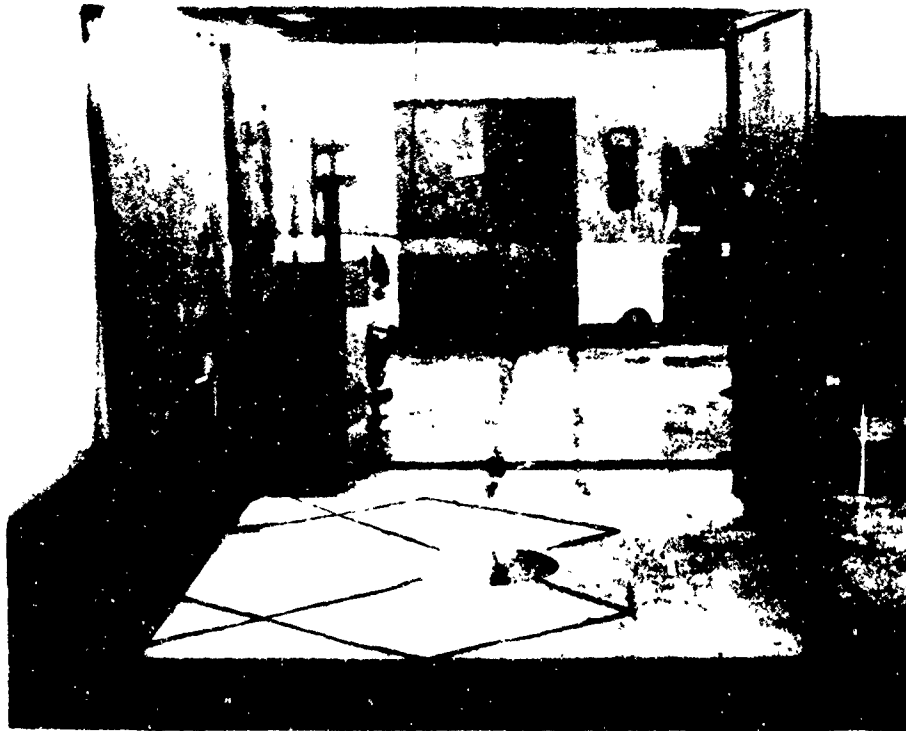
(a) Overall arrangement
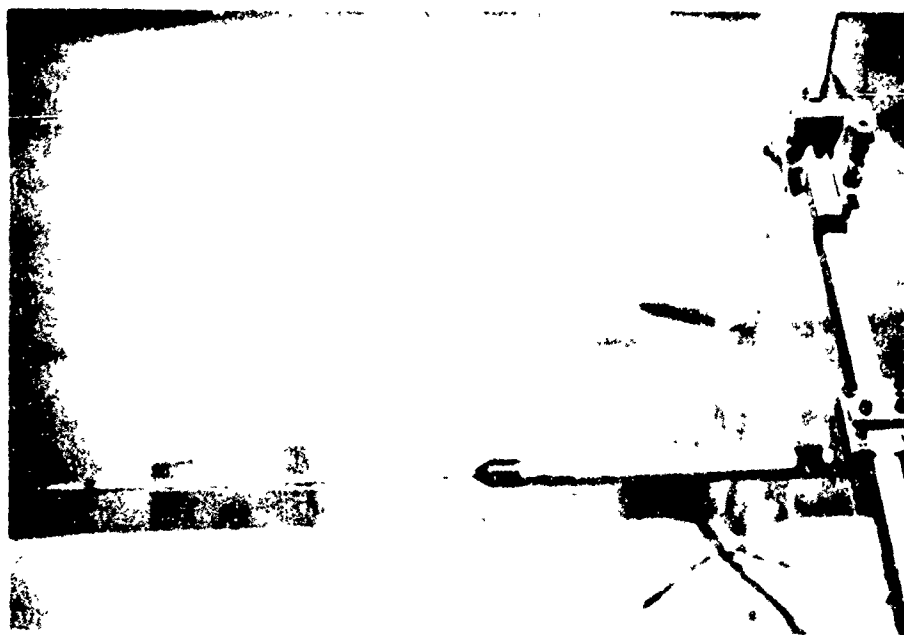
(b) Hot-wire traversing mechanism
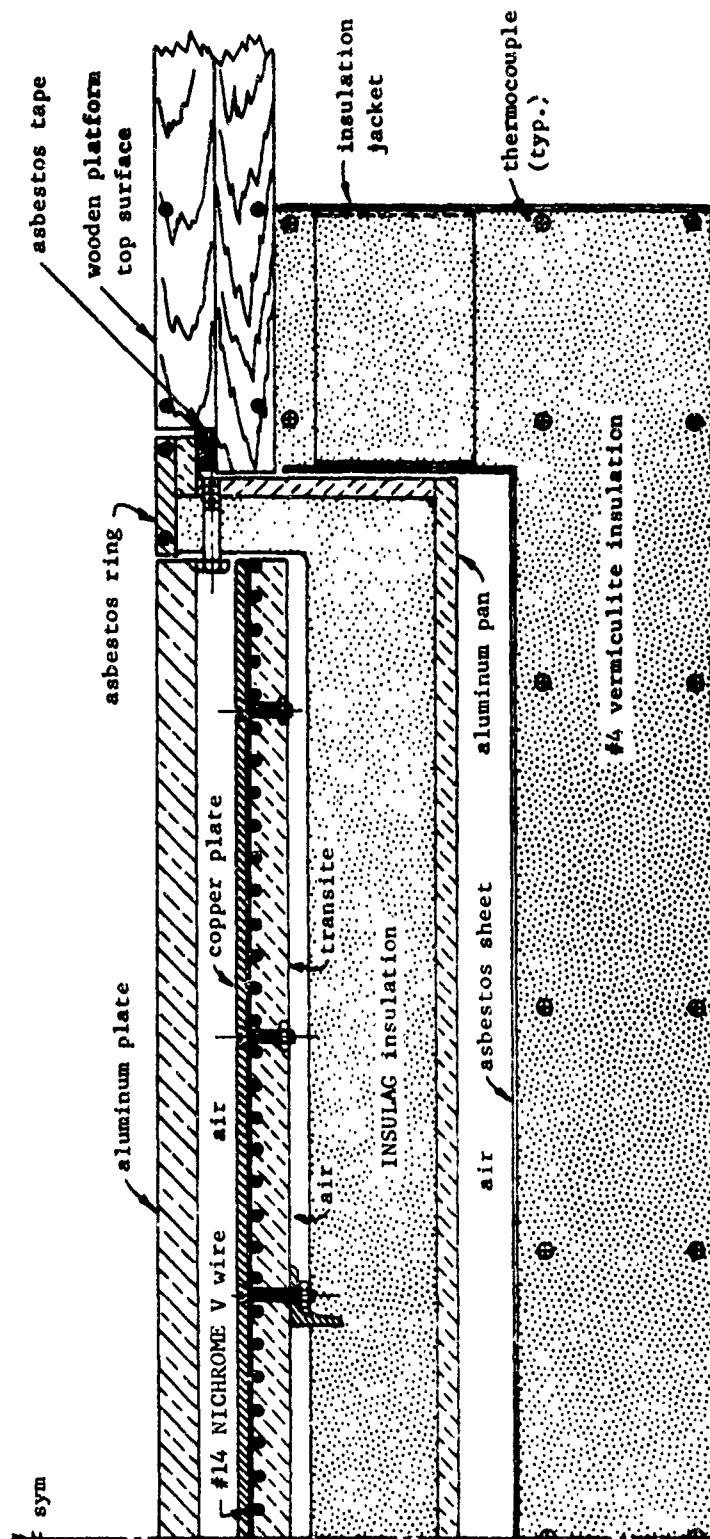
Figure 1. Experimental apparatus

87

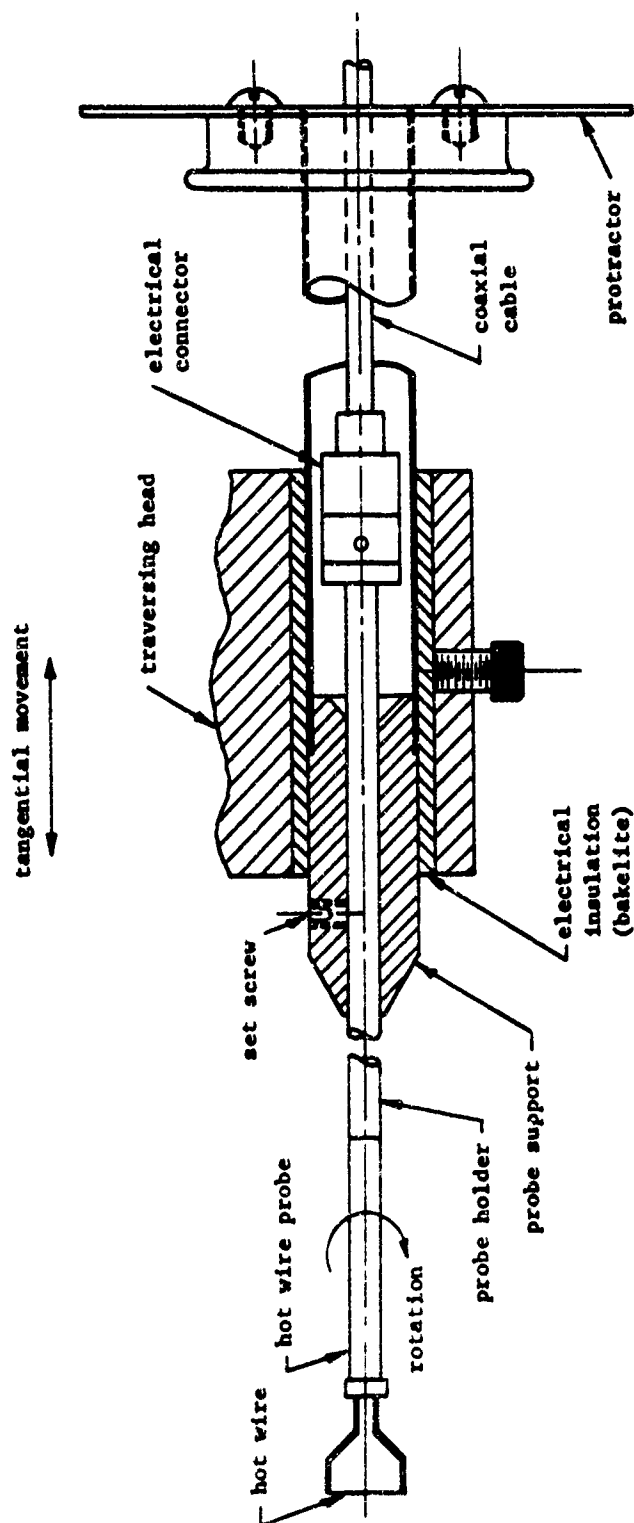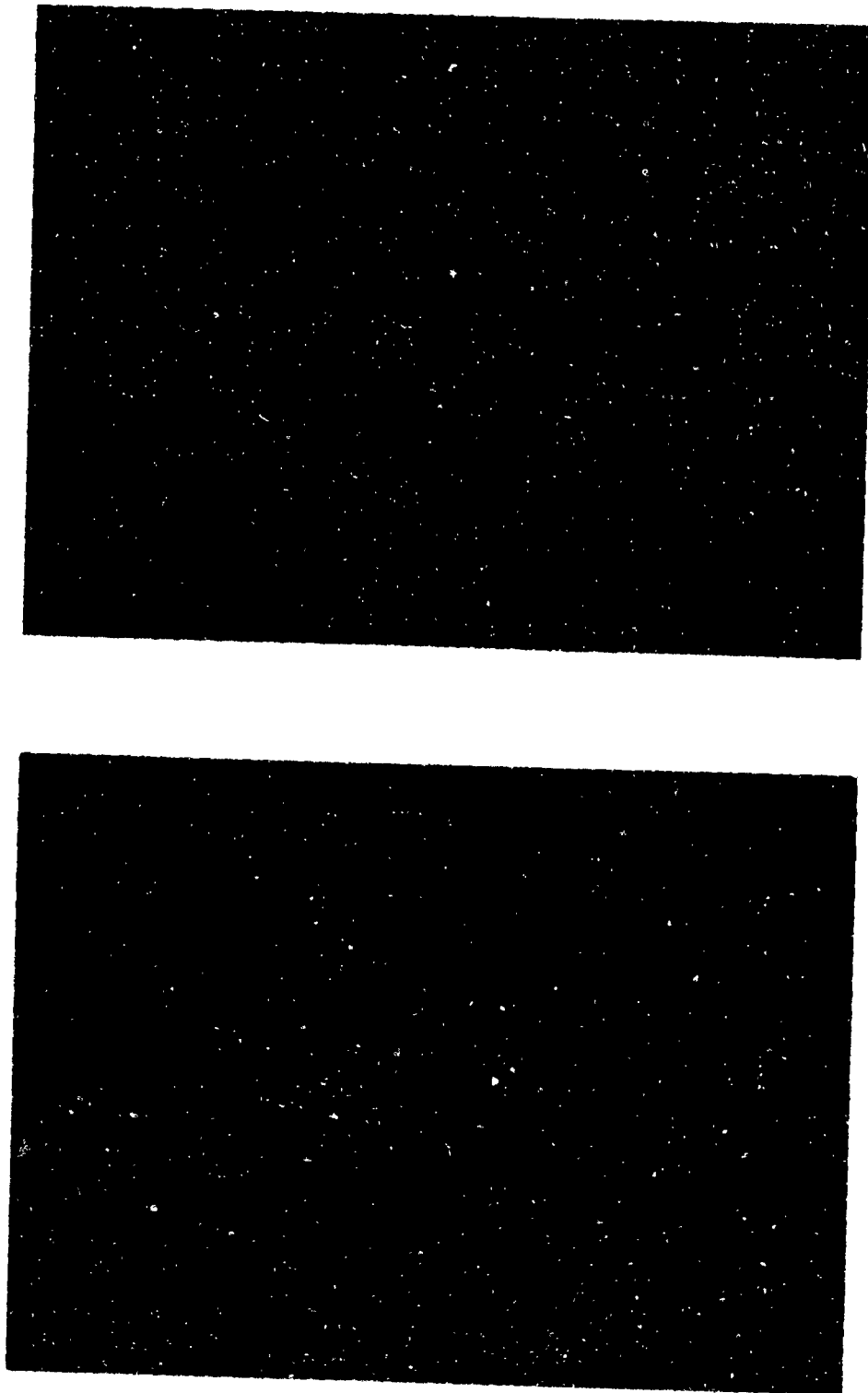Figure 2. Heater installation (approximately half actual size).

The following labels appear in the figure:

- asbestos tape
- wooden platform top surface
- insulation jacket
- thermocouple (typ.)
- asbestos ring
- aluminum plate
- copper plate
- air
- #14 NICHROME V wire
- transite
- air
- INSULAG insulation
- aluminum pan
- air
- asbestos sheet
- #4 vermiculite insulation
- ℄ sym

88

Figure 3. Hot wire probe mounting (approximately to scale).

tangential movement

electrical
connector

coaxial
cable

protractor

traversing head

electrical
insulation
(bakelite)

set screw

hot wire probe

hot wire

rotation

probe holder

probe support

(a) $\theta_p = 520^\circ F$ (b) $\theta_p = 410^\circ F$

Figure 4.   Shadow pictures.

Figure 5. Whirling column (θ_p = 520°F).

#50 bottom drilled holes,
#24 A.W.G. Cu-constantan
thermocouple, welded
junction first inserted
in place then filled
the void space with
liquid aluminum.

aluminum alloy
2024T351
QQ A 250/4
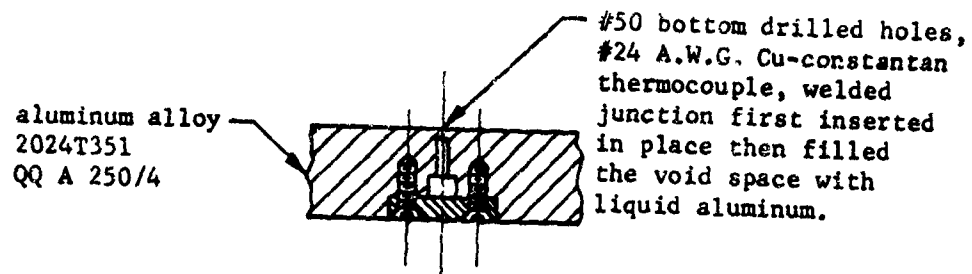
Typical Thermocouple
Installation
actual size
A - A

This side
facing down
in installation

A

A

4" (typ.)

2"

4"

1"

3"

24" dia.
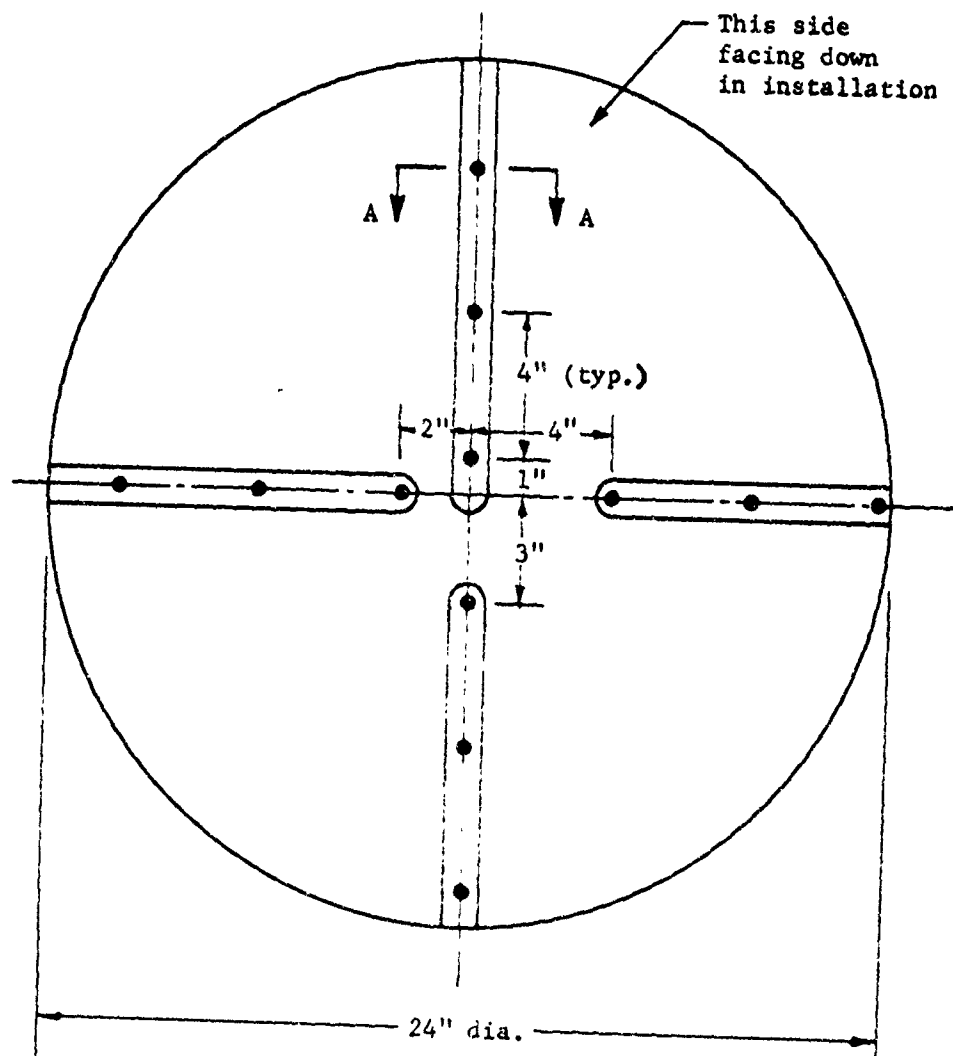
Figure 6. Thermocouple installation in the heated aluminum plate.
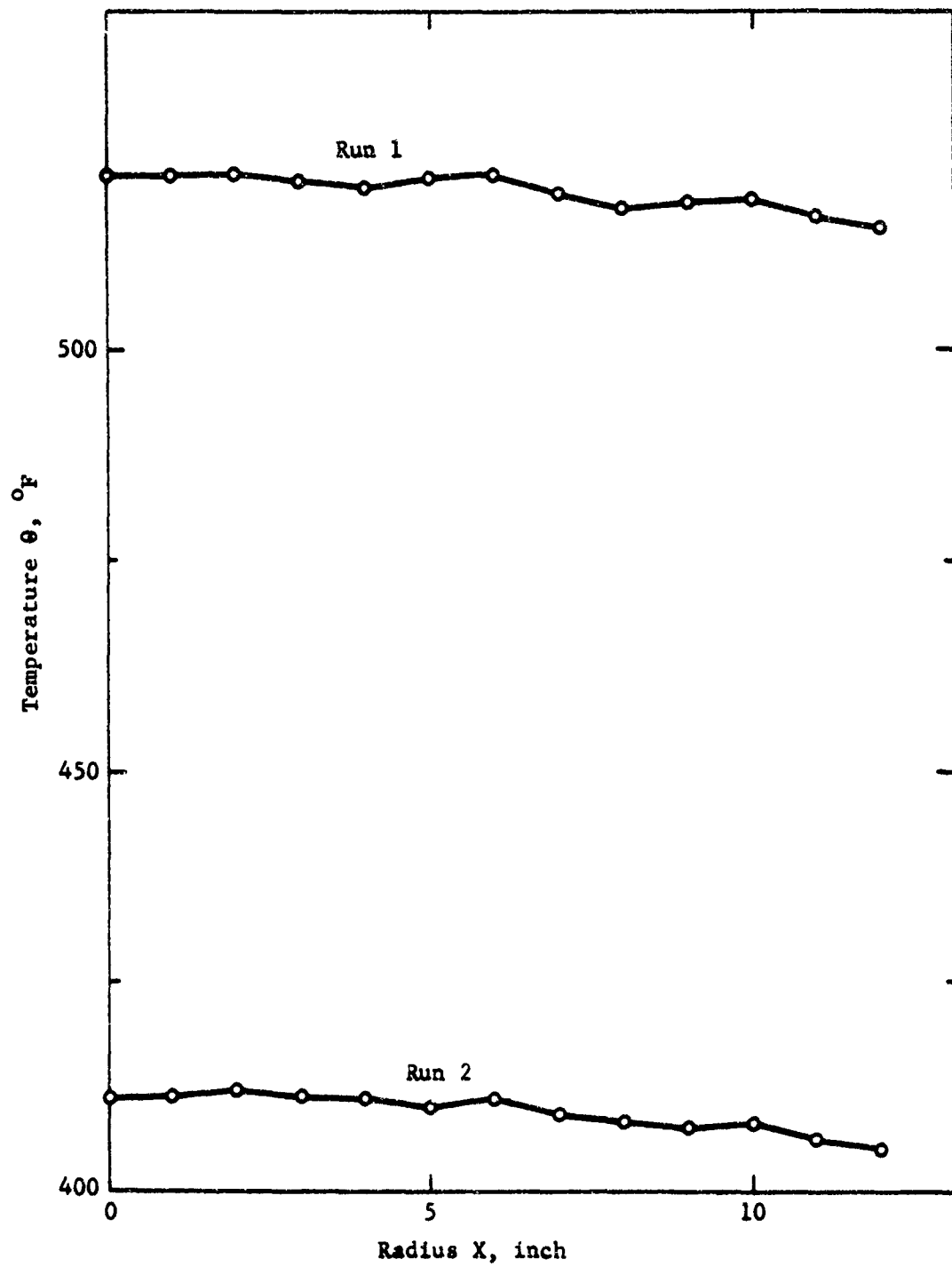
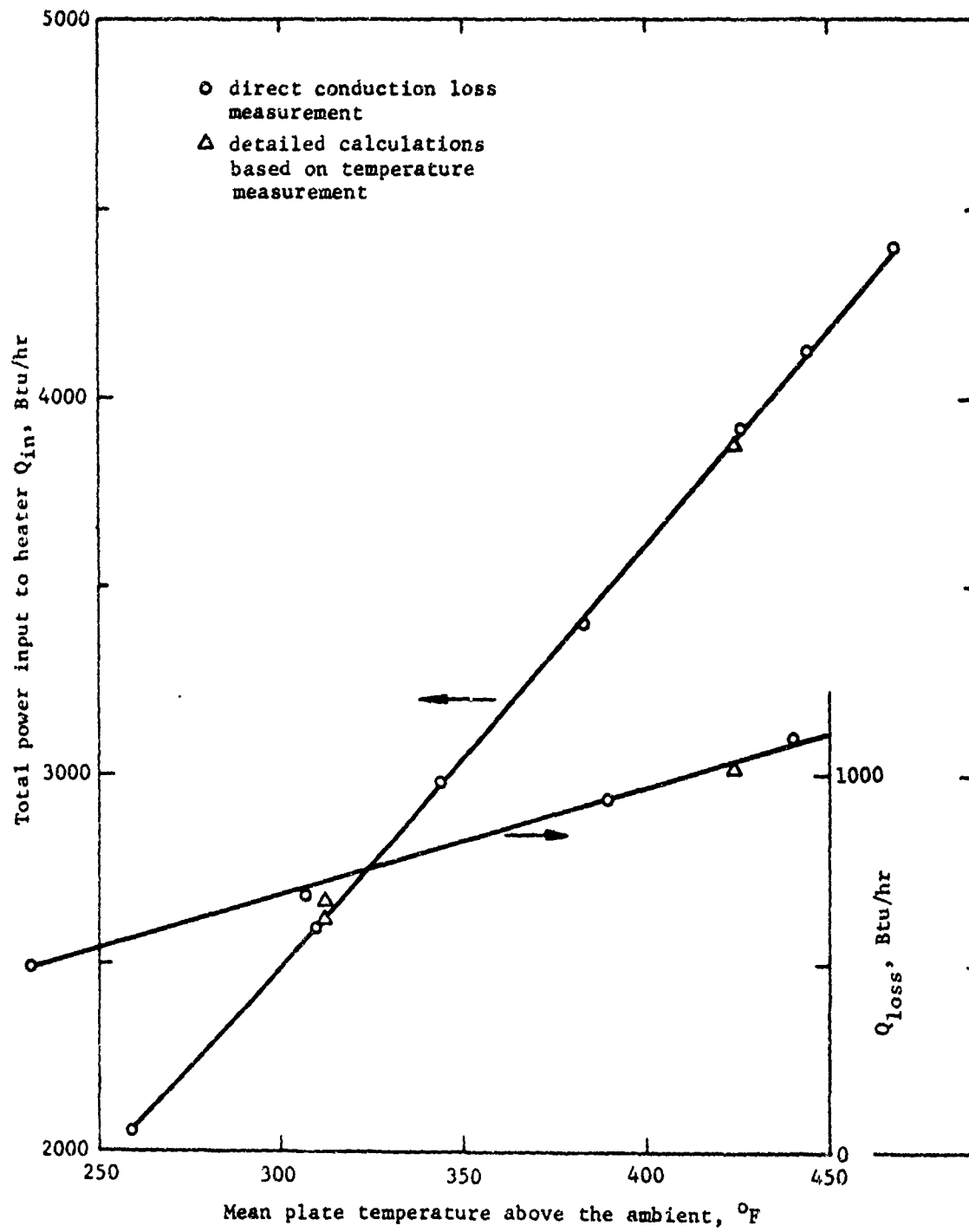Figure 7. Temperature distribution in the heated aluminum plate.
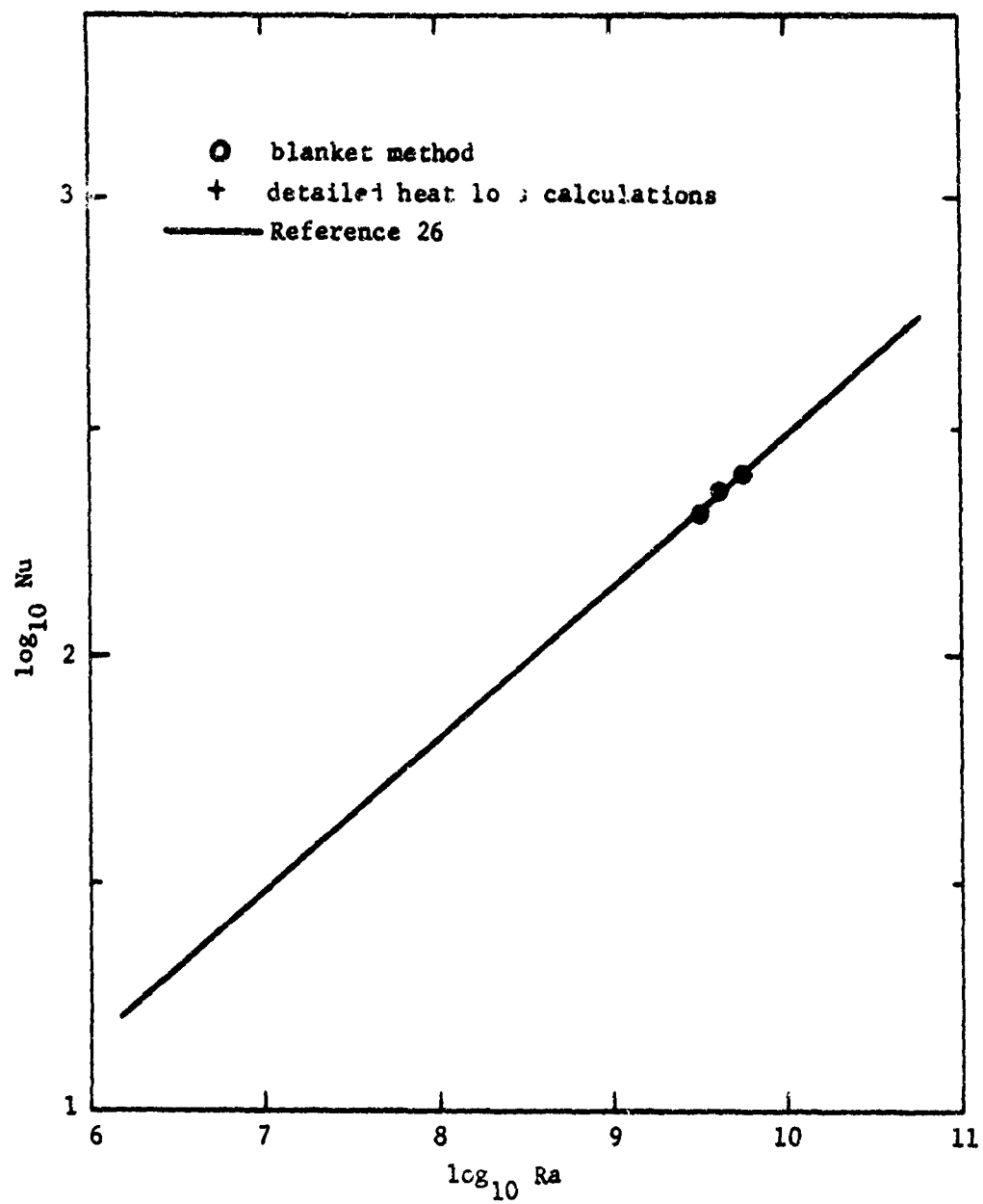
Figure 8. Heater performance.

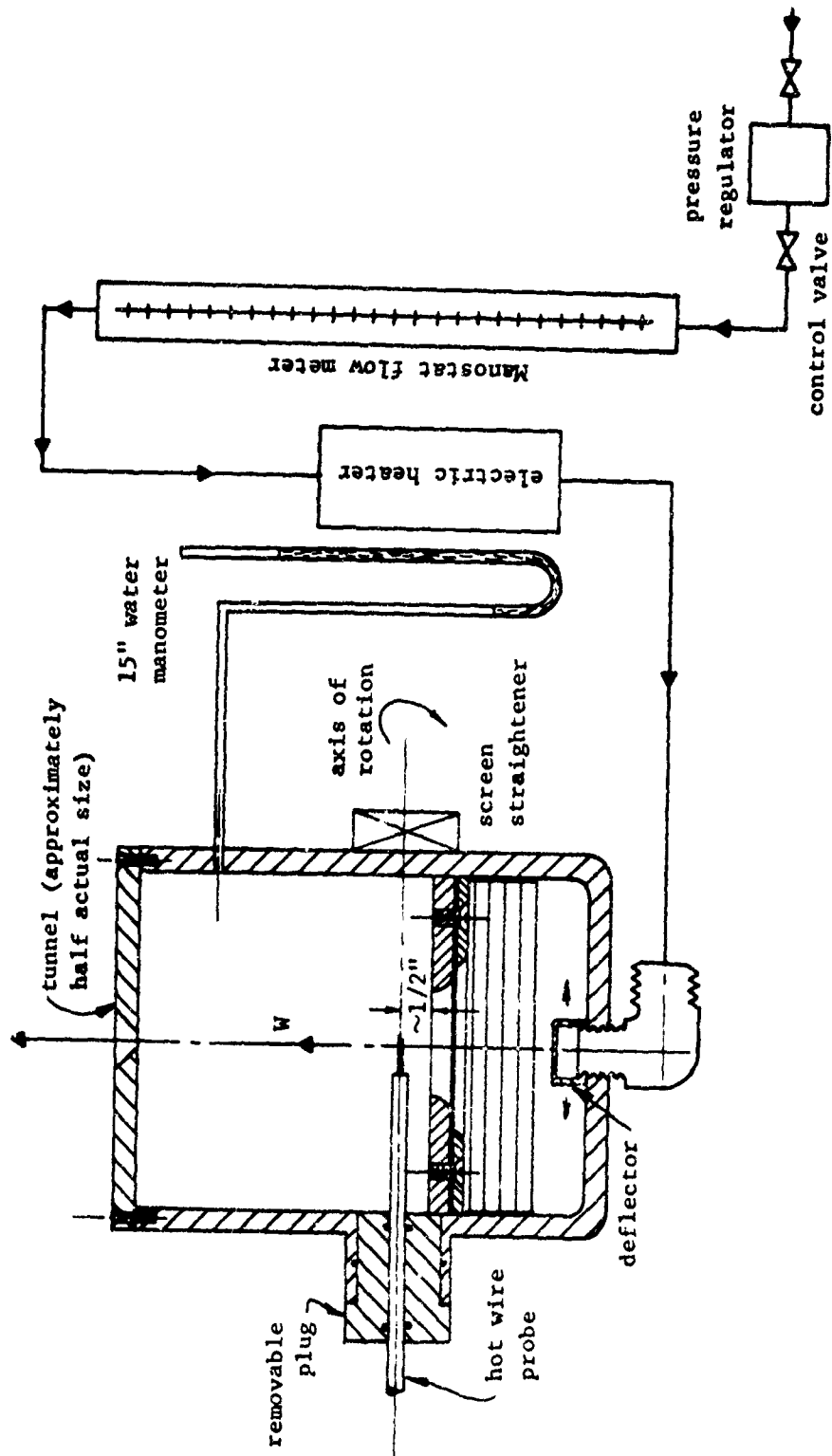Figure 9. Heat transfer correlation.

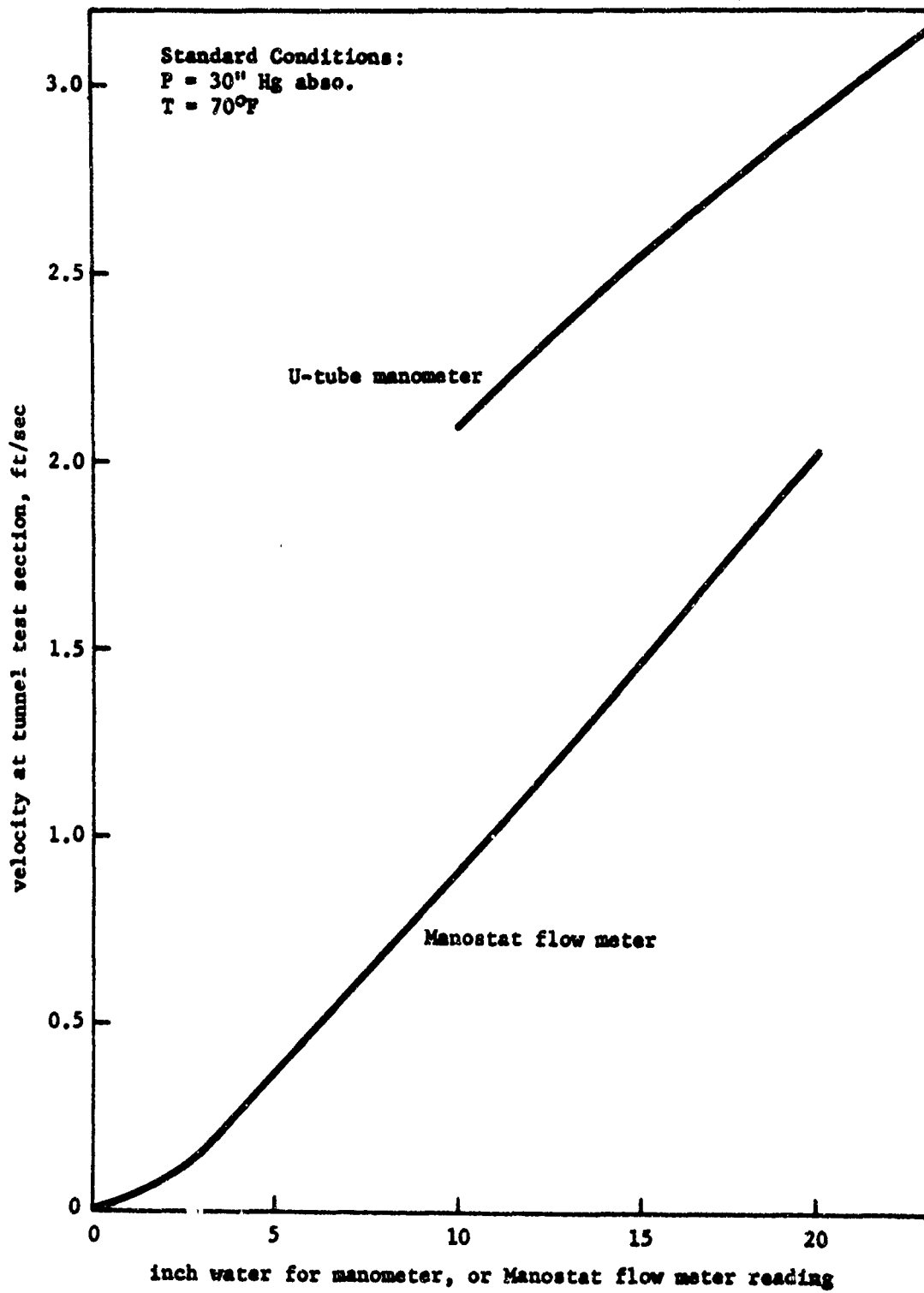Figure 10. Hot wire calibration tunnel – schematic.
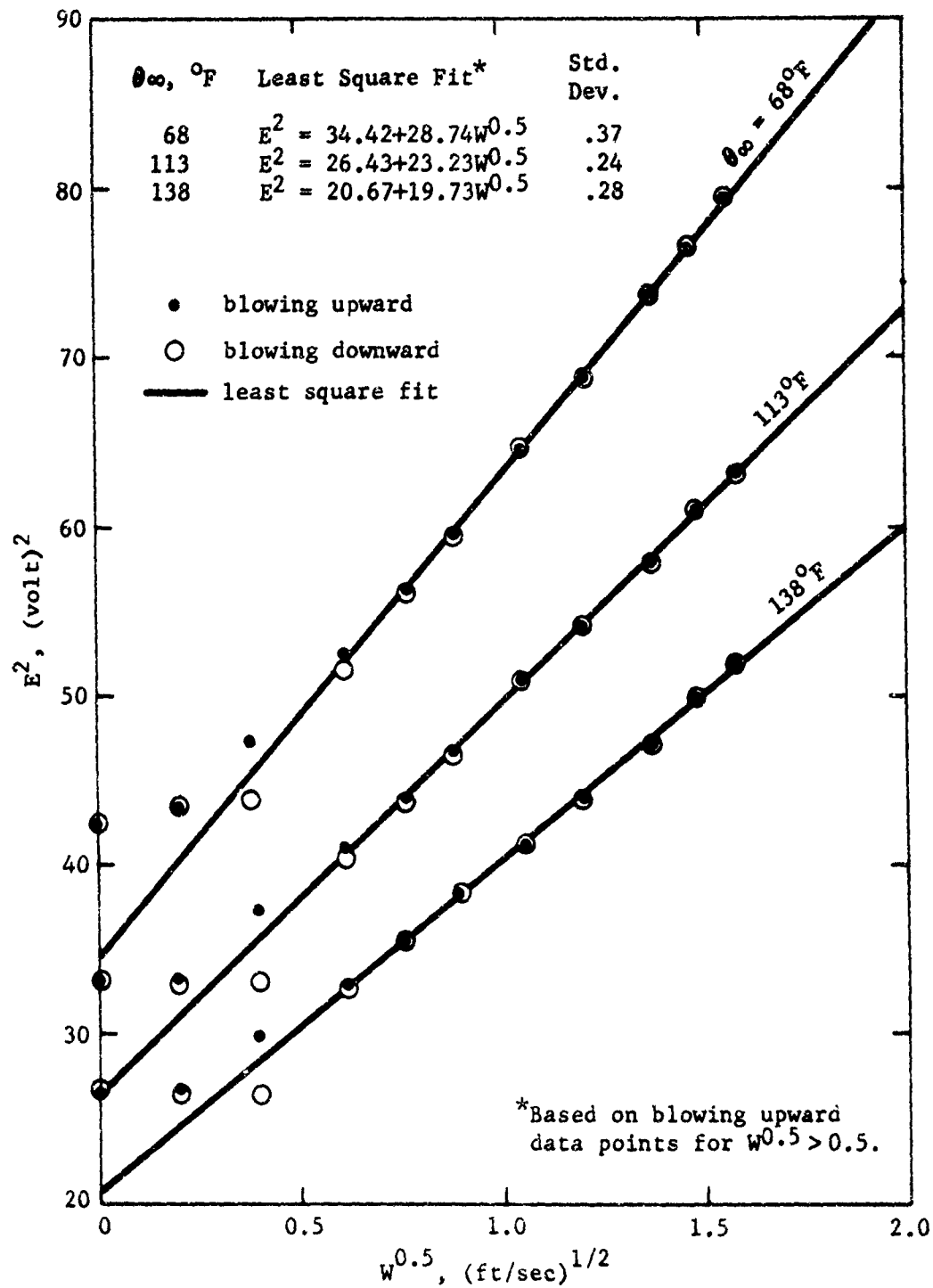
Figure 11.   Tunnel velocity calibrations.

Figure 12. Hot-wire calibrations (0.001" dia. x 0.5" long platinum wire, positioned horizontally, estimated wire temperature = 300°F).
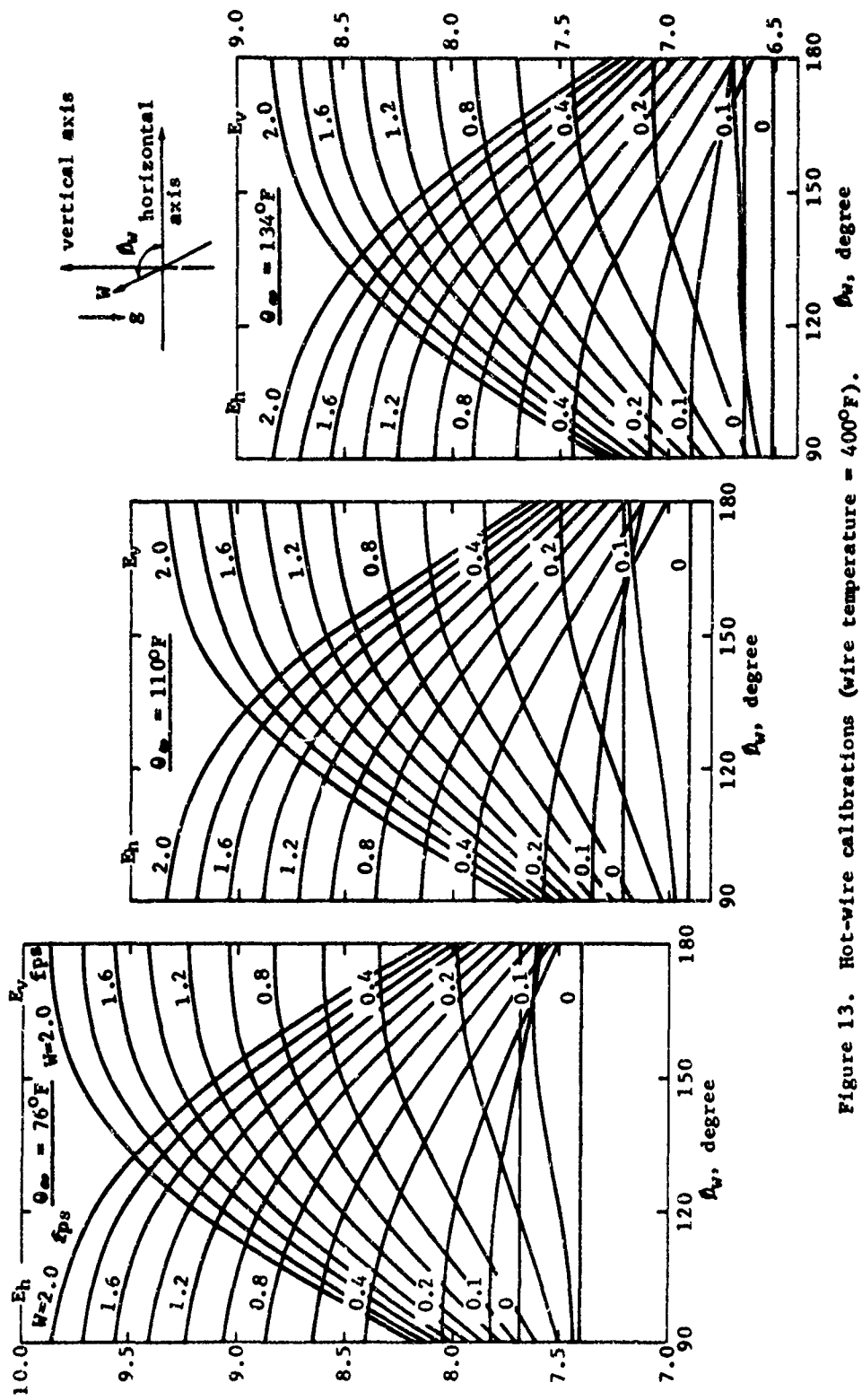
Figure 13. Hot-wire calibrations (wire temperature = 400°F).
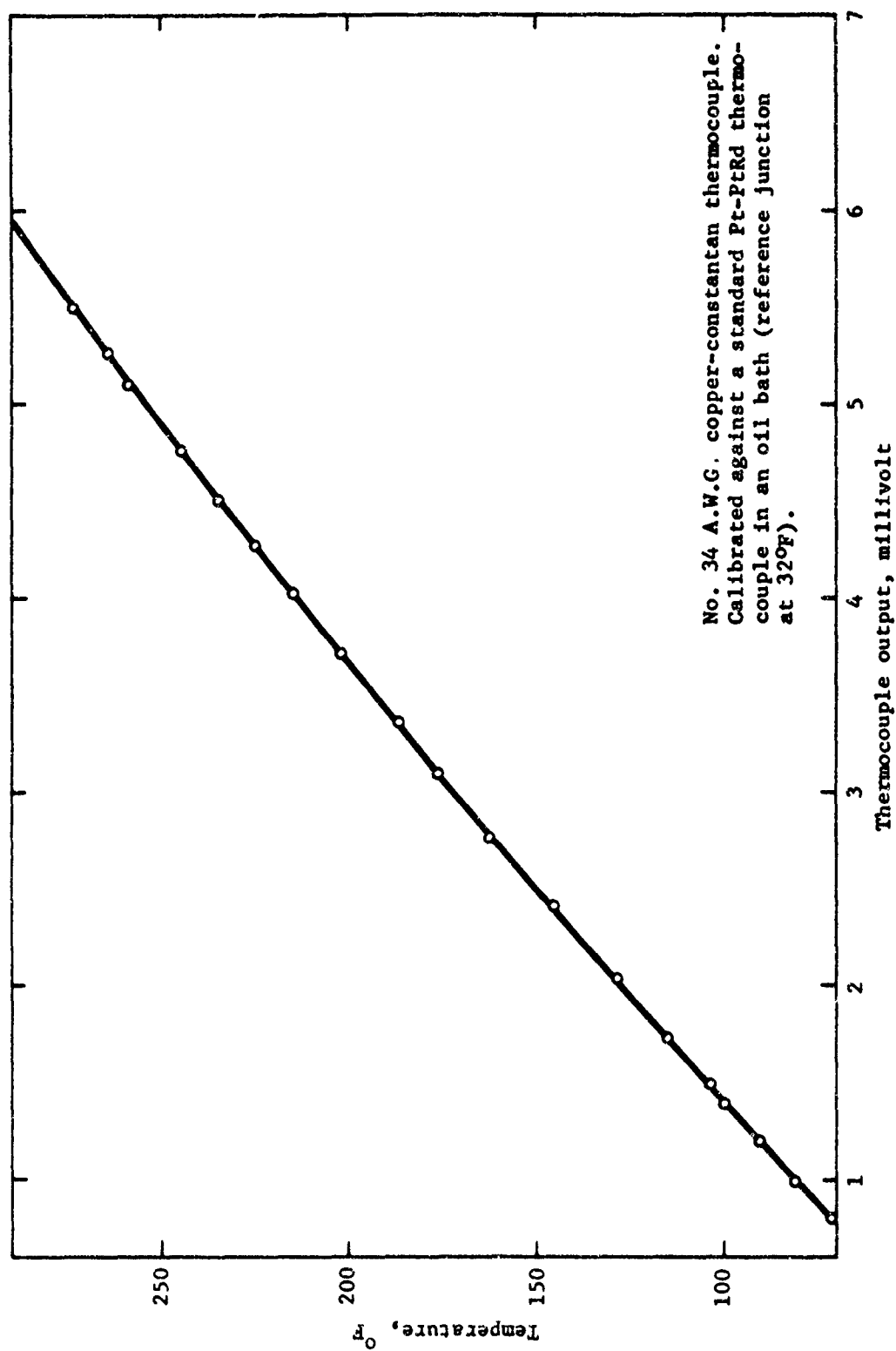
Figure 14. Thermocouple calibrations.

No. 34 A.W.G. copper-constantan thermocouple. Calibrated against a standard Pt-PtRd thermocouple in an oil bath (reference junction at 32°F).
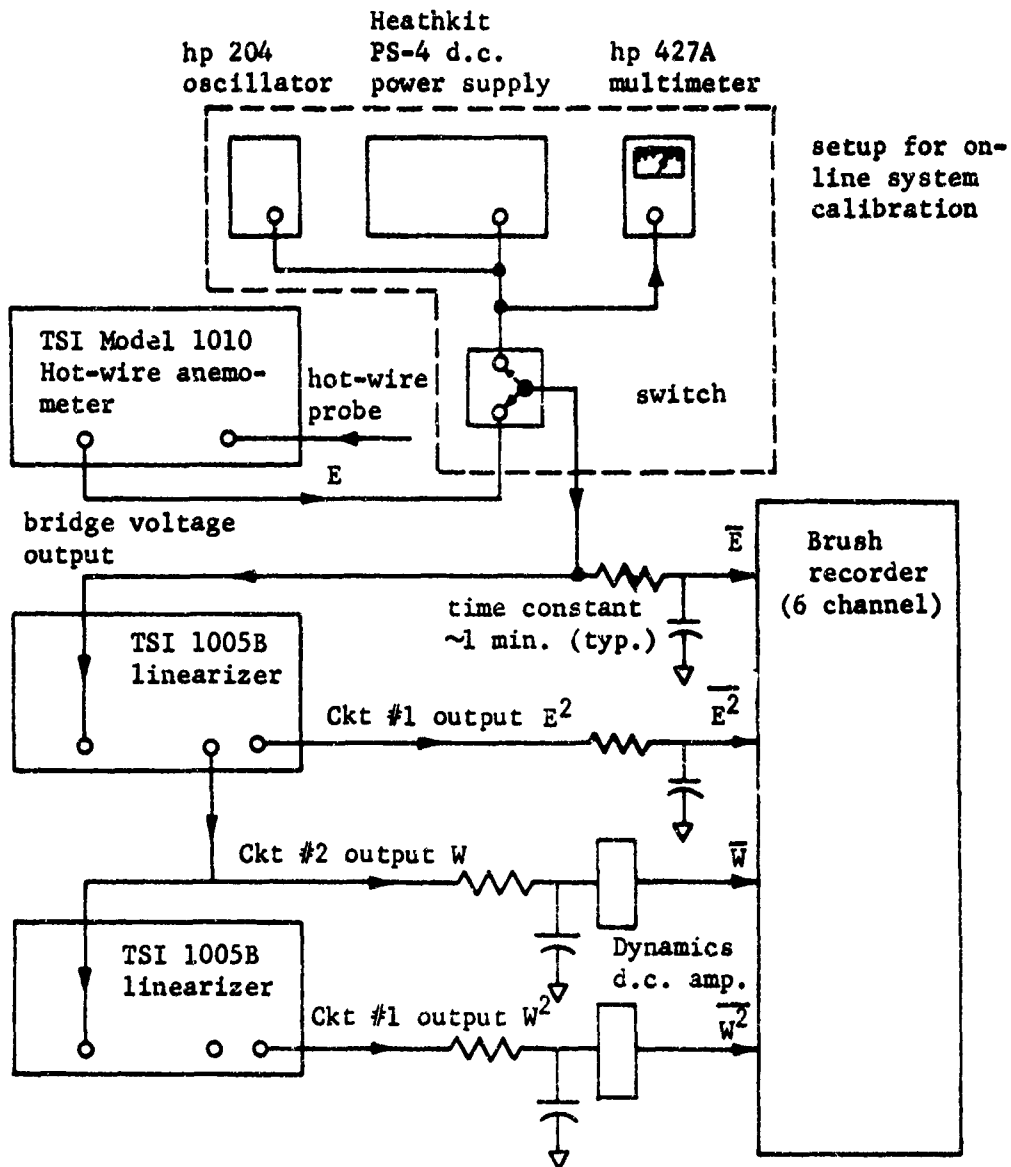
Figure 15. Hot-wire data recording setup - schematic.

,001" dia.
Pt wire

thermocouple
wire leads

#34 Cu-const.
thermocouple

hot wire probe
holder

hot wire
probe

set screw

3/16"

3/16"

thermocouple
support assy.

actual size

Figure 16. Thermocouple and hot wire probe arrangement.

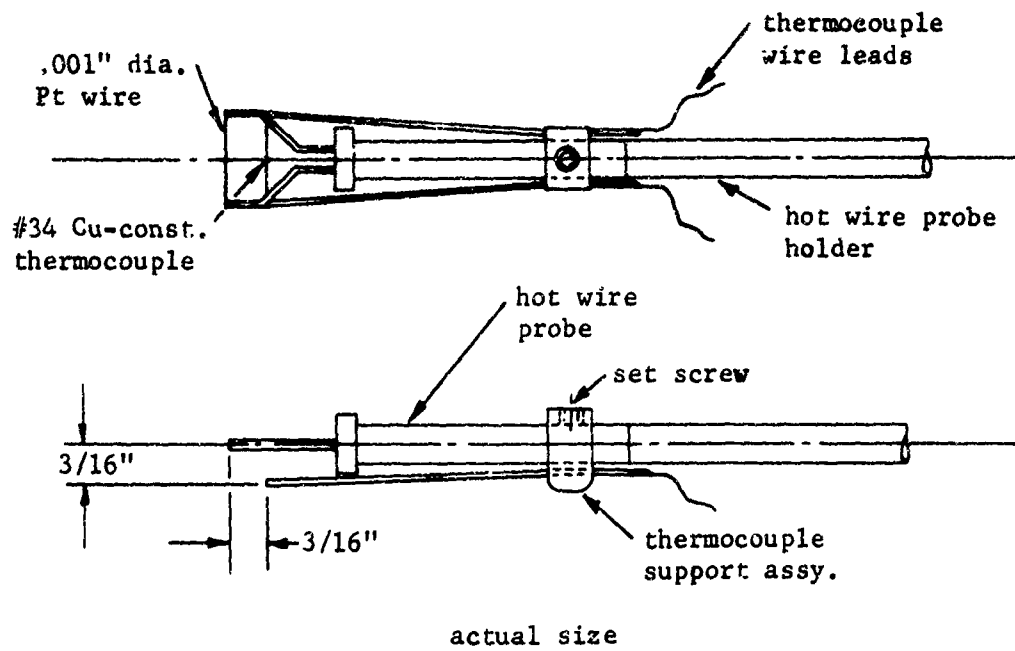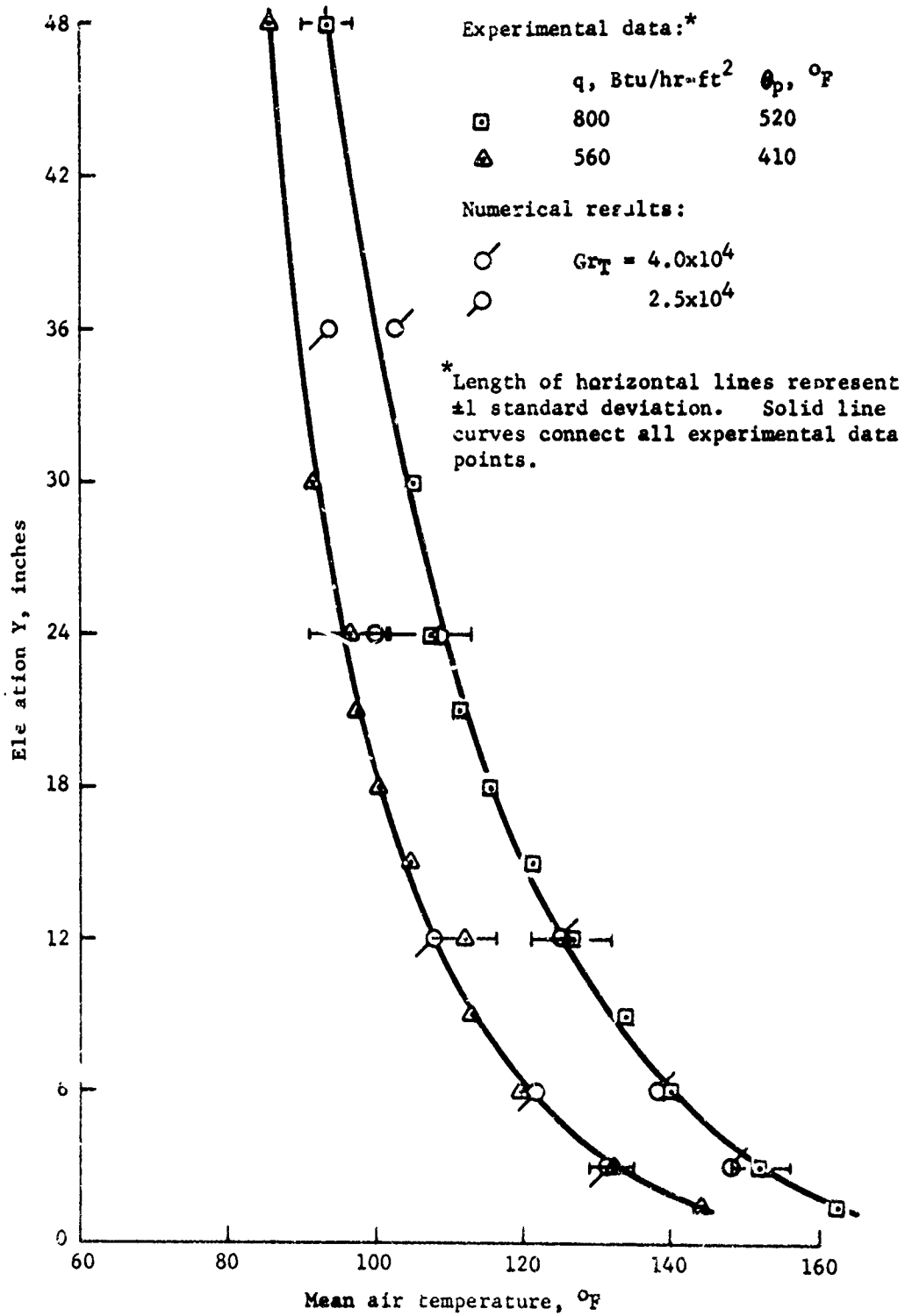Figure 17. Centerline temperature profiles.

103
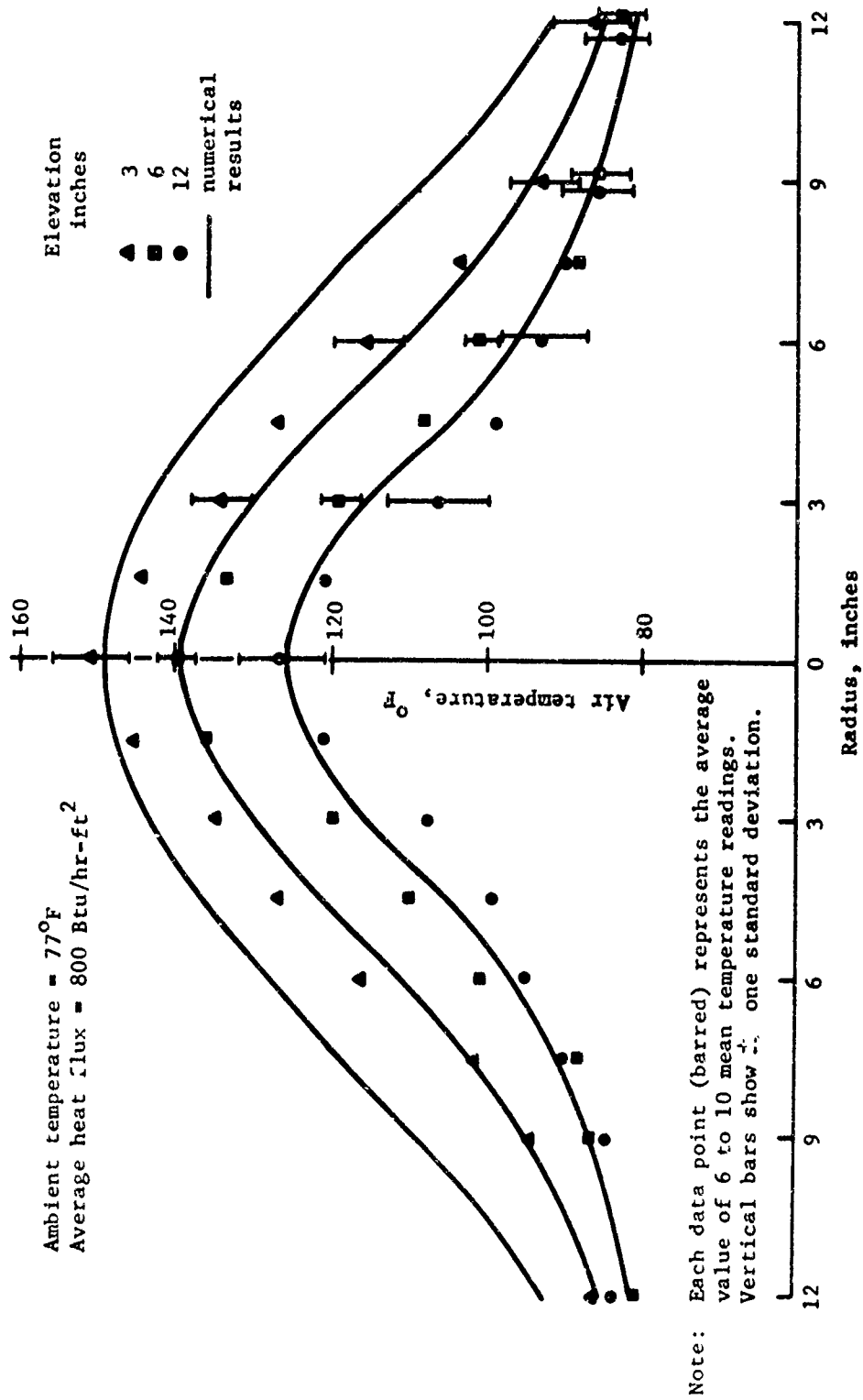
Figure 18. Horizontal temperature profiles ($\theta_p = 520°F$).

Note: Each data point (barred) represents the average value of 6 to 10 mean temperature readings. Vertical bars show $\pm$ one standard deviation.
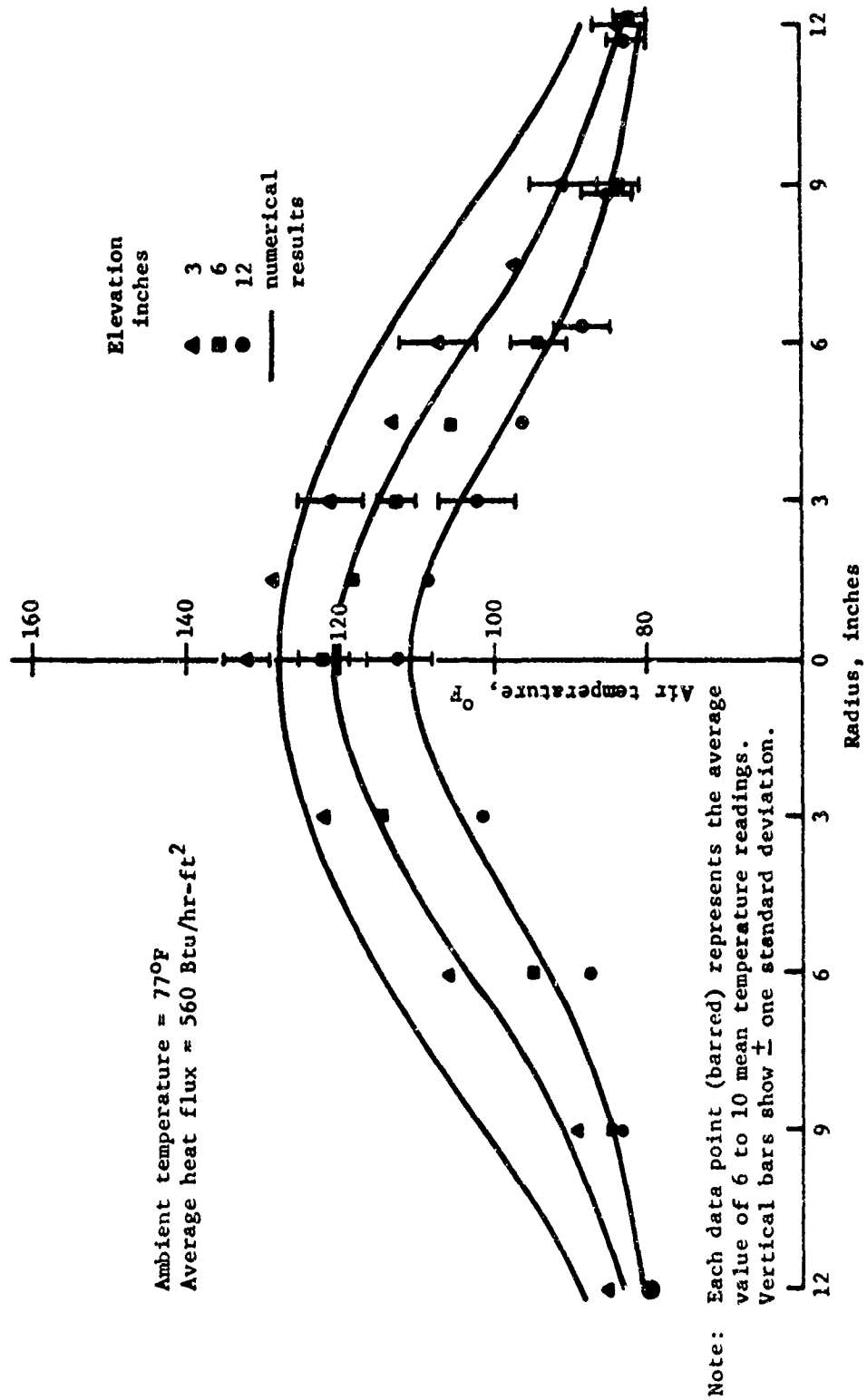
Figure 19. Horizontal temperature profiles ($\theta_p = 410°F$).

Thermocouple lead wires:
Copper – enamel and cotton
insulation
Constantan – cotton
insulation

probe support
(see Figure 3)

horizontal axis

set screw

.025" O.D. x .013" I.D.
stainless steel tubing

thermocouple bead
D = 1/32 in.

bare wire portion
d = 0.0063" dia.

L = 3"

l = .4"
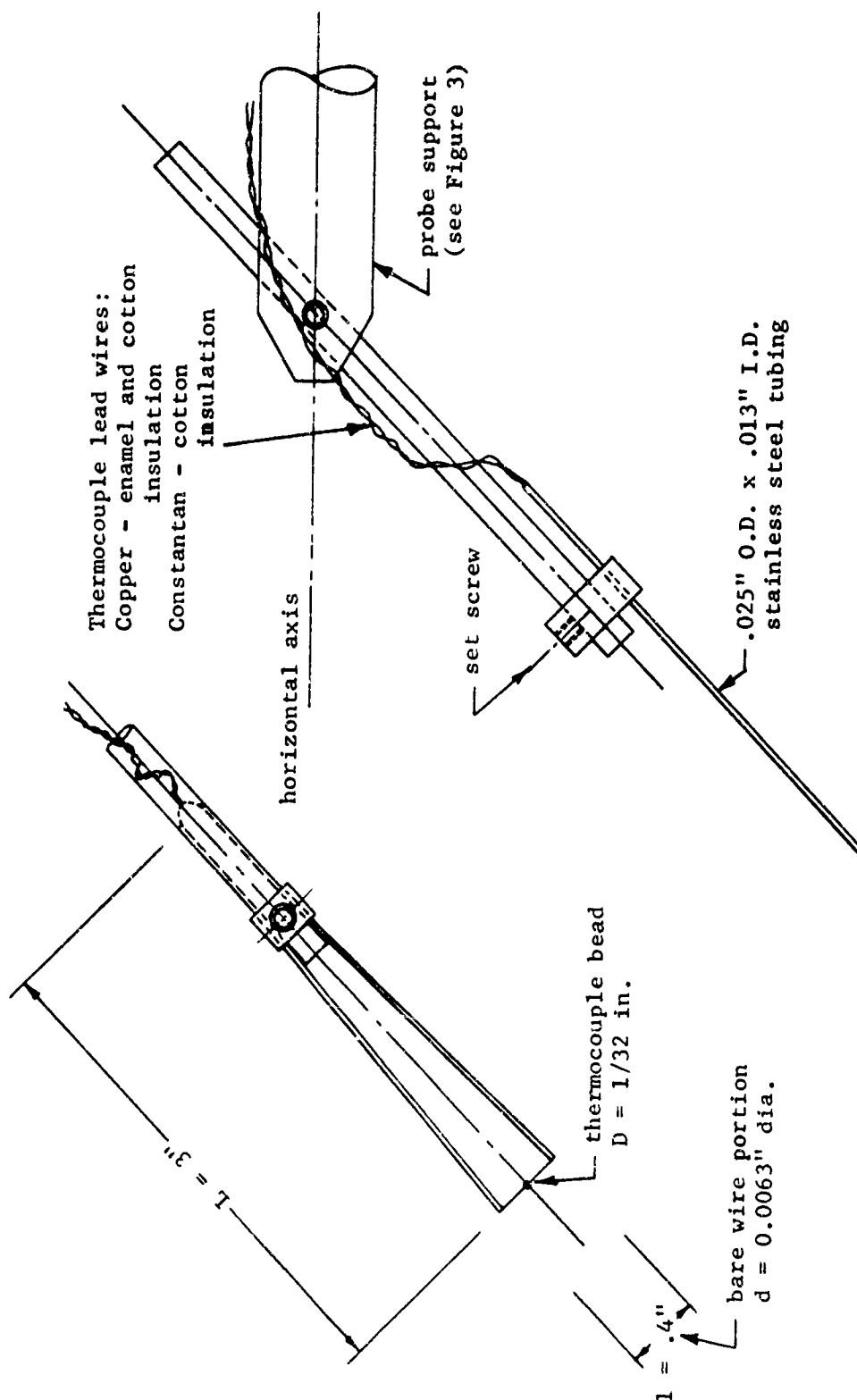
Figure 20. Thermocouple mounting for temperature measurements near the plate.
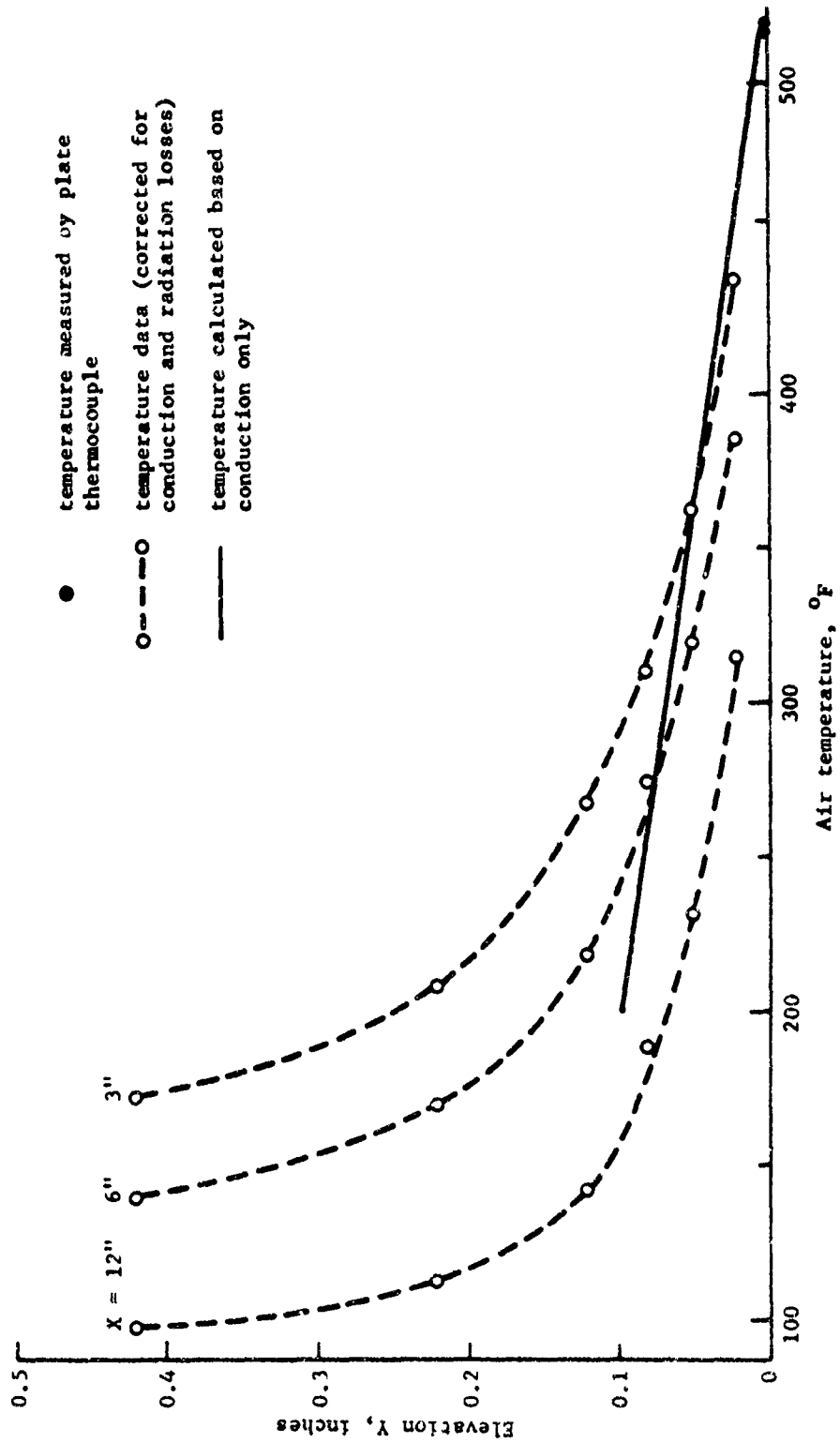
Figure 21. Temperature distribution near the plate ($\theta_p = 520°F$).
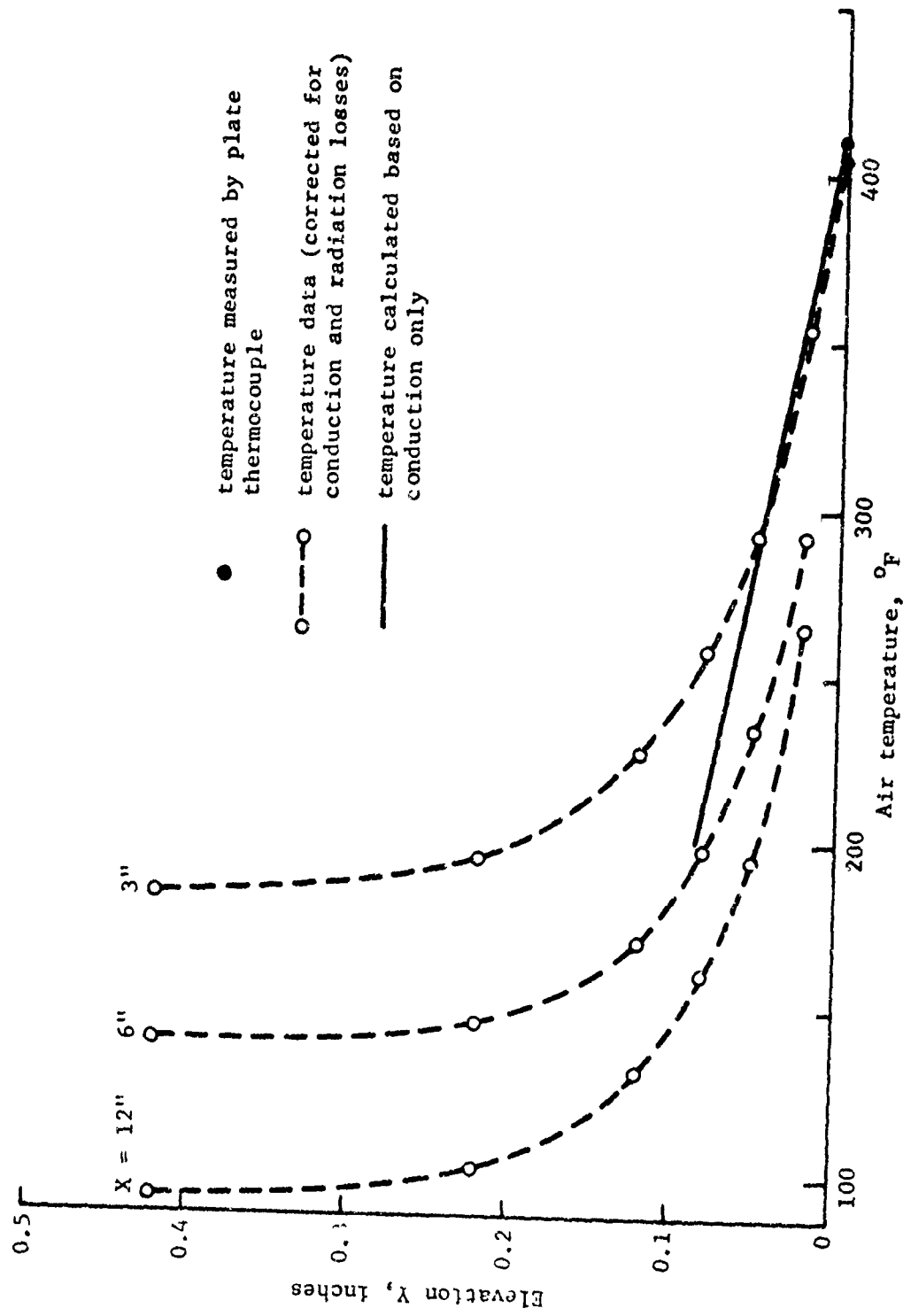
Figure 22. Temperature distribution near the plate ($\theta_p = 410°F$).
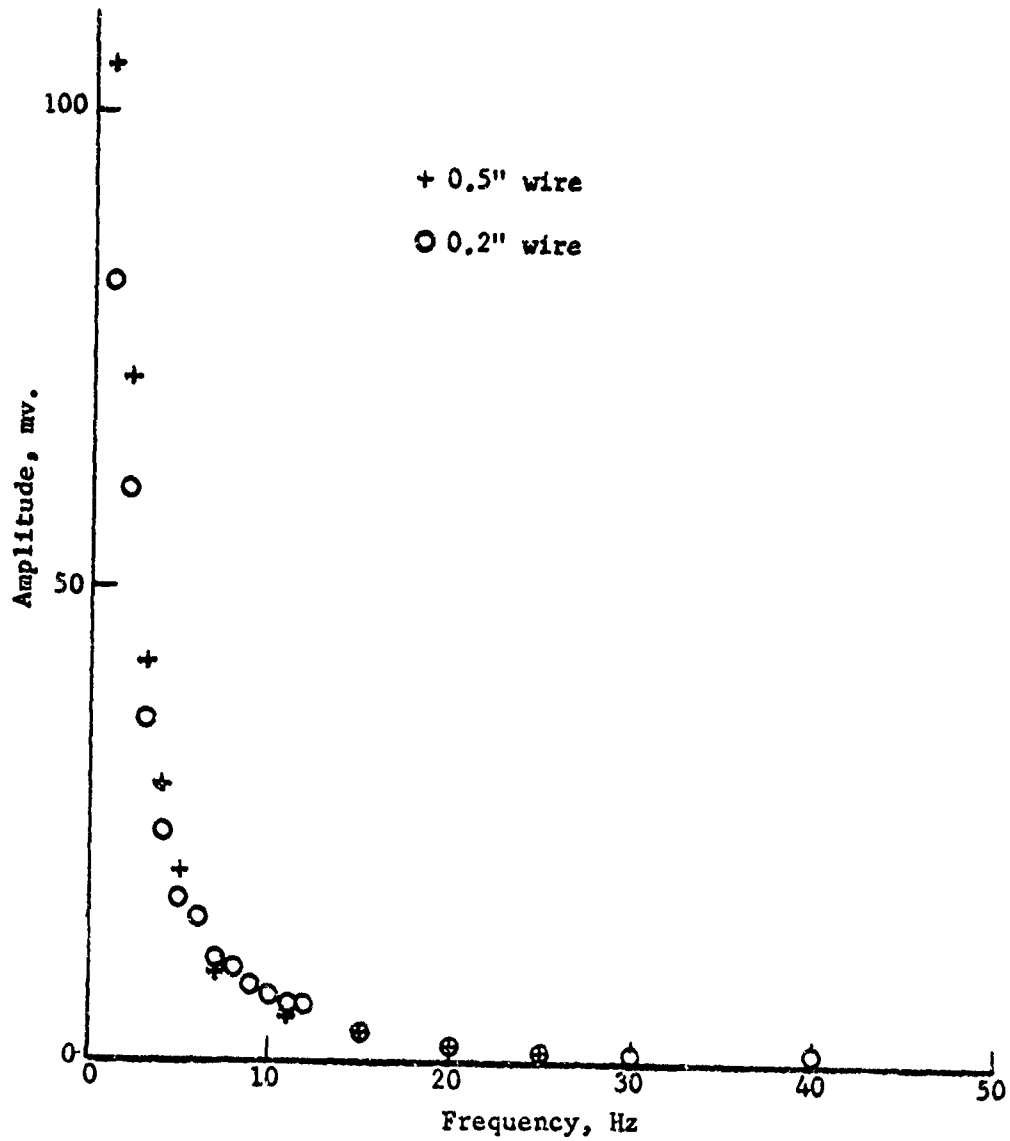
Figure 23. Comparison of wave analyzer outputs for different wire lengths (θ_p = 520°F, X = 6", Y = 6", wire horizontal).
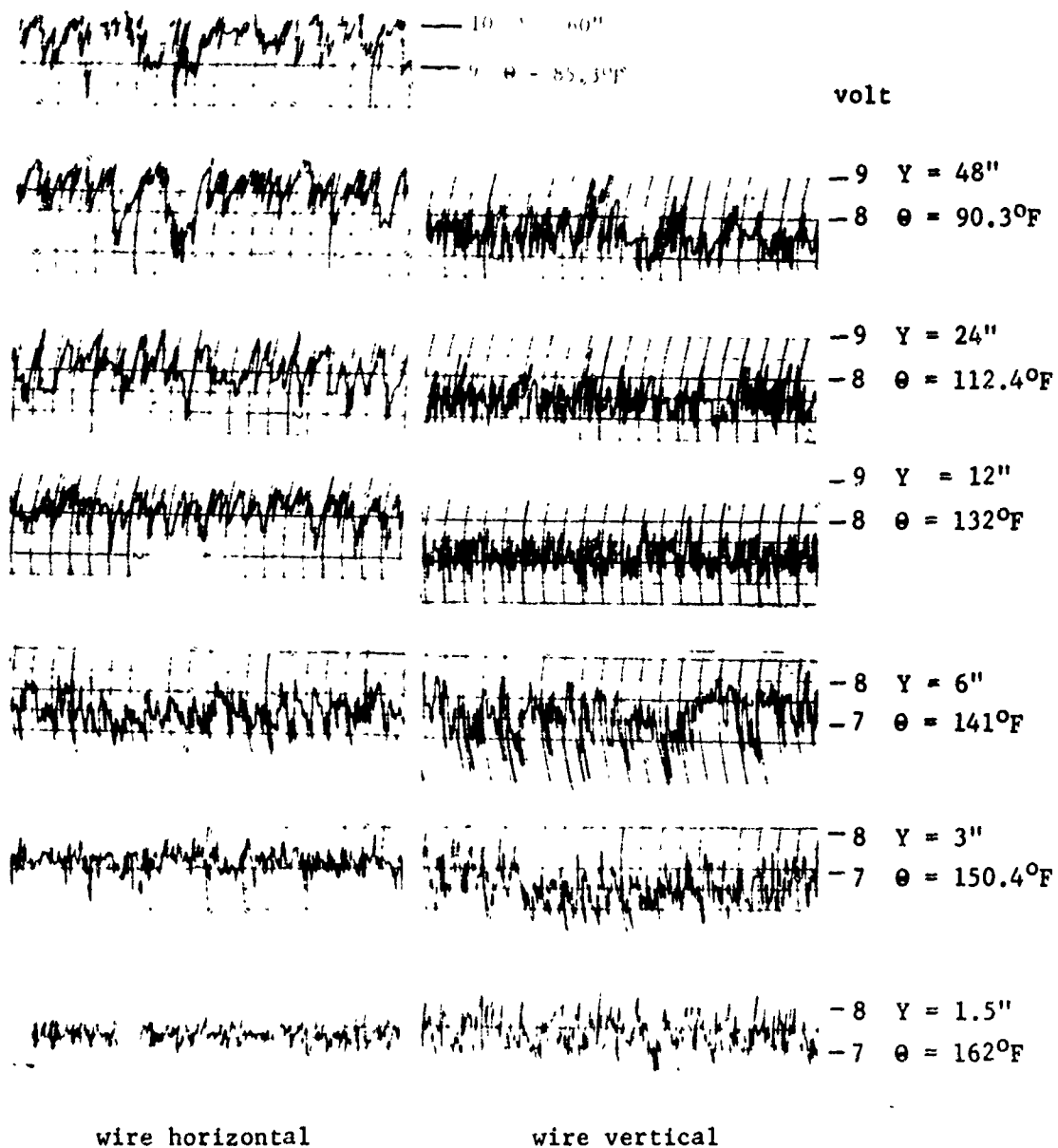
Figure 24.   Hot-wire bridge voltage output ($X = 0$, $\theta_p = 520^\circ F$).
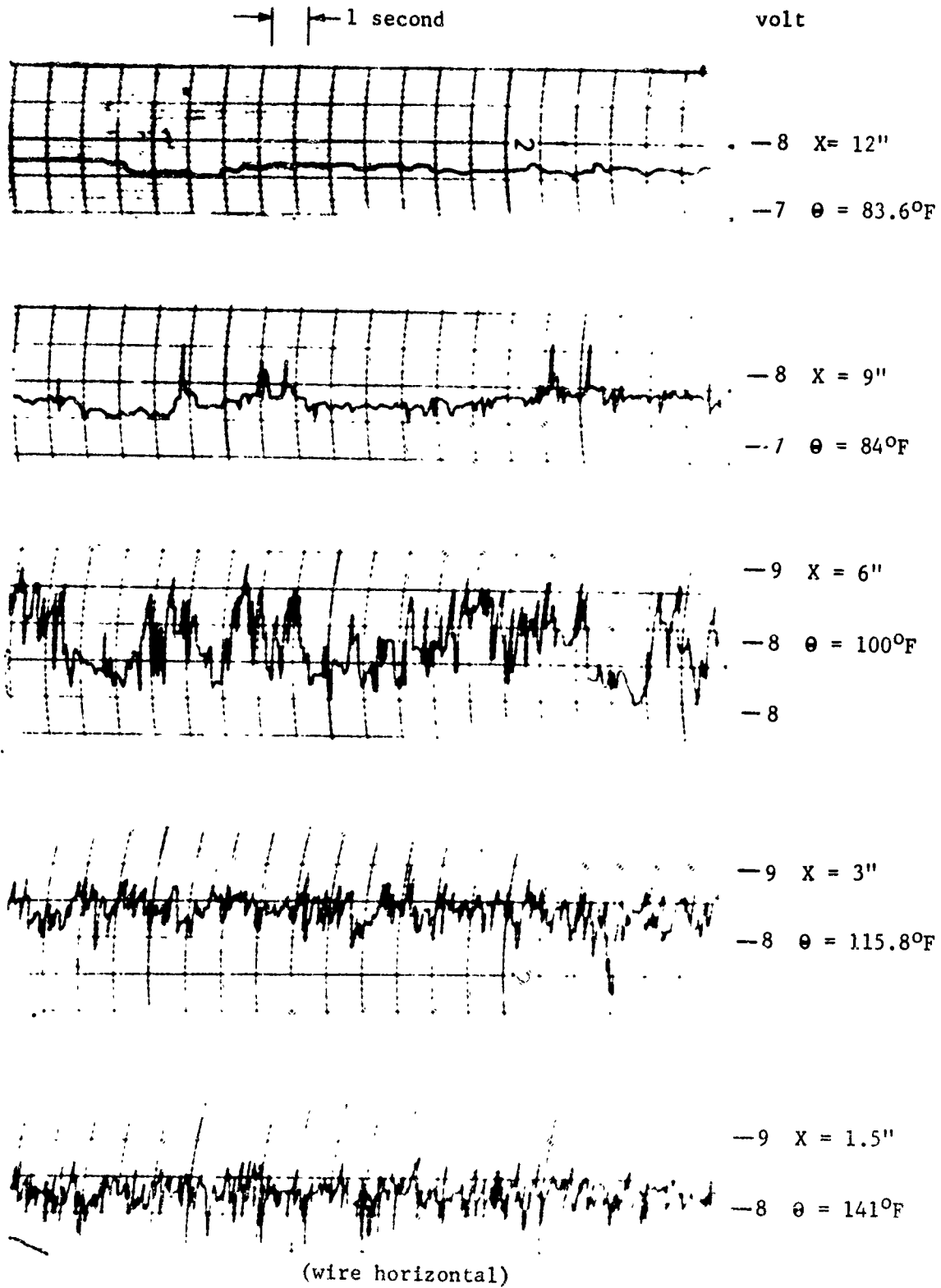
Figure 25. Hot-wire bridge voltage output ($Y = 6$", $\Theta_p = 520^\circ F$).
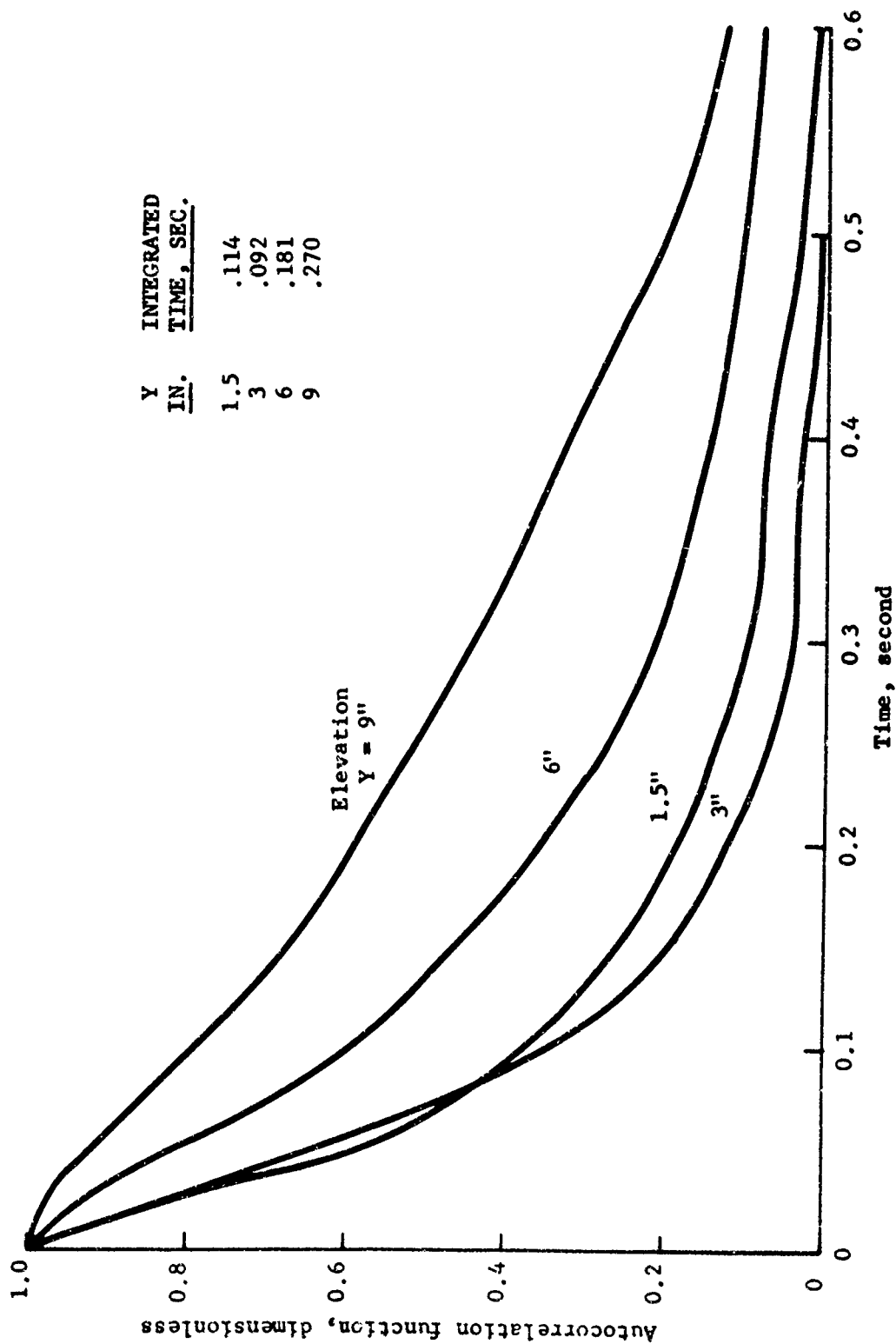
Figure 26. Autocorrelation function of hot-wire bridge voltage output for centerline locations (wire horizontal, $\theta_p = 520^\circ F$)
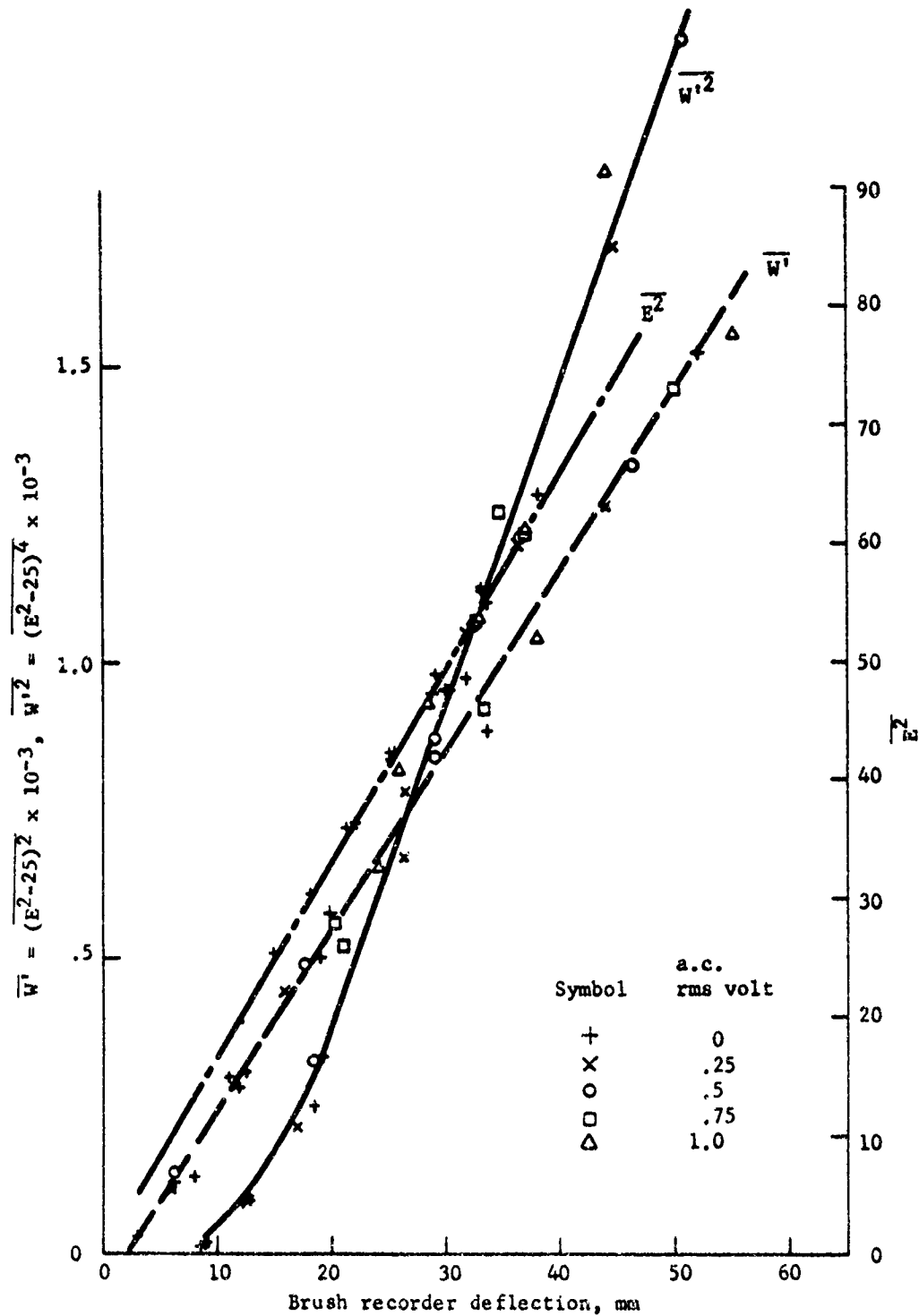
Figure 27. Calibrations of hot-wire data taking system using d.c. plus a 60 Hz a.c. as input.

(a) X = 0, Y = 1.5"

(b) X = 0, Y = 3"

Angle between wire and the horizontal, degrees
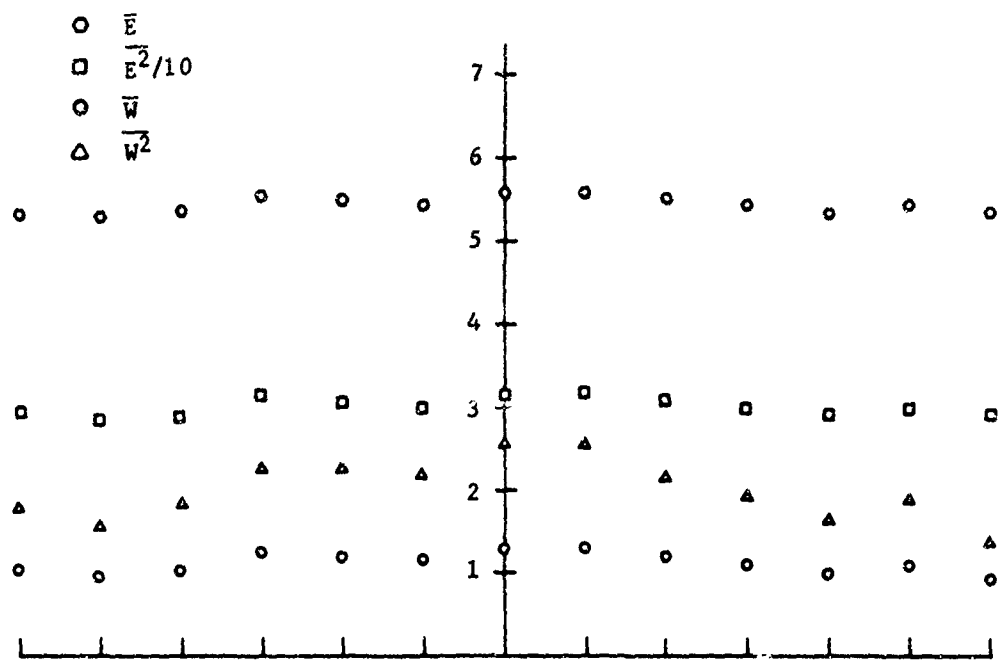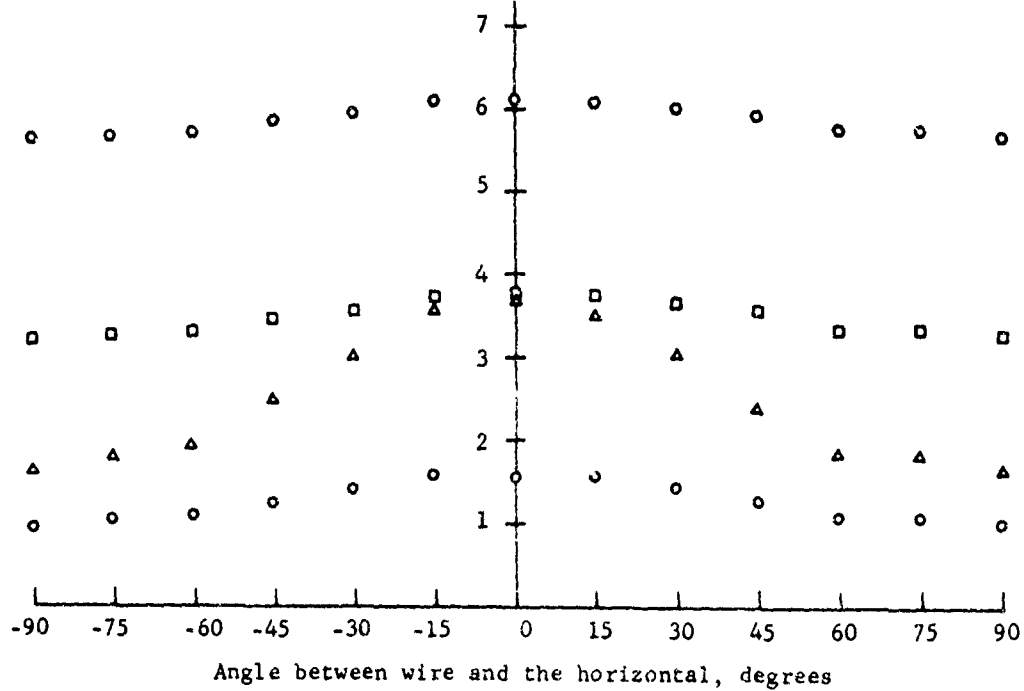
Figure 28. Hot-wire data - bridge voltage and its moments ($\theta_p = 520^\circ$F).

(c) X = 0, Y = 6"

Angle between wire and the horizontal, degrees

(d) X = 0, Y = 12"

Figure 28. (Continued)

(e) X = 3", Y = 3"

(f) X = 3", Y = 6"

Angle between wire and the horizontal, degrees

Figure 28. (Continued)

(g) X = 6", Y = 3"

(h) X = 6", Y = 6"

Angle between wire and the horizontal, degrees
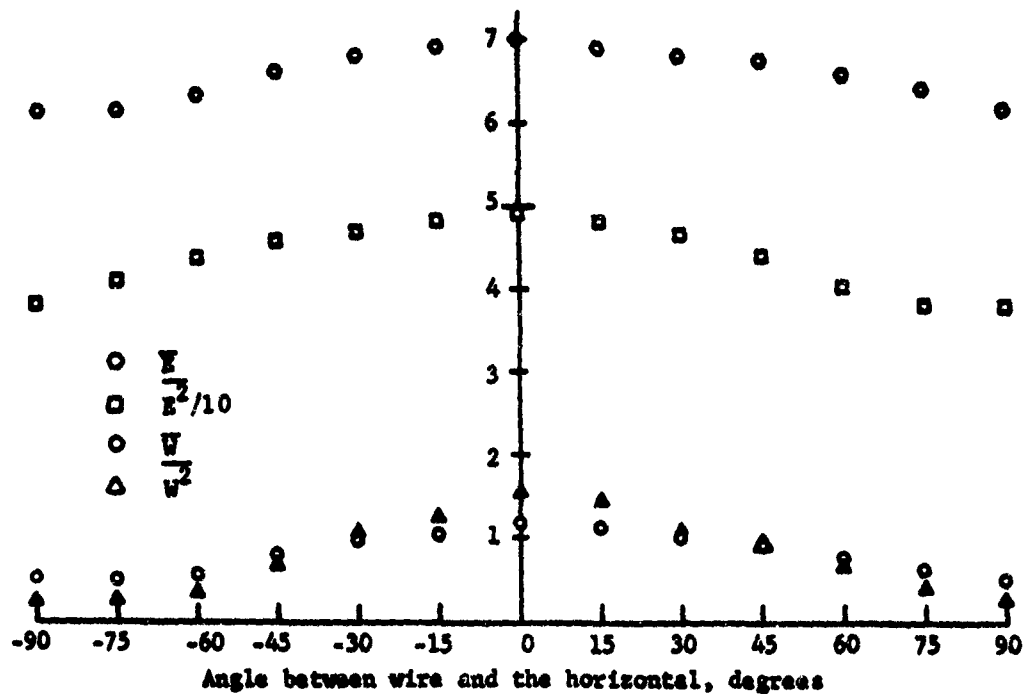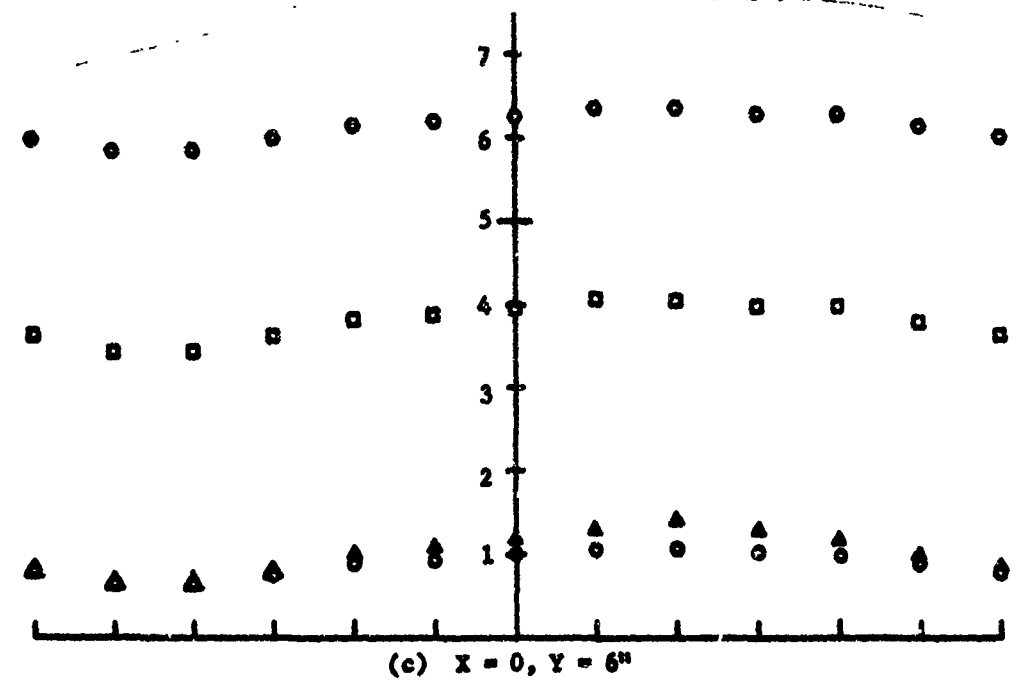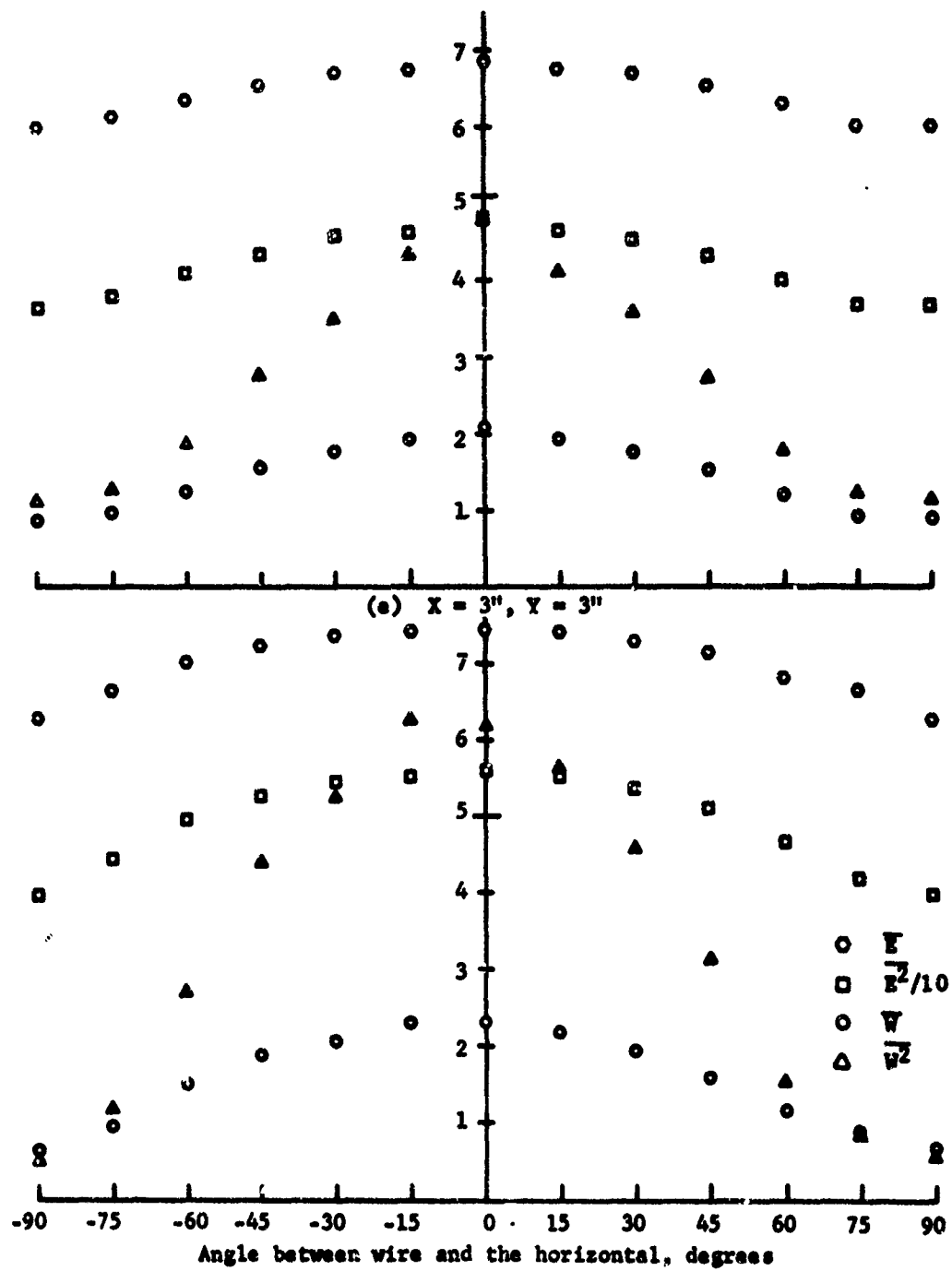
Figure 28 (Continued)
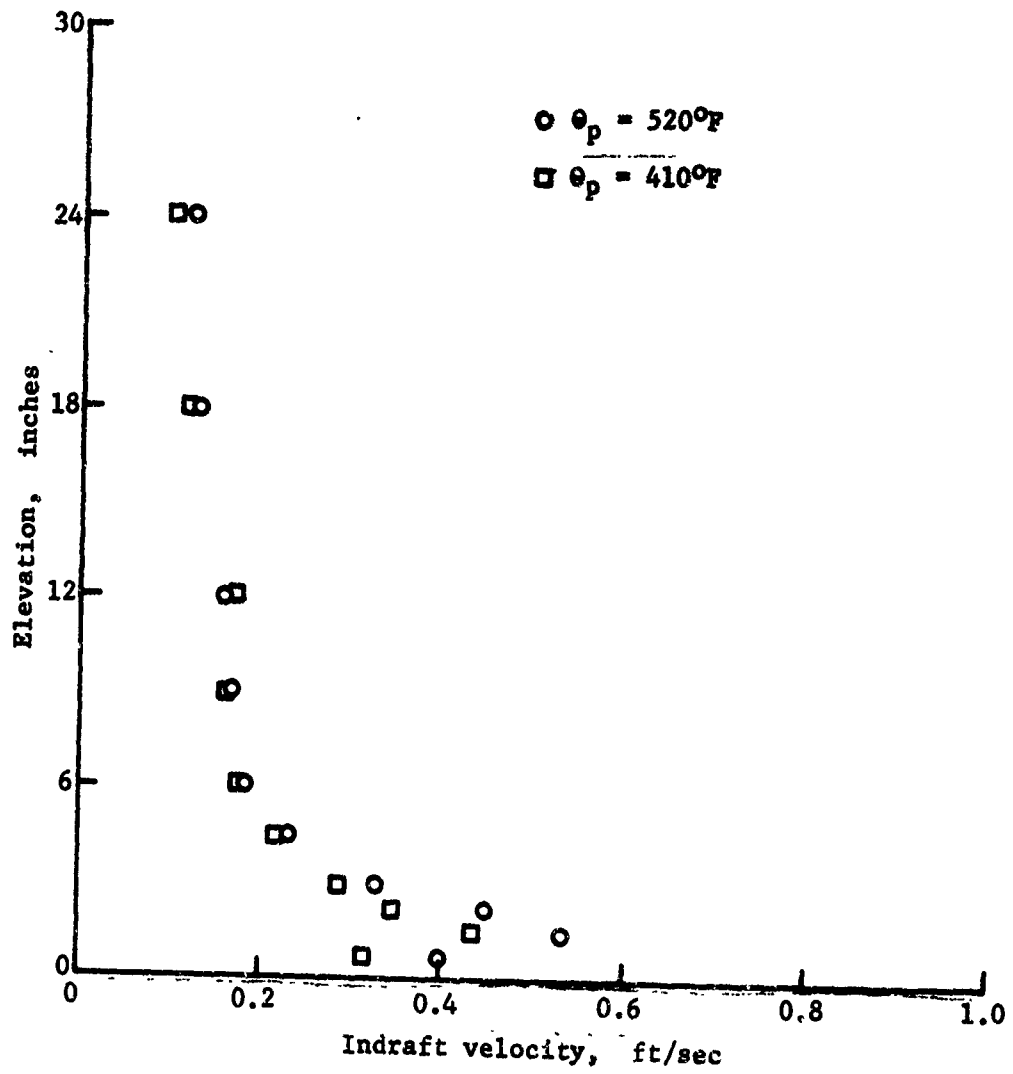
Figure 29.   Indraft profiles (X = 12").

Figure 31. Typical simulated hot-wire data, k2=0 (normalized by the corresponding value at β_w=0°).

Figure 30. Typical simulated hot-wire data, k2=0.1 (normalized by the corresponding value at β_w = 0°).

(a) Shape parameter $\mathcal{R}_0$

(b) Shape parameter $\mathcal{R}_1$

Figure 32. Simulated hot-wire data

(c) Shape parameter $\mathcal{R}_2$

(d) Effective flow velocity W/V_m
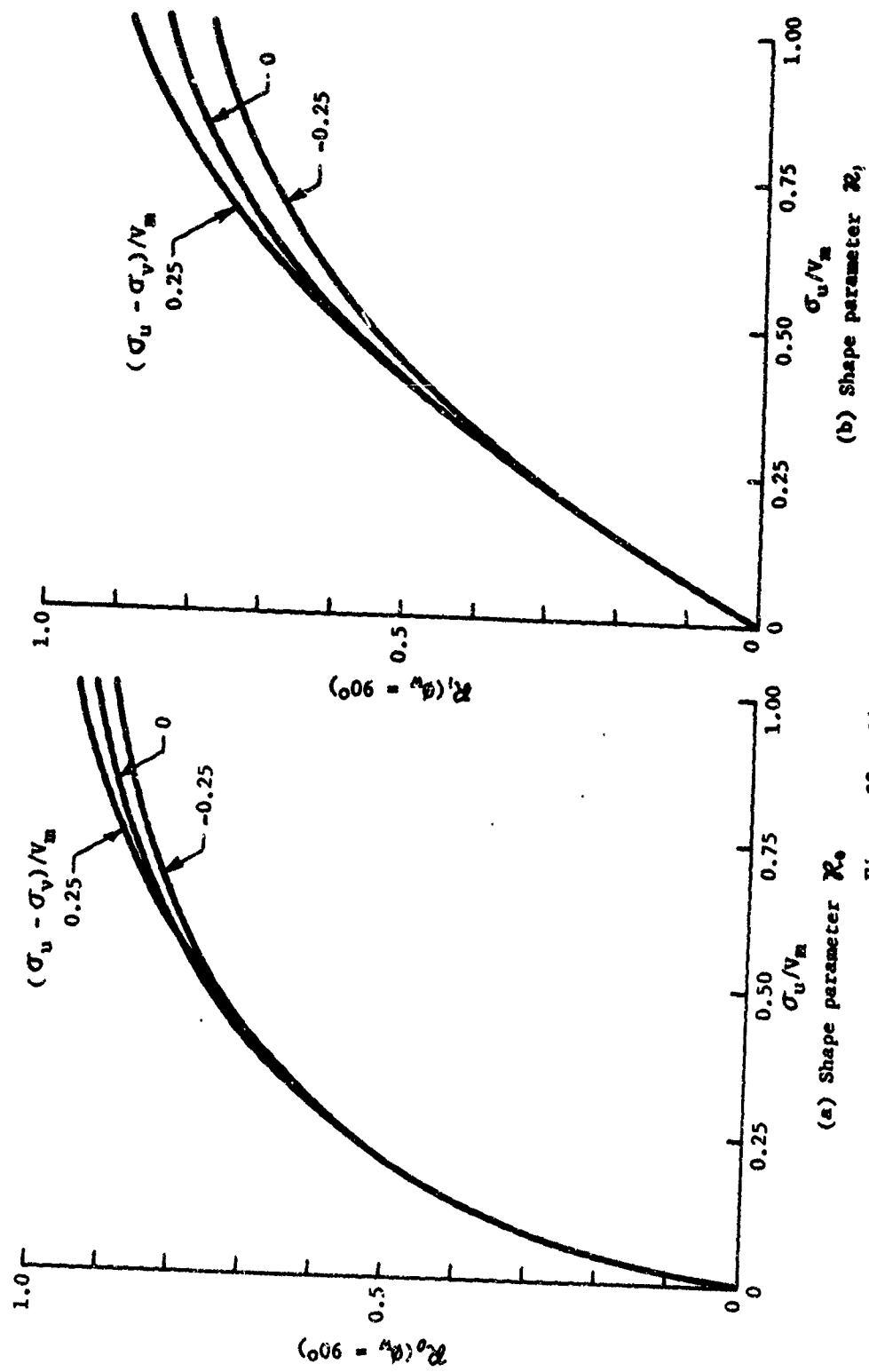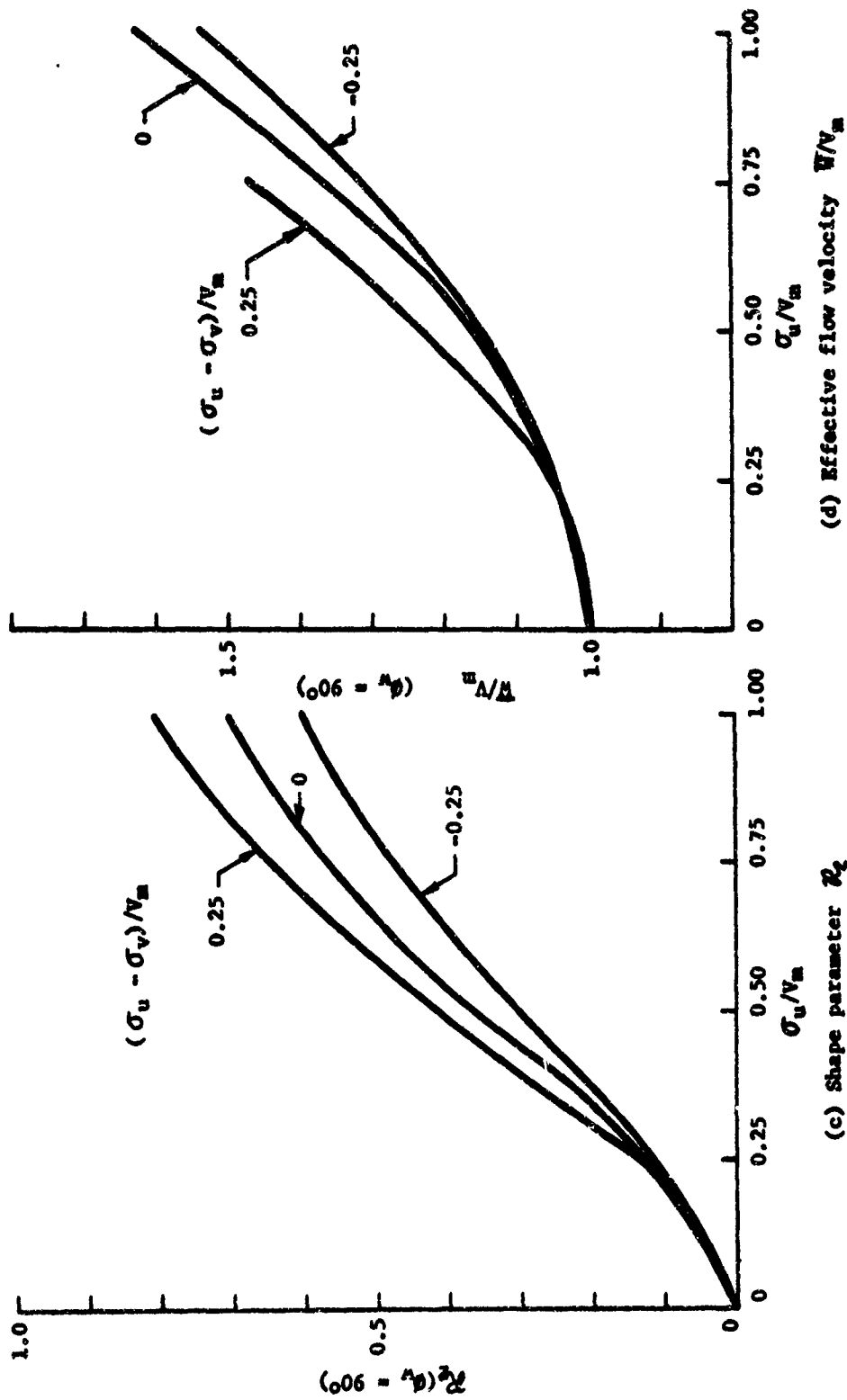
Figure 32 (continued)
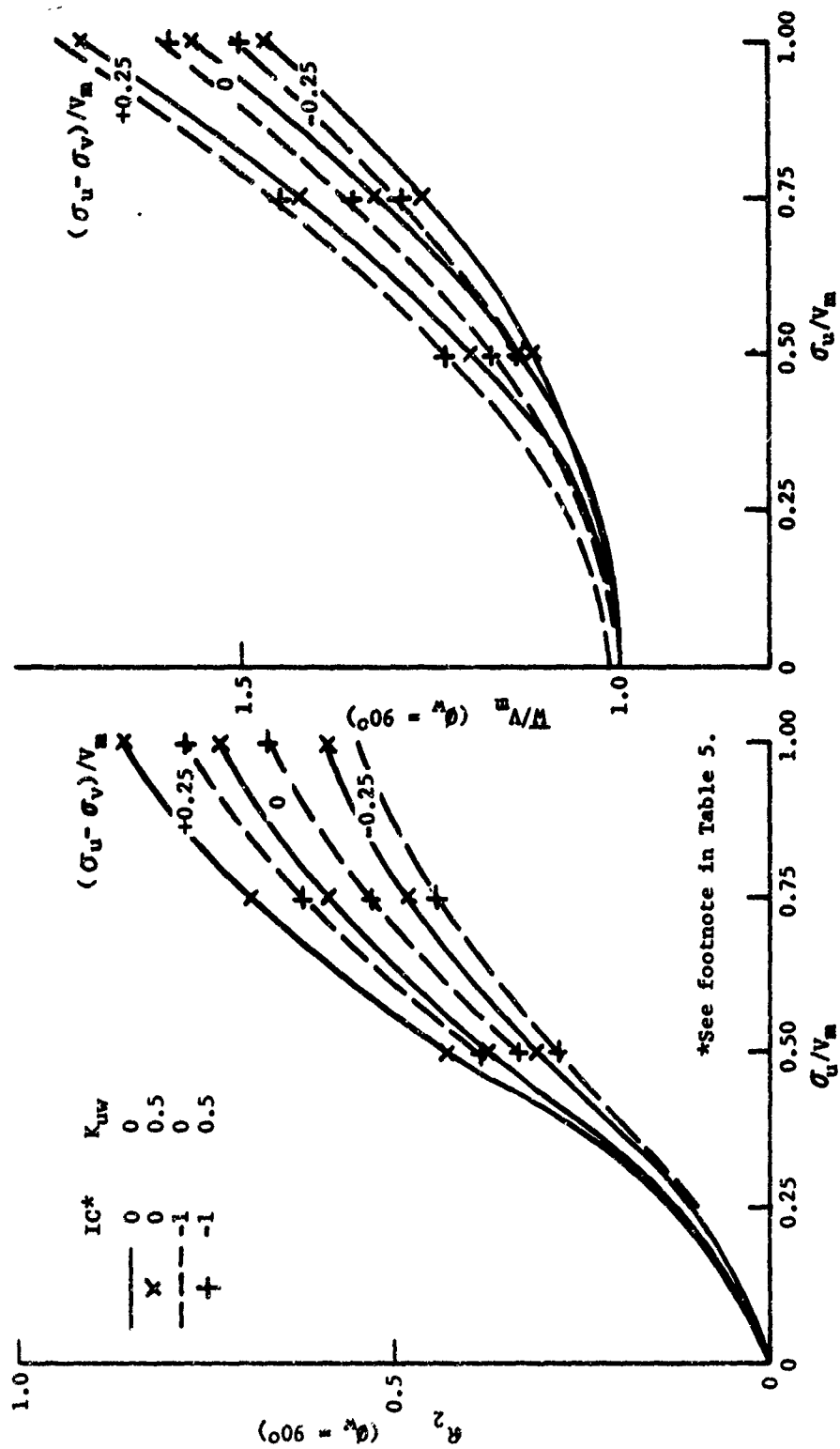
Figure 33. Simulated hot-wire data - effects of assumptions.
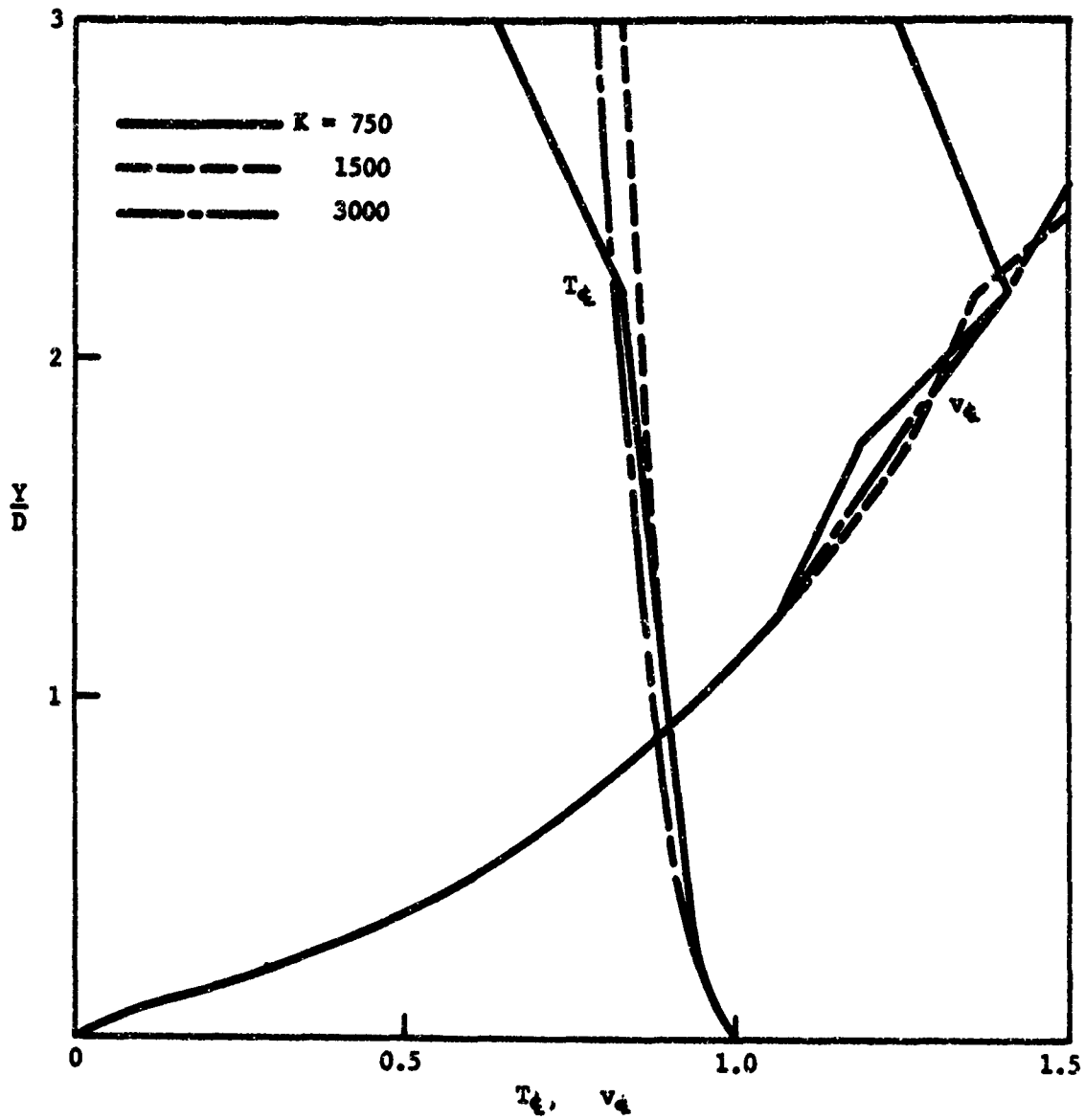
Figure 34. Numerical results at various stages of calculations for a transformed coordinate system (grid system = 17 x 17, 1-9, $C_1 = C_2 = 4$, $Gr_T = 7.43 \times 10^9$, $Pr = 0.708$).
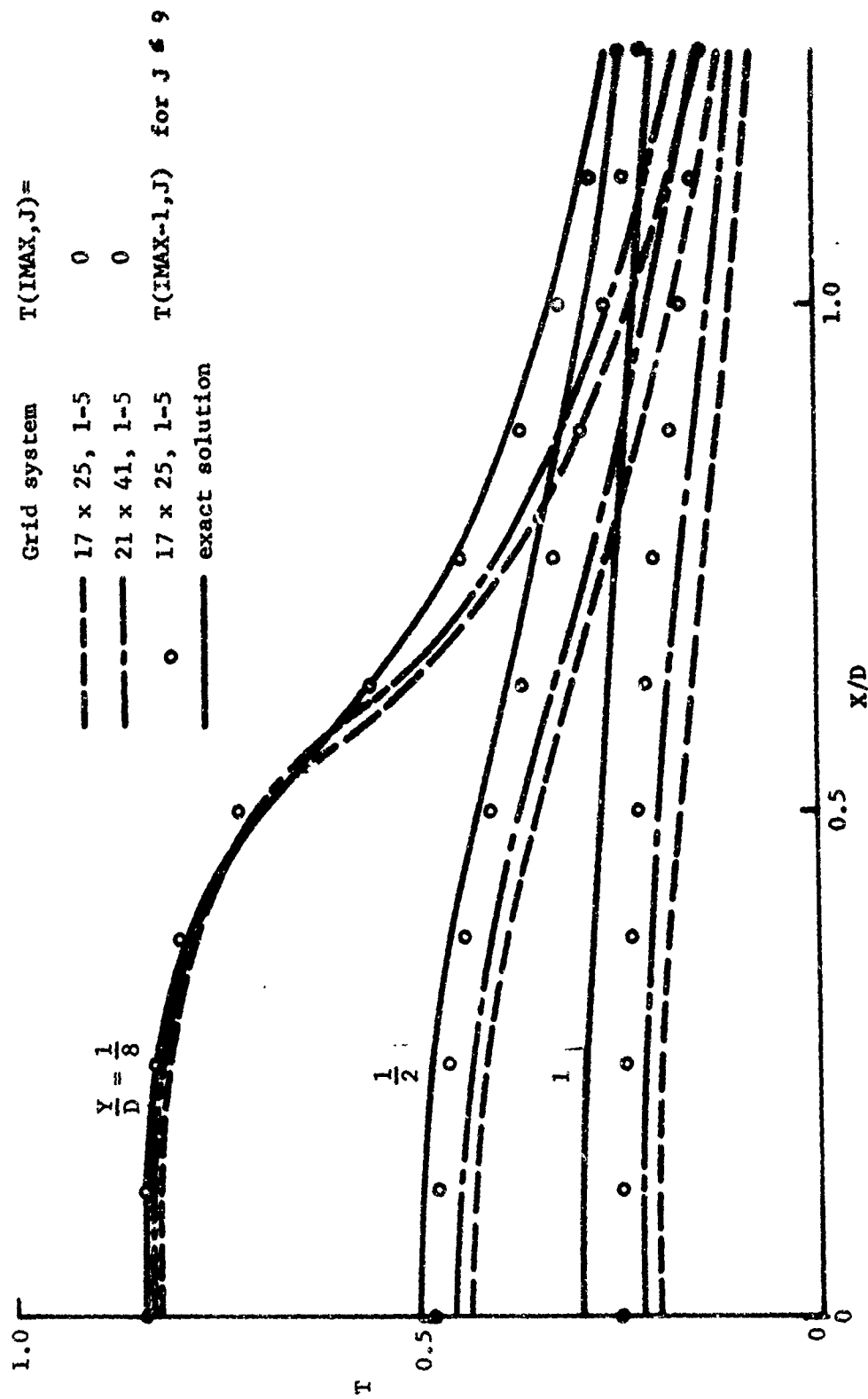
Figure 35. Comparison of numerical results for non-flow condition with exact solution of diffusion equation).
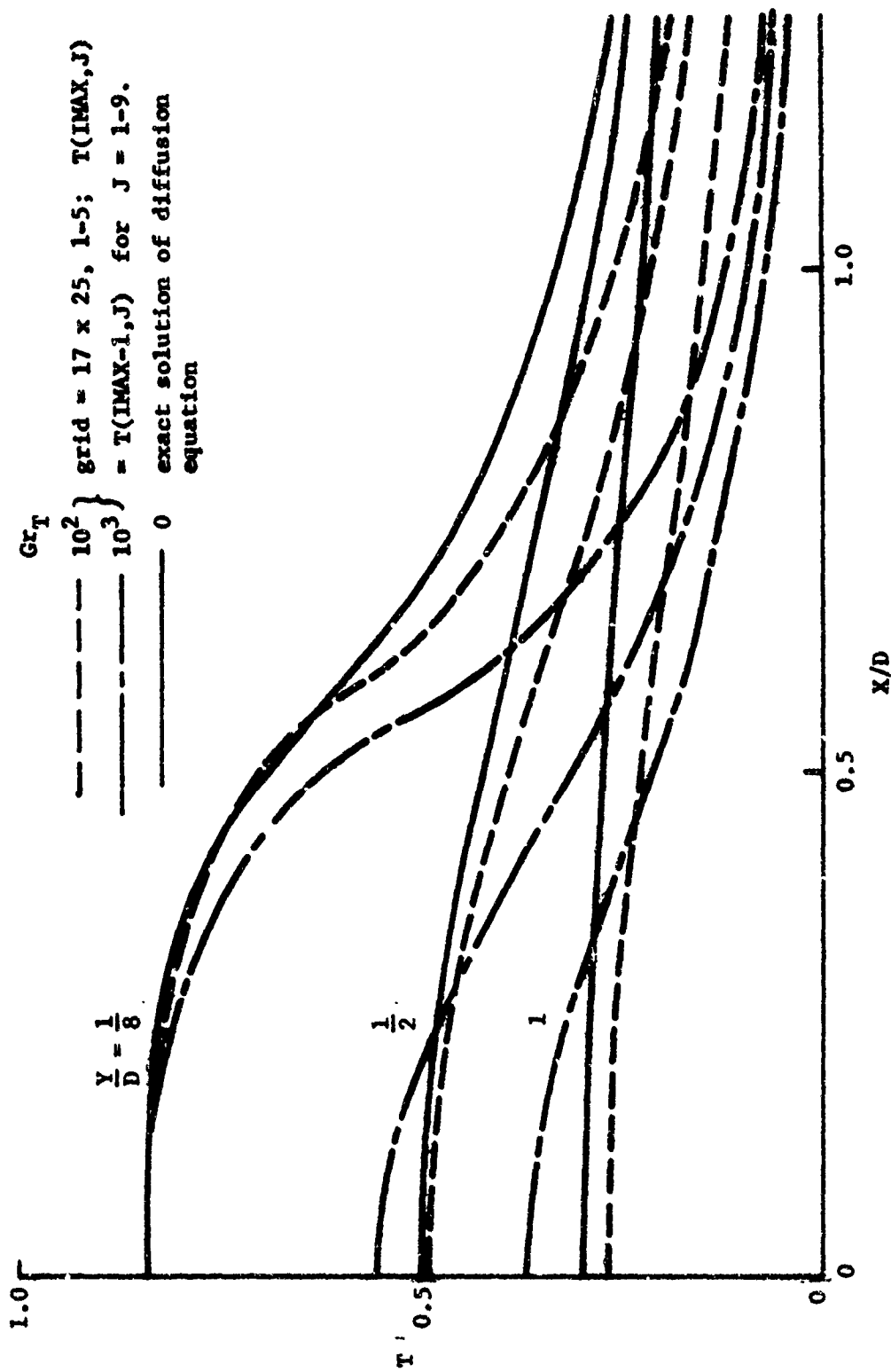
Figure 36. Comparison of numerical results for small Gr_T with the exact solution of diffusion equation
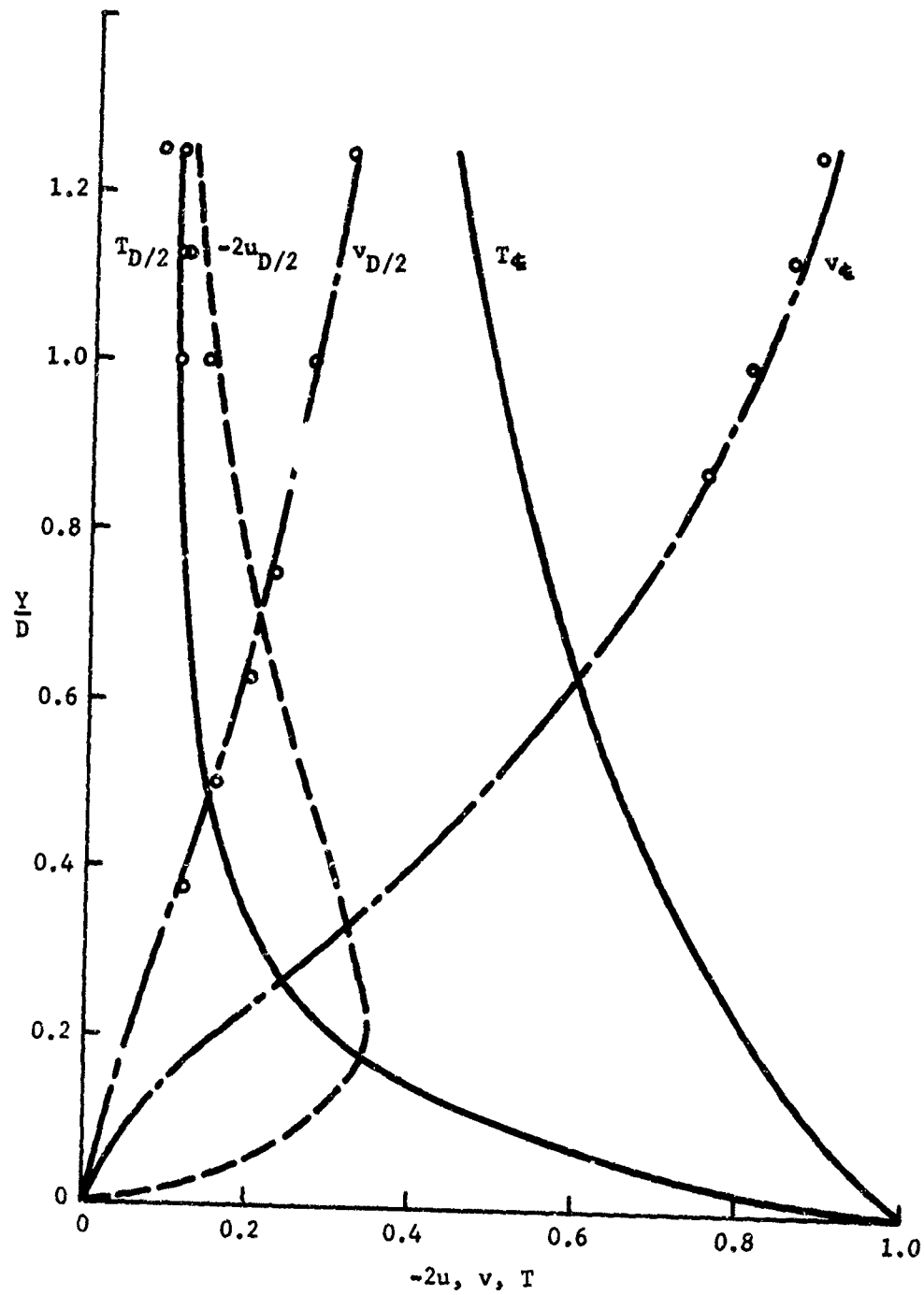
Figure 37. Effects of domain of calculations on the numerical results - vertical extent ($Gr_T = 10^4$, $Pr = 0.708$).
(Lines shown are for grid systems: 17 x 17, 1-5; 17 x 21, 1-5; 17 x 25, 1-5. o shows the deviation of the results of a 17 x 13, 1-5 system from the lines).
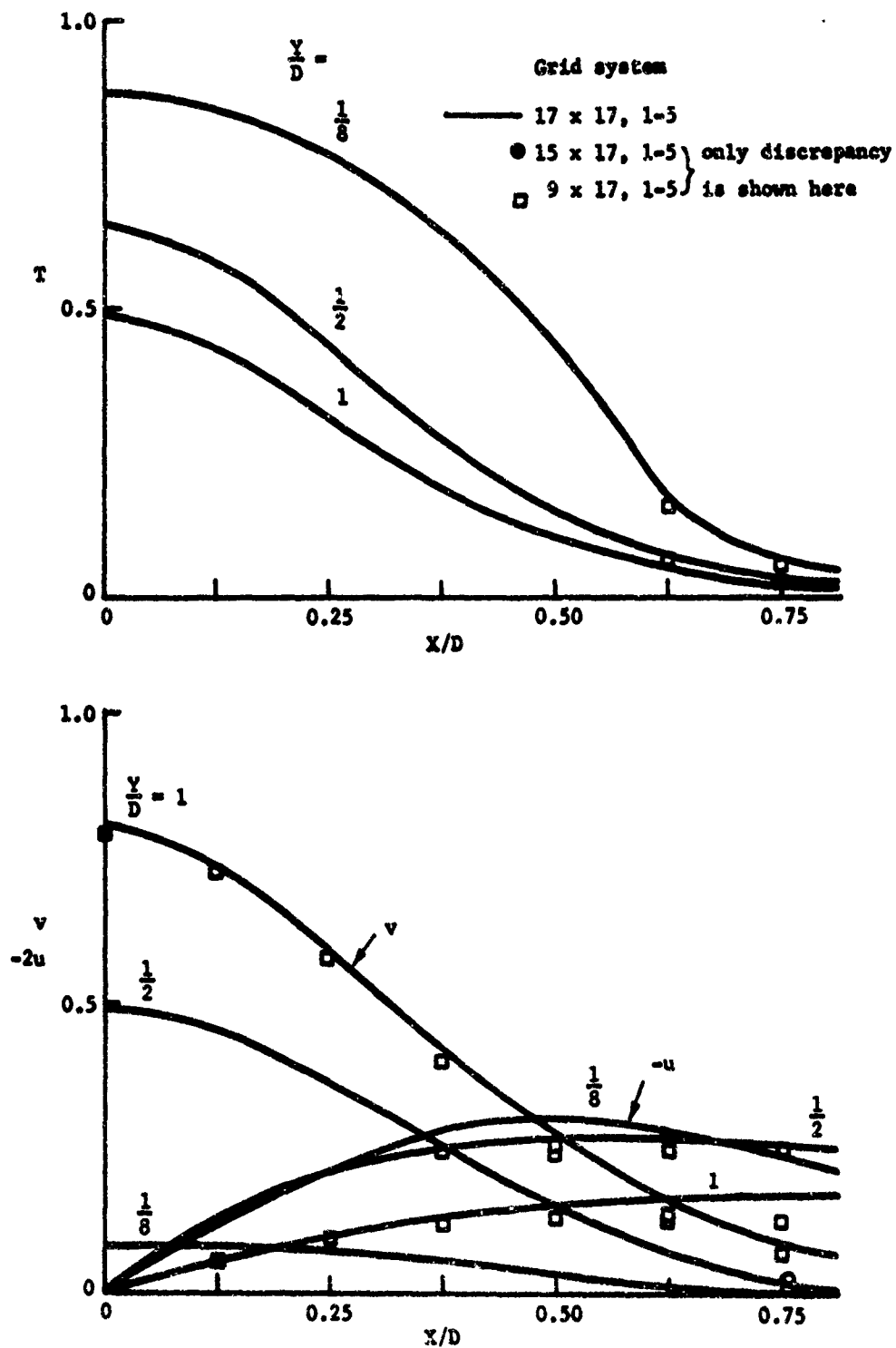
Figure 38. Effects of domain of calculations on the numerical results - horizontal extent.
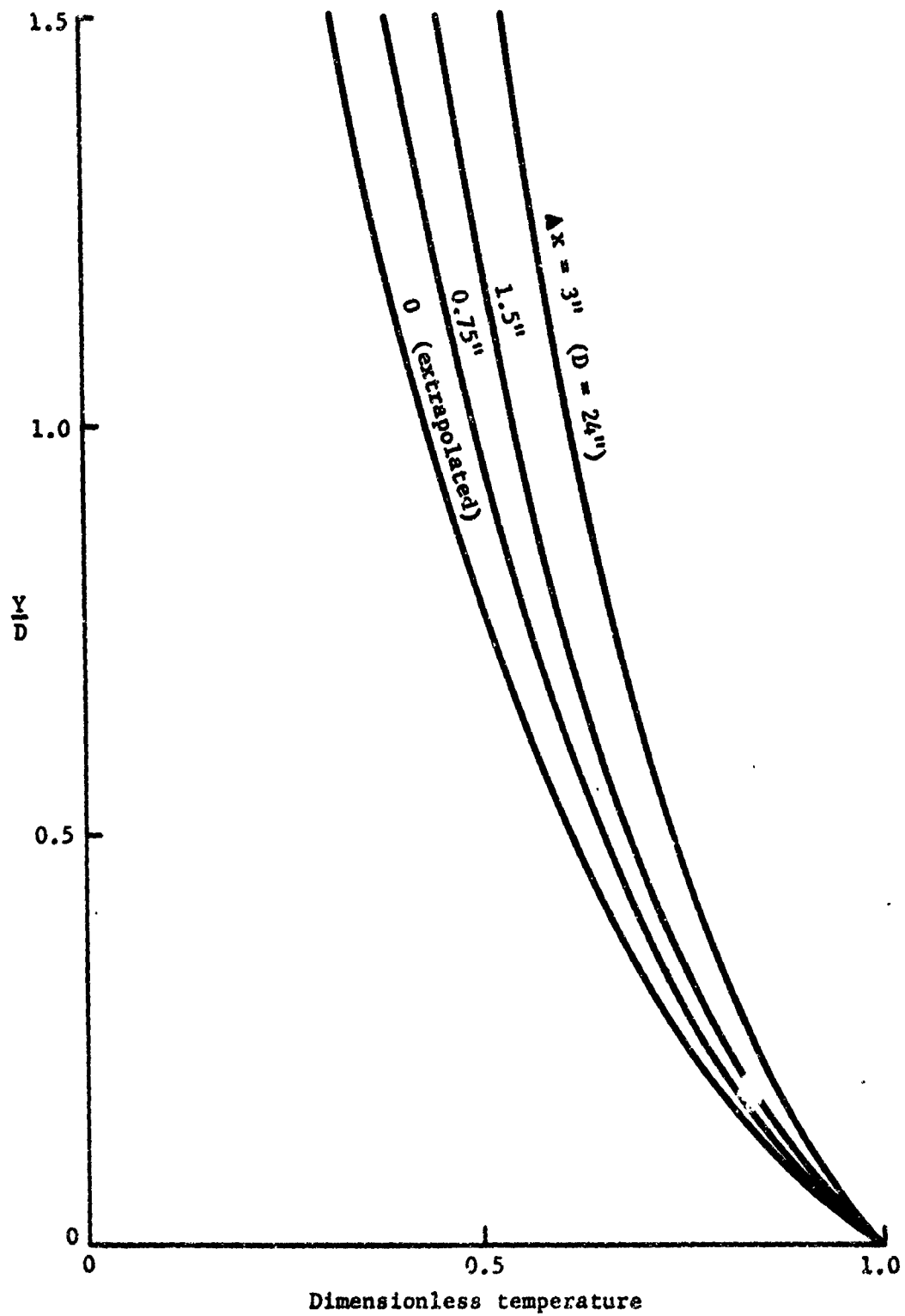
Figure 39. Effect of mesh spacing on centerline temperature ($Gr_T = 10^5$).
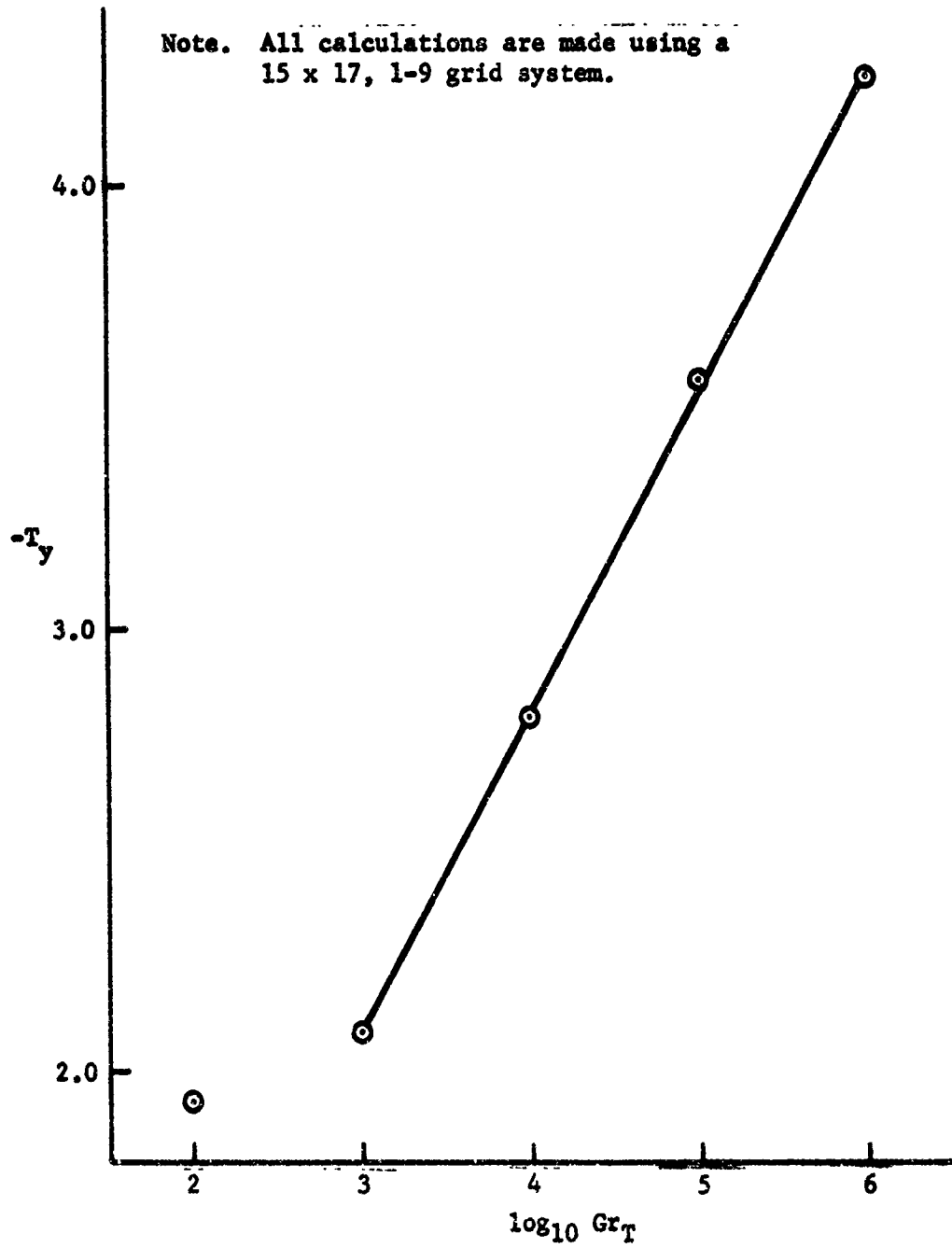
Figure 40. Relationship between T_y and Gr_T.
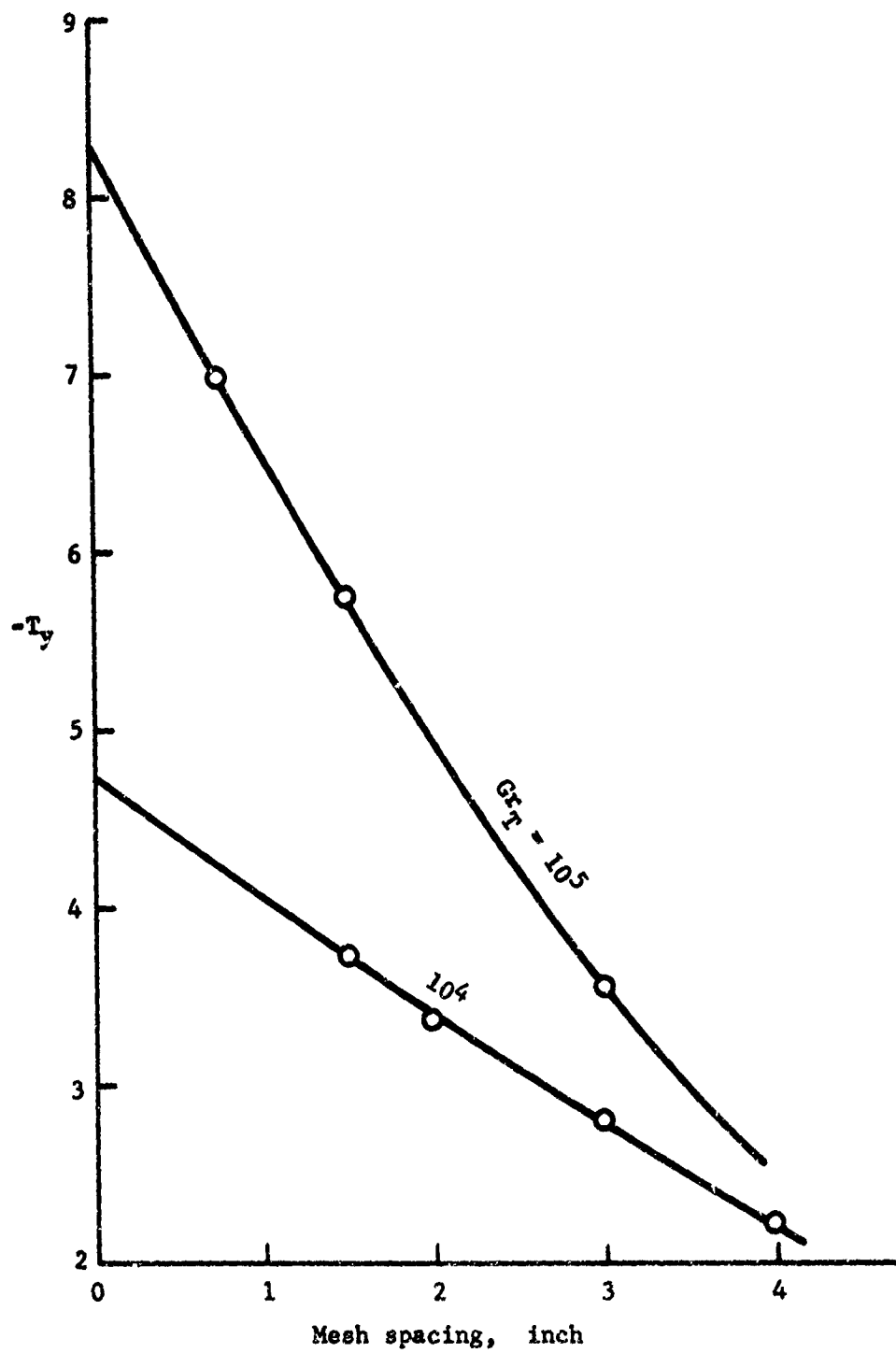
Figure 41. Effect of mesh spacing on T_y.
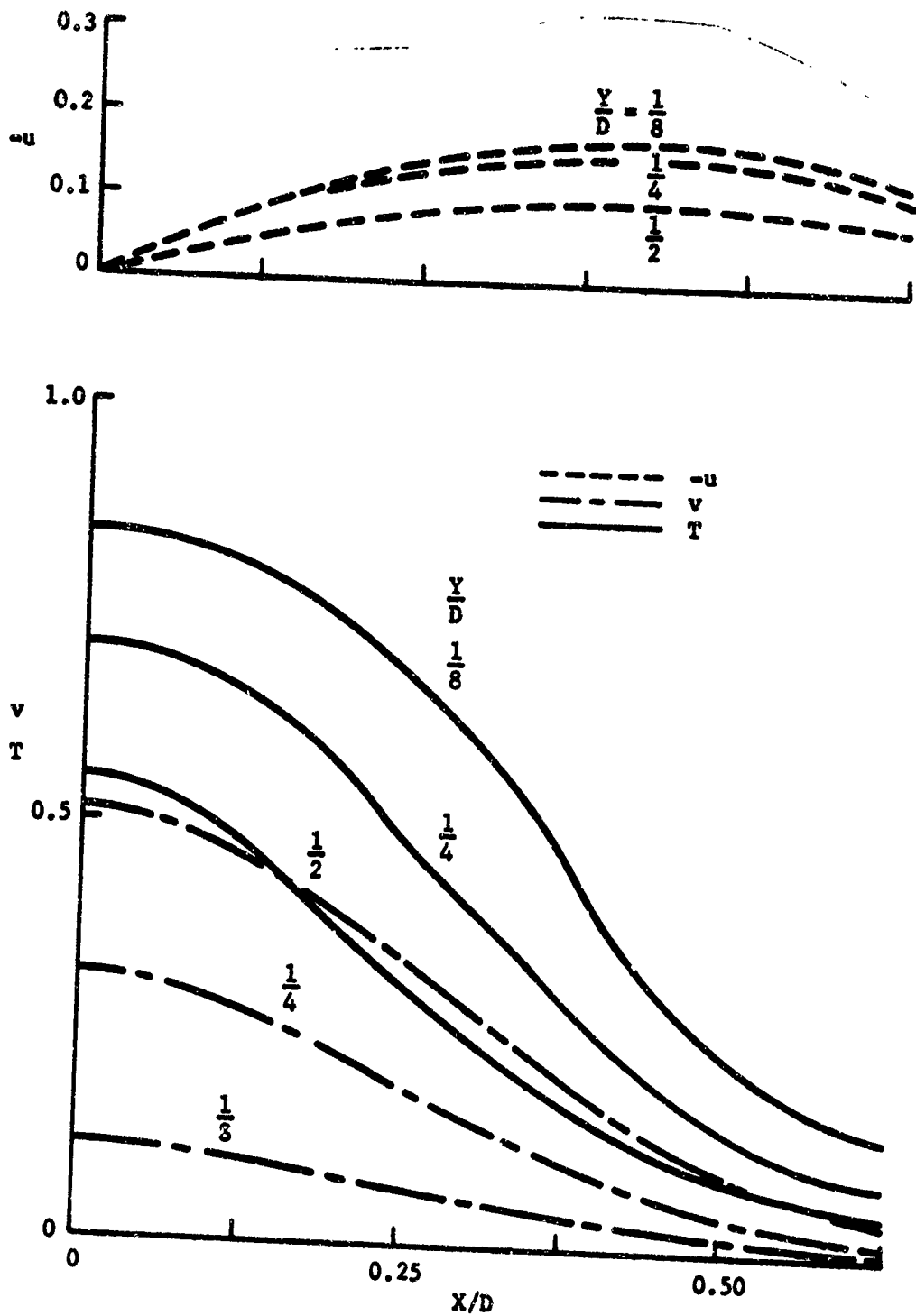
Figure 42. Numerical results for $Gr_T = 10^4$ (extrapolated to correspond to $\Delta x \to 0$).
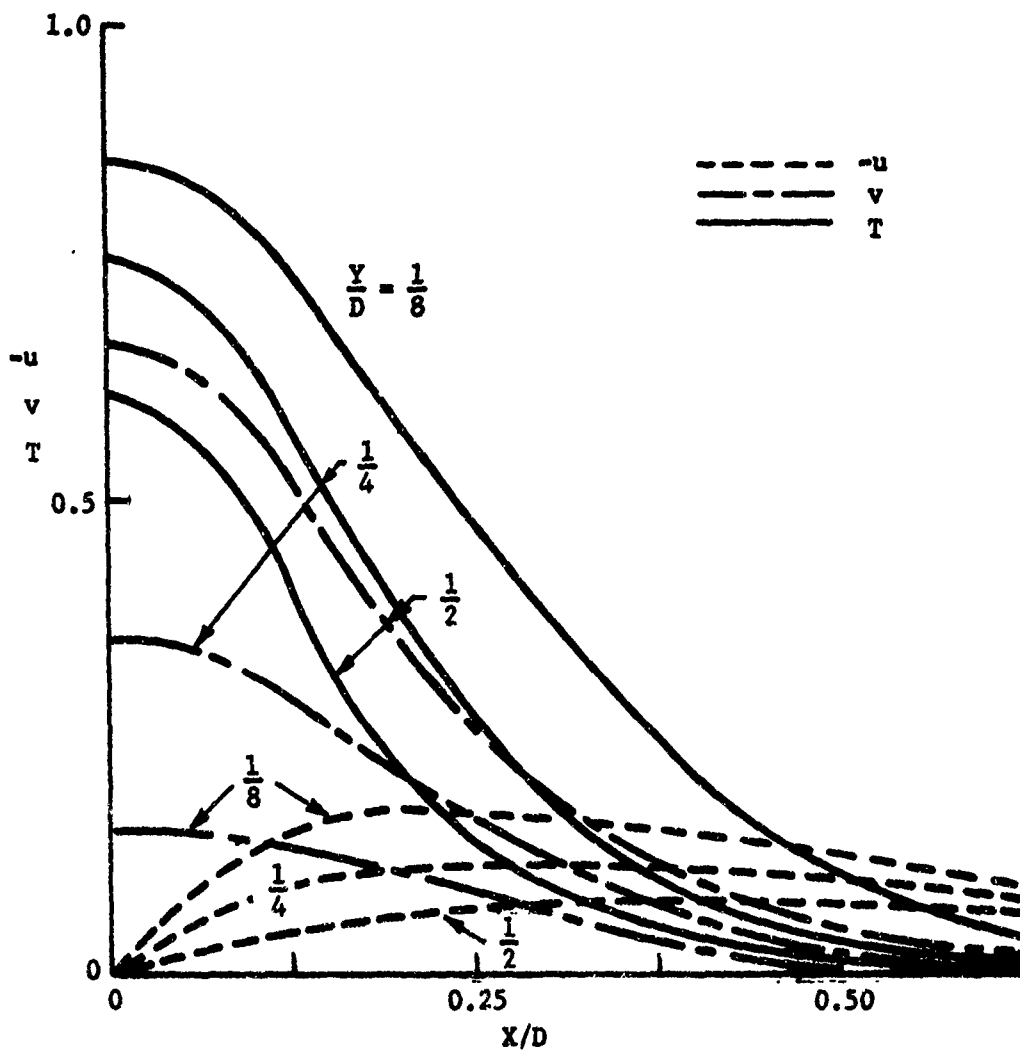
Figure 43. Numerical results for $Gr_T = 10^5$ (extrapolated to correspond to $\Delta x \rightarrow 0$).
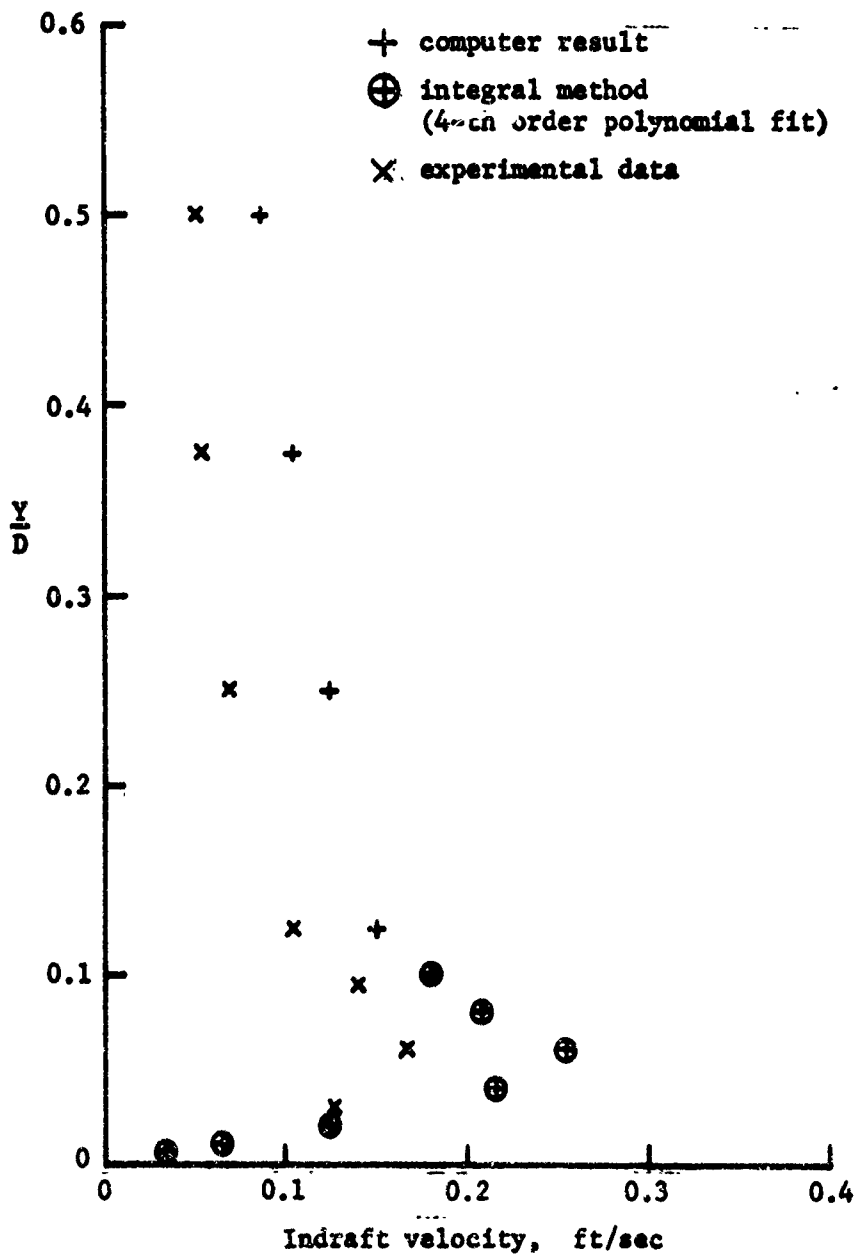
Figure 44. Indraft velocity profile near the ground (θ_p = 520°F, X = 12", U_c = 3.2 ft/sec).
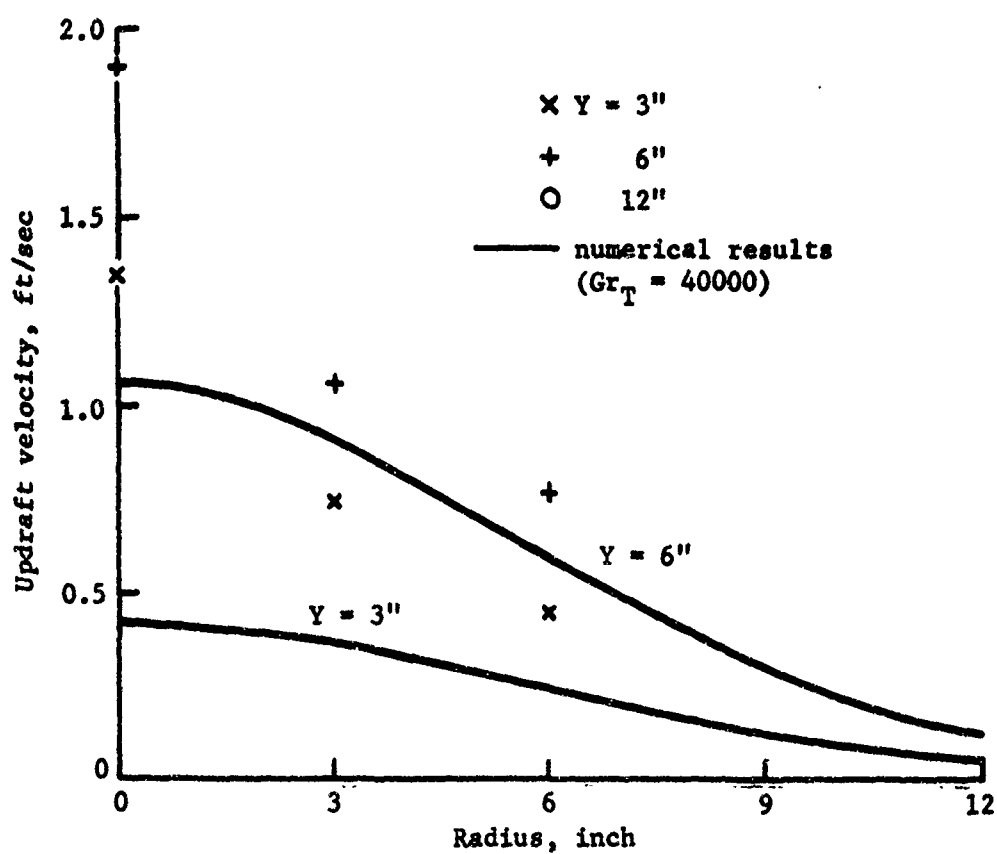
Figure 45. Comparison of updraft data with numerical results ($\Theta_p = 520^{\circ}F$).

BIBLIOGRAPHY

1. Boussinesq, P. J., _Theoric Analytique de La Chaleur_, Vol. II, Gauthier-Villars, Imprimeur-Libraire, Paris, 1903.

2. Howard, L. N., "Heat Transfer by Turbulent Convection," _Journal of Fluid Mechanics_, Vol. 17, 1963, pp. 405-432.

3. Townsend, A. A., "Temperature Fluctuations over a Heated Horizontal Surface," _Journal of Fluid Mechanics_, Vol. 5, 1959, pp. 209-241.

4. Morton, B. R., G. I. Taylor, and J. S. Turner, "Turbulent Gravitational Convection from Maintained and Instantaneous Sources," $^\sim\tau$ _Proceedings of the Royal Society_, Vol. 234A, 1956, pp. 1-22.

5. Fujii, T., "Theory of the Steady Laminar Natural Convection above a Horizontal Line Heat Source and a Point Heat Source," _International Journal of Heat and Mass Transfer_, Vol. 6, 1963, pp. 597-606.

6. Brodowicz, K., and W. .. Kierkus, "Experimental Investigation of Laminar Free Convection Flow in Air above Horizontal Line with Constant Heat Flux," _International Journal of Heat and Mass Transfer_, Vol. 9, 1966, pp. 81-93.

7. Lee, S. L., and H. W. Emmons, "Natural Convection above a Line Fire," _Journal of Fluid Mechanics_, Vol. 11, 1961, pp. 353-368.

8. Morton, B. R., "On the Dynamics of Fire Plume Convection," DASIAC Special Report 59, October 1967, Defense Atomic Support Agency.

9. Wilkes, J. O., "The Finite Difference Computation of Natural Convection in an Enclosed Rectangular Cavity," Ph.D. Thesis, University of Michigan, Ann Arbor, Michigan, 1963.

10. Fromm, J. E., _Methods in Computational Physics_, Vol. 3, Edited by B. Alder, Academic Press, New York, 1964, pp. 345-382.

11. Hellums, J., and S. Churchill, "Computation of Natural Convection by Finite Differences," Paper No. 118 presented at International Heat Transfer Conference in Denver, Colorado, 1961.

12. MacGregor, R. K., "The Natural Convection of Fluids in Rectangular Vertical Enclosures," Ph.D. Thesis, University of Washington, Seattle, Washington, 1967.

13. Nielsen, H. J., "Fire Storm Environmental Model," Report to office of Civil Defense (Contract OCD-PS-64-50), 1965.

14. Lewis, R. D., J. W. Foreman, H. J. Watson, and J. R. Thornton, "Laser Doppler Velocimeter for Measuring Flow-Velocity Fluctuations," The Physics of Fluids, Vol. 11, No. 2, 1968, pp. 433-435.

15. Foreman, J. W., R. D. Lewis, J. R. Thornton, and H. J. Watson, "Laser Doppler Velocimeter for Measurement of Localized Velocities in Liquids," IEEE Proceedings, Vol. 54, 1966, pp. 424-425.

16. Thomson, J., "On a Changing Tessellated Structure in Certain Liquids," Proceedings Glasgow Philosophical Society, Vol. 13, 1882, p. 469.

17. Benard, H., "Les Tourbillons Cellulaires Dans une Nappe Liquide," Revue Generale Des Sciences, 1900, pp. 1261-1271, and 1309-1328.

18. Rayleigh, L., "On Convection Currents in a Horizontal Layer of Fluid when the Higher Temperature is on the Underside," Scientific Paper, Vol. 6, 1916, pp. 432-446.

19. Chandrasekhar, S., Hydrodynamic and Hydromagnetic Stability, Oxford University Press, New York, 1961.

20. Ramdas, L. A., "Surface Convection and Variation of Temperature near a Hot Surface," Indian Journal of Physics, Vol. 7, 1932, p. 1.

21. Ramdas, L. A., "Convective Phenomena near a Heated Surface," Proceedings of Indian Academy of Science, Vol. 37, 1953, p. 300.

22. Croft, J. F., "The Convective Regime and Temperature Distribution above a Horizontal Heated Surface," Quarterly Journal of Royal Meteorological Society, Vol. 84, 1958, pp. 418-427.

23. Priestley, C. H. B., "Convection from a Large Horizontal Surface," Australian Journal of Physics, Vol. 7, 1954, pp. 176-201.

24. Priestley, C. H. B., "Free and Forced Convection in the Atmosphere near the Ground," Proceedings of the Royal Meteorological Society, Vol. 81, 1955, pp. 144-157.

25. Schmidt, E., Proceedings of the 4th International Congress of Applied Mechanics, Cambridge, 1934, p. 92.

26. Fishenden, M. and O. A. Saunders, An Introduction to Heat Transfer, Oxford, 1950, p. 95.

27. Jakob, M., Heat Transfer, Vol. I, Chapter 25, John Wiley and Sons, Inc., New York, 1949.

28. Tritton, D. J., "Turbulent Free Convection above a Heated Plate Inclined at a Small Angle to the Horizontal," _Journal of Fluid Mechanics_, Vol. 16, 1963, pp. 282-312.

29. Gaines, E., panel chairman, "Project FLAMBEAU," Defense Atomic Support Agency Special Report 59, October 1967.

30. Parker, W. J., R. C. Corlett, and B. T. Lee, "An Experimental Test of Mass Fire Scaling Principles," Paper No. WSCI 68-14, 1968, spring meeting, Western States Section, The Combustion Institute, University of Southern California, April 1968.

31. Lee, B. T., "Mass Fire Scaling with Small Electrically Heated Models," Paper presented at Central States Section, The Combustion Institute, University of Minnesota, March 1969.

32. Stewartson, K., "On the Free Convection from a Horizontal Plate," _Z. Angew. Math. Phy._, Vol. 9, 1958, pp. 276-281.

33. Deardorff, J. W., "A Numerical Study of Two-Dimensional Parallel-Plate Convection," _Journal of the Atmospheric Sciences_, Vol. 21, July 1964, pp. 419-438.

34. Fromm, J. E., "Numerical Solution of the Nonlinear Equations for a Heated Fluid Layer," _The Physics of Fluids_, Vol. 8, 1965, pp. 1757-1759.

35. Suriano, F. J. and K. T. Yang, "Laminar Free Convection about Vertical and Horizontal Plates at Small and Moderate Grashof Numbers," _International Journal of Heat and Mass Transfer_, Vol. 11, 1968, pp. 473-490.

36. Kane, T. J., and K. T. Yang, "Laminar Free Convection about a Horizontal Disk at Small Grashof Numbers," Technical Report 67-21, Heat Transfer and Fluid Mechanics Laboratory, Department of Mechanical Engineering, University of Notre Dame, Notre Dame, Indiana, 1967.

37. Corlett, R. C., "A Contemplative Study of Mass Fire Problems - Scaling Laws and Mathematical Formulation," R port submitted to Naval Radiological Defense Lab., San Francisco, California, O.C.D. Work Unit 2536 F, September 1966.

38. Morton, B. R., "Modeling Fire Plumes," 10th Symposium (International) on Combustion, The Combustion Institute, Pittsburgh, Pennsylvania, 1965, pp. 973-982.

39. Tritton, D. J., "The Use of a Fibre Anemonmeter in Turbulent Flows," *Journal of Fluid Mechanics*, Vol. 16, 1963, pp. 269-281.

40. Collis, D. C., "Forced Convection of Heat from Cylinders at Low Reynolds Numbers," *Journal of Aeronautical Science* Vol. 23, 1956, pp. 697-698.

41. Collis, D. C., "Two-Dimensional Convection from Heated Wires at Low Reynolds Numbers," *Journal of Fluid Mechanics*, Vol. 6, 1959, pp. 357-384.

42. Hinze, J. O., *Turbulence*, Chapler 1, McGraw-Hill Book Company, Inc., New York, 1959.

43. Torrance, K. E., "Comparison of Finite-Difference Computations of Natural Convections," *Journal of Research*, National Bureau of Standards, Vol. 72B, 1968, pp. 281-301.

44. Champagne, F. H., C. A. Sleicher, and O. H. Wehrmann, "Turbulence Measurements with Inclined Hot-Wires, Part I. Heat Transfer with Inclined Hote-Wire," *Journal of Fluid Mechanics*, Vol. 28, 1967, pp. 153-175.

45. Schlichting, H., *Boundary Layer Theory*, 4th ed. McGraw-Hill Book Company, Inc., New York, 1960, Chapters 3, 12, 14.

46. Crocco, L., "A Suggestion for the Numerical Solution of the Steady Navier-Stokes Equations," *AIAA Journal*, Vol. 3, 1965, pp. 1824-1829.

47. Neumann, J. von, and R. D. Richtmyer, "A Method for the Numerical Calculations of Hydrodynamic Shocks," *Journal of Applied Physics*, Vol. 21, 1950, pp. 232-237.

48. Pearson, C. E., "A Computational Method for Viscous Flow Problems," *Journal of Fluid Mechanics*, Vol. 21, No. 4, 1965, pp. 611-622.

49. Burstein, S. Z., "Numerical Methods in Multidimensional Shocked Flows," *AIAA Journal*, Vol. 2, 1964, pp. 2111-2117.

50. Richtmyer, R. D. and K. W. Morton, *Differerce Methods for Initial-Value Problems*, 2nd ed., Interscience Publishers, New York, 1967,

51. Ames, W. F., *Nonlinear Partial Differential Equations in Engineering*, Academic Press, New York, 1965, Chapler 7.

52. Murgai, M. P. and H. W. Emmons, "Natural Convection above Fires," *Journal of Fluid Mechanics*, Vol. 8, 1960, pp. 611-629.

53. Pearson, C. E., verbal communication.

54. Jackson, J. D., *Classical Electrodynamics*, John Wiley & Sons, Inc., New York, 1963, pp. 89-93.

55. Lees, Sidney, "Uncertainly and Imprecision," *Trans. ASME Series D, Journal of Basic Engineering*, Vol. 88, 1966, pp. 369-378.

56. Corlett, R. C., "Digital Computer Calcuation of Mass Fire Flow Fields,: Problems and Prospects," Defense Atomic Support Agency Special Report 59, October 1967, pp. 158-169.

57. Byram, G. M., "Scaling Laws for Modeling Mass Fires," Paper No. WSCI 66-15, Western States Section, The Combustion Institute (1966).

58. Kreith, F., *Principles of Heat Transfer*, International Textbook Company, Scranton, 1960.

59. Janes, E. T., *Information Theory and Statistical Mechanics*, "Brandeis Summer Institue, 1962, Statistical Physics," Ed. K. W. Ford, Benjamin, Inc., New York, 1963.

Appendix A

MOTIVATION OF RESEARCH

The origin of this project was an attempt to study the gross flow behavior in the vicinity of large unconfined fires. This problem has been the subject of several investigations during the past decade (29, 30, 31, 37). Experimental observations suggest that, in general, the physical behavior of a large fire may be described in terms of the four zones shown below (56):
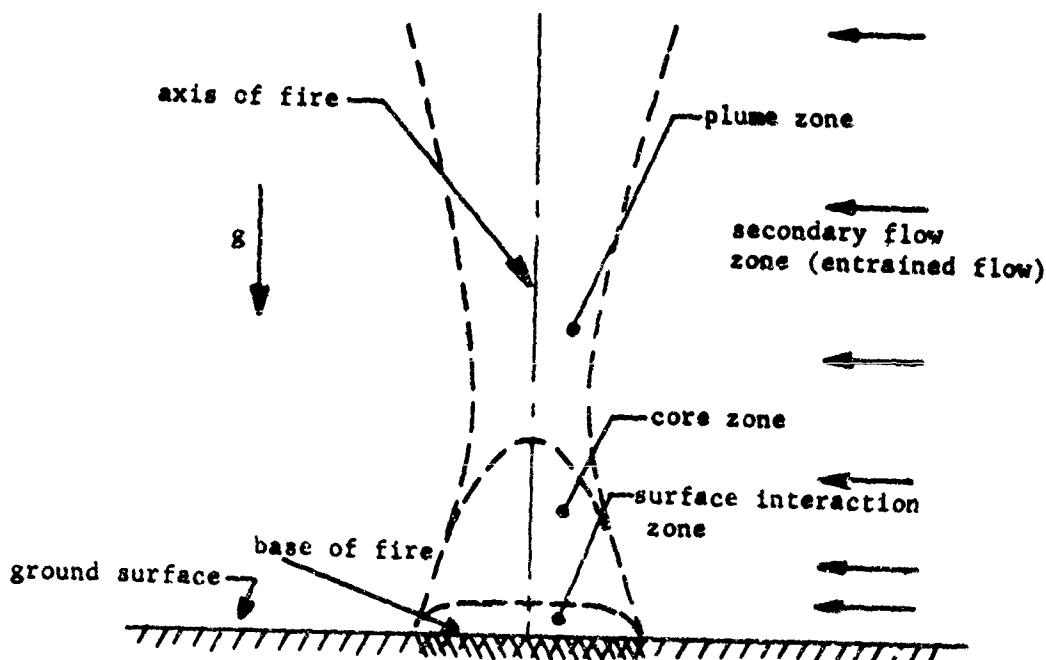
1. ## Plume Zone

   Above the fire there is a rising current of heated gases. The zone where this current is the dominant feature is called the fire

convection plume. Entrainment of ambient air and, therefore, cooling
of the rising column take place. The flow is fully turbulent. Fire
whirls may sometimes be present. The affected cross section of the
surrounding air gradually widens along the path of the ascending
mass of the hot gases until its momentum is balanced by entrained
ambient air. The flow behavior in the plume zone resembles that of
a free jet. The boundary layer assumptions are valid and under some
circumstances similarity solutions may be obtained. Mathematical and
experimental investigations of the plume have been fruitful (e.g.,
references 4, 5, 6, 7, 8, 52).

2. Secondary Flow Zone

This is the "upstream" region of cold air outside the fire. In an
otherwise still ambient atmosphere, the fluid motion in this zone
is due solely to the pressure defect resulting from the buoyancy of
the hot ascending gases. The entrainment and the associated indraft
are largest at altitudes relatively near the base of the fire. This
indraft is substantial for large fires; it tends to prevent the
outward lateral propagation of the fire. Thus when the indraft is
large enough all the burning may be confined in a relatively stationary
region. This is one reason why the ground indraft is so important
in fire behavior.

3. Surface Interaction Zone

This is the region of fuel supplies such as buildings, trees, etc.
Major destructive burning and the release of gaseous fuels take place

in this zone. Inside this zone are intricate interactions of heat and mass transfer, chemical reactions, and air entrainment. In the start-up phase of a mass fire, ignition, spreading and the interactions between individual small fires occur in this zone. The burning process in this region is usually incomplete. In a large area fire, this zone, although the source of energy supply, is usually confined in a region very close to the ground level and is very small compared with that of the whole region which is significantly influenced by the fire (Reference 29). It is believed that the detailed physico-chemical phenomena associated with combuation in this region are only local effects, and that the large scale convective motion in a fire is governed primarily by the heat release. Thus, for modeling purposes, we assume that the detailed knowledge of phenomena in this zone is not essential on understanding of the gross flow behavior of large fires.

4. Core Zone

Near the base of the fire is a region linking the surface interaction zone, the secondary flow of fresh air and the convection plume above. Here the pressure defect driving the low elevation secondary flow is developed. The winds, temperature, and oxygen concentration experienced by the surface interaction zone are determined by the core phenomena. The general understanding of the physics in this zone is essential to the studying of fire flow fields. The flow field in this zone cannot be described mathematically by the boundary layer type

formulation as used for convection plume calculations (4,5,6,7,8,52).
This aspect is demonstrated by Stewartson (32) with an example of
the natural convection above a heated horizontal plate.

The fire problems studied to date have been concerned primarily with
the convection plume well above the fire. Solutions are based on free
boundary layer approximations and the assumptions of small density
changes and similarity profiles. Results of these calculations are in
good agreement with available experimental data (4,5,7,52). Experimental
investigations of the behavior of large fires have been carried out by
personnel of Pacific Southwest Forest and Range Experiment Station.
Wood piles or simulated houses covering areas up to forty acres were
burned. Although numerous data were collected, only a very limited
amount of fire flow field data have so far been made available to the
public (29).

Due to the complexity of the details of the fire problem and the
prohibitive cost of field experiments, it is desirable to utilize
mathematical models to the greatest extent feasible. A logical start
is to try for an approximate description of the large scale flow features
with a simple mathematical model, and to then attempt to fill the gaps
by adjustment to agree with field data as available.

As discussed earlier, the flow field generated by a fire is driven
primarily by free convection effects resulting from the heating of the
air in the proximity of the fire. We regard the combustion processes
in the surface interaction zone as local in nature. We then assume

further that the heat release from the fire is the dominant factor which govern the gross behavior of the fire flow field so that the fact of combustion may be modeled by prescribed temperature or heat flux distribution at the base of the fire.

A limiting case of this is the free convection field produced by a prescribed uniform heat source. Hopefully, this will qualitatively describe the gross features of the flow induced by a large area fire and will provide a starting point for the fluid mechanical study of a fire-like flow field. Once the problems associated with this fluid mechanical model are overcome, as a second step, a more realistic model including fuel and air mixing, followed by gas phase combustion, could be developed, for example, by simulated spatial distribution of sources of heat and mass.

For mathematical simplicity, the free convection due to a horizontal heated, circular surface flush with the ground surface in an otherwise still ambient is considered as the model. This model provides a flow field which describes the basic features of a large fire as discussed earlier in this appendix.

The free convection model has also been considered as an approach to the scaling of the indraft velocity due to an area fire (31,37,57). By a dimensional analysis, Byram (57) has shown that preserving the Grashof number between model and prototype is impossible for any useful length scaling ratio. Fortunately, at the expected magnitude of Gr in a fire ($\sim 10^{15}$), the flow is fully turbulent and molecular transport

phenomena have been postulated unimportant. Thus if Gr can be neglected, for geometrically similar models, the heat flux and indraft velocity are proportional to the square-root of the length scale. The validity of this concept has been demonstrated experimentally by Lee (31) as conclusively as possible with the limited data available (30).

Appendix B

ENERGY BALANCE

The calculations for the energy balance terms summarized in Table 1 are discussed in this appendix. Three types of energy loss are considered here:

    a. Radiative losses from the aluminum plate, the asbestos ring, and the floor.

    b. Convective losses from the asbestos ring and the floor.

    c. Conductive losses through the insulation jacket and the floor.

As an example, the calculations for Run No. 1 are described below:

1. **Radiative Losses**

The following equation was used for all radiative loss calculations:

$$Q_r = \epsilon \sigma A(\theta^4 - \theta_\infty^4) \quad \text{Btu/hr}$$

where $\theta_\infty (=537^\circ R)$, $\sigma(=.1714 \times 10^{-8}$ Btu/hr-ft^2-R^4), ϵ, and A are, respectively, the ambient temperature, Stefan-Boltzmann constant, emissivity, and heat transfer area.

2. **Convective Losses**

From the experimental correlation Nu $= 0.141$ Ra$^{1/3}$ (Reference 26) and the definition of $q_c = h\Delta\theta$, we estimate:

$$q_c = 0.141k \left[Pr \frac{g\beta}{\nu^2} \right]^{1/3} \Delta\theta^{4/3}$$

Using the property values for air at $\theta_\infty(58)$, the above expression may be simplified to:

$$Q_c = 0.243 \Delta\theta^{1.33} A \quad \text{Btu/hr.}$$

The calculated energy losses for the above two items are summarized below:

Part Name	Aluminum Plate	Asbestos Ring	Floor
ϵ	.05	.96	.91
A, ft^2	3.18	.84	1.6
θ, $^\circ R$	979	740	597
Q_r, Btu/hr	229	294	110
Q_c, Btu/hr	---	231	86

3. Conductive Losses

These losses are from the insulation jacket and partly from the floor. The temperature at two points along various heat transfer paths were measured (see Figure 2 for thermocouple locations). The total heat transfer surface was divided into several parts. For each of these surfaces, an average temperature drop was obtained from the measured temperature data. Since the conduction surface area, the length of path, and the thermal conductivity (No. 4 vermiculite, see footnote on p. 15) are known, the heat transfer was calculated by:

$$Q = -k \frac{\Delta\theta}{\Delta Y} A \quad \text{Btu/hr.}$$

The calculated total conductive loss through the insulation jacket was 347 Btu/hr and the conductive loss through the floor was 45 Btu/hr.

Appendix C

TEMPERATURE CORRECTIONS

The temperature indicated by the thermocouple is corrected for losses due to radiation and conduction. We refer to the detailed configuration of the thermocouple give in Figure 20.

Heat is transferred to the exposed surface (0.4" long) of the thermocouple wire by convection and lost from the same surface by radiation. Heat is also lost by conduction through the portion of the thermocouple wire in the stainless steel tubing. For thermal equilibrium, we require that $q_{conv} = q_{cond} + q_{rad}$; this gives:

$$A_{conv} h(\theta_a - \theta_t) = A_{cond} k_{wire} (\theta_t - \theta_\infty)/L + A_{rad} \sigma \epsilon (\theta_t^4 - \theta_\infty^4)$$

where

$A_{conv} = A_{rad} = \pi d \ell(\ell - D) + \pi D^2 = 7.29 \times 10^{-5} \text{ ft}^2$

$A_{cond} = \pi d^2/4 = 2.16 \times 10^{-7} \text{ ft}^2$

$k_{wire} = k_{copper} + k_{constantan} = 218 + 12.8 = 231 \text{ Btu/hr-ft-R}$

$\epsilon = \text{emissivity} = 0.8$

$\sigma = .1714 \times 10^{-8} \text{ Btu/hr-ft}^2\text{-R}^4$

$\theta_\infty = \text{ambient temperature} = 537^\circ R$

$\theta_a = \text{true mean temperature of the air, } ^\circ R$

$\theta_t = \text{mean temperature indicated by thermocouple output, } ^\circ R$

$L = \text{length of conduction path} = 0.25 \text{ ft (see Figure 20).}$

Substituting the appropriate values into the above equation and rearranging, we get:

$$\Delta\theta = \theta_a - \theta_t = 2.75 \frac{\theta_t - \theta_\infty}{h} + \frac{.1374}{h} \left[\left(\frac{\theta_t}{100} \right)^{4\cdot} - \left(\frac{\theta_\infty}{100} \right)^4 \right] \qquad (C-1)$$

where the first term on the right hand side of the equation is the correction due to conduction loss in $^\circ F$ and the last term is the correction due to radiation loss in $^\circ F$.

Consider the heat transfer surface in the exposed portion of the thermocouple as composed of a sphere of diameter D (for the bead) and a circular cylinder of diamter d (for the wire); an equivalent wire diameter weighted by surface area was used for heat transfer coefficient calculations.

$$d_e = \frac{(\pi d \ell)d + (\pi D^2)D}{\pi d \ell + \pi D^2} = 0.0142".$$

At an assumed air temperature (e.g., that calculated based on conduction only), the properties of air may be found in Appendix III of Reference 58), with the local mean velocity from velocity measurements, the local Reynolds number may be calculated. From heat transfer correlation (e.g., Reference 58, Figure 7-3), the heat transfer coefficient h may be calculated. The temperature corrections thus obtained are shown in Figures 21 and 22. A numerical example is given below.

Consider the point X = 0, Y = 0.02" for Run 1 (Figure 21). The local mean velocity was obtained from interpolation between the points

Y = 0 and 3". Q_a was estimated to be 458°F. The following additional data were used:

V = 0.009 ft/sec

θ_t = 782°R

k = .0224 Btu/hr-ft-F

ν = 4.3 x 10^{-4} ft^2/sec

Re = Vd_e/ν = 0.024

since this Reynolds number is so small (forced convection data unavailable), the actual heat transfer is in the free convection regime. Setting Ra = PrGr = $PrRe^2$ and using Figure 7-3, Reference (58), we get:

$$Nu = 0.51$$

$$h = Nu(k/d_e) = 9.5 \ Btu/hr-ft^2-F.$$

Substituting the appropriate values into Equation (C-1), we get:

$$\Delta\theta = 116°F$$

Finally,

$$\theta_a = \theta_t + \Delta\theta = 438°F$$

Error Analysis

In the above calculation procedure, we need to estimate the values of θ_a and V for computing the heat transfer coefficient h. From the dependence of h on the governing parameters, it can be shown that h depends only weakly on the value of θ_a and more strongly on V. Experimental heat transfer correlation (Reference 58) shows that the change of Nu is very gradual in the range of our interest (Ra $\sim 10^{-4}$). Spot

checking of the results were made and it was found that an error of $20^\circ F$ on θ_a would result $1^\circ F$ and a 20% error of V would result a $5^\circ F$ change in the temperature corrections. Since $20^\circ F$ is larger than the possible variation in our temperature measurements and 20% error in V is a reasonable upper bound, the estimated error in our temperature corrections would be less than $6^\circ F$.

The source of error during data taking was basically due to the drifting of the recorder chart paper, (1 mm is a quite noticeable amount). This drift would represent a maximum possible error of 0.1 mv in the thermocouple output, or an error of $\sim 5^\circ F$. Consequently, the total possible error in our temperature measurements would be approximately $11^\circ F$. Since the main contribution of correction is due to radiation loss which increases rapidly with the wire temperature, it is clear that the amount of correction and hence the associated error will be greatly reduced when the thermocouple gets away from the plate.

Appendix D

DERIVATION OF EQUATION (5-4)

$$\overline{W'} = \overline{(E^2-A')^2} = \overline{\left[(E^2-A) + (A-A')\right]^2} = \overline{(E^2-A)^2} + 2(A-A')\overline{(E^2-A)} + (A-A')^2$$

Multiplying by C_1 and rearranging the first of Equation (5-4) will result.

$$\overline{W'^2} = \overline{(E^2-A')^4} = \overline{\left[(E^2-A) + (A-A')\right]^4}$$

$$= \overline{(E^2-A)^4} + 4(A-A')\overline{(E^2-A)^3} + 6(A-A')^2\overline{(E^2-A)^2}$$

$$+ 4(A-A')^3\overline{(E^2-A)} + (A-A')^4$$

Since,

$$\overline{(E^2-A)^3} = \overline{\left[(E^2-\overline{E^2}) + (\overline{E^2}-A)\right]^3}$$

$$= \overline{(E^2-\overline{E^2})^3} + 3\overline{(\overline{E^2}-A)}\overline{(E^2-\overline{E^2})^2} + 3\overline{(\overline{E^2}-A)^2(E^2-\overline{E^2})} + \overline{(\overline{E^2}-A)^3}$$

$$= \overline{(E^2-\overline{E^2})^3} + 3\overline{(\overline{E^2}-A)}\ \overline{\left[(E^2-A) - (\overline{E^2}-A)\right]^2} + \overline{(\overline{E^2}-A)^3}$$

$$= \overline{(E^2-\overline{E^2})^3} + 3\overline{(\overline{E^2}-A)}\ \overline{\left[(E^2-A)^2 - (\overline{E^2}-A)^2\right]} + \overline{(\overline{E^2}-A)^3}$$

$$= \overline{(E^2-\overline{E^2})^3} + 3\overline{(\overline{E^2}-A)}\overline{(E^2-A)^2} - 2\overline{(\overline{E^2}-A)^3}$$

We have,

$$\overline{W'^2} = \overline{(E^2-A)^4} + 4(A-A')\overline{(E^2-\overline{E^2})^3} + 12(A-A')\overline{(\overline{E^2}-A)}\overline{(E^2-A)^2} - 8(A-A')\overline{(\overline{E^2}-A)^3}$$

$$+ 6(A-A')^2\overline{(\overline{E^2}-A)^2} + 4(A-A')^3\overline{(\overline{E^2}-A)} + (A-A')^4. \tag{D-1}$$

Multiplying by C_1^2 and neglecting the term $4C_1^2(A-A')\overline{(E^2-\overline{E^2})^3}$, the second of Equation (5-4) will result.

This neglected term is not zero in general but is very small relative to the retained terms for an assumed probability density of E. To illustrate, let this distribution be Gaussian,

$$P(E) = \frac{\lambda}{\sqrt{\pi}} \exp\left[-\lambda^2(E-\bar{E})^2\right]$$

where $\bar{E}$ is the average of E; $\lambda^2 = (2\sigma_E^2)^{-1}$ and σ_E = variance of E.

Letting $u = \lambda(E-\bar{E})$ we have

$$\overline{E^2} = \int_{\infty}^{\infty} E^2 \ PdE = \frac{1}{\sqrt{\pi}}\int_{-\infty}^{\infty}\left|\frac{u}{\lambda} + \bar{E}\right|^2 e^{-u^2}du = \bar{E}^2 + \frac{1}{2\lambda^2}$$

$$\overline{(E^2-\overline{E^2})^3} = \int_{\infty}^{\infty}(E^2-\overline{E^2})^3 PdE$$

$$= \frac{1}{\sqrt{\pi}}\int_{\infty}^{\infty}\left[\left(\frac{u}{\lambda} + \bar{E}\right)^2 - \left(\bar{E}^2 + \frac{1}{2\lambda^2}\right)\right]^3 e^{-u^2} \ du$$

$$= \frac{1}{\lambda^6\sqrt{\pi}}\int_{\infty}^{\infty}\left[u^2 + 2\lambda\bar{E} \ u - 1/2\right]^3 e^{-u^2} \ du$$

$$= \frac{1}{\lambda^6}(1 + 6\lambda^2 \ \bar{E}^2)$$

or,

$$\overline{(E^2-\overline{E^2})^3} = 8 \ \sigma_E^4 \ (1 + 3\bar{E}^2)$$

From the data given in Table 6, the value of $\overline{(E^2-\overline{E^2})^3}$ and hence the neglected term $4C_1^2C_2\overline{(E^2-\overline{E^2})^3}$ can be calculated. Calculations show that this term is on the order of $10^{-3} - 10^{-5}$ and its adjacent terms in Equation (D-1) are on the order of 1. Therefore, the neglect of this term does not introduce apprecialbe error and is well justified.

Appendix E

RANDOM VARIABLE ALGORITHMS -

NUMERICAL SIMULATION OF HOT-WIRE DATA

Two basic schemes for obtaining the random variables for hot-wire
data simulation are described in this appendix. The parameters to be
specified consist of the standard deviation of the fluctuations and
correlation coefficients as defined in Equations (5-8) and (5-9). In
this procedure, a set of four random numbers are generated for computing
the normalized fluctuating velocities as defined in Equation (5-7). The
computation involved is such that the fluctuating velocities are consistent
with the specified correlation coefficients. The algorithms for these
computations are described below.

For convenience of discussion, the flow variables $(\overline{U}, \overline{V}, \overline{W}, \overline{T})$ in
Equation (5-7) are redesignated by ϕ_i, $i = 1, 2, 3, 4$; thus the correla-
tion coefficients become $\overline{\phi_i \phi_j}$. The problem is to compute a random
sequence of sets of ϕ_i consistent with the specified set of values of
$\overline{\phi_i \phi_j}$. Two schemes for obtaining ϕ_i are described below.

NORMAL DISTRIBUTION SCHEME

Let ψ_i be independent random variables with zero mean and unity
standard deviation. Let P be the probability distribution function of
the flow variables ϕ_i, and set:

$$\phi_i = \sum_{j=1}^{4} \alpha_{ij} \, \psi_j \qquad (E-1)$$

where α_{ij} are constants. Noting that the Jacobian C of transformation between ϕ_i-space and ψ_i-space is a constant.

$$\overline{\phi_i \phi_j} = \frac{1}{C} \int_{all\psi_i} \sum_{k,\ell=1}^{4} \alpha_{ik} \alpha_{j\ell} \psi_k \psi_\ell \, Pd\psi_i$$

$$= \frac{1}{C} \sum_{k,\ell=1}^{4} \alpha_{ik} \alpha_{j\ell} \overline{\psi_k \psi_\ell} = \frac{1}{C} \sum_{k=1}^{4} \alpha_{ik} \alpha_{jk} \qquad (E-2)$$

It is convenient to choose $C = 1$. The quantity ψ_i satisfy:

$$\overline{\psi_k \psi_\ell} = \delta_{k\ell}$$

where $\delta_{k\ell}$ is the Kronecker delta. Letting:

$$\overline{\phi_i \phi_j} = K_{ij} + \delta_{ij}, \text{ and}$$

$$\alpha_{ij} = \delta_{ij} - a_{ij}$$

we have,

$$\overline{\phi_i \phi_j} = K_{ij} + \delta_{ij} = \sum_{k=1}^{4} (\delta_{ik} - a_{ik})(\delta_{jk} - a_{jk})$$

whence

$$a_{ij} = \frac{1}{2} \left[\sum_{k=1}^{4} a_{ik} a_{jk} - K_{ij} \right] \qquad (E-3)$$

Note here that if the ϕ's are independent then $\overline{\phi_i \phi_j} = \delta_{ij}$, K_{ij} and a_{ij} as perturbation about an uncorrelated distribution. This method has been found to converge rapidly, Equation (E-3) is the basis for an iterative solution for the a_{ij} starting with $a_{ij} = 0$. Once a_{ij} are computed, the values α_{ij} and hence ϕ_i can be computed.

An approach to measurement problems based on principle of least bias has been discussed by Lees (55) and Janes (59). Following the formalism presented by Lees, we find that if only first and second moments of the flow variables (u, v, w, ϕ') are prescribed, e.g., $\overline{u}$, $\overline{v}$, σ_u^2, $\overline{uv}$, etc., the least biased distribution function consistent with the given set of moments and correlation coefficients is given by Equation (E-1) with the ϕ's Gaussian. Gaussian distribution was chosen for all basic calculations.

AN ALTERNATIVE GENERAL SCHEME

This scheme is the same as above except for higher correlations and is designed for consideration of a number of random number probability distributions. For a given set of correlation coefficients $\left|\overline{\phi_i \phi_j}\right| \leq 1$, the following set of relations are first written:

$$\overline{\phi_1 \phi_2} = a$$

$$\overline{\phi_2 \phi_3} = b_1 \overline{\phi_1 \phi_2} + b_2$$

$$\overline{\phi_3 \phi_4} = b_1 + b_2 \overline{\phi_1 \phi_2} \qquad\qquad (E-4)$$

$$\overline{\phi_1 \phi_4} = c_1 + c_2 \overline{\phi_1 \phi_2} + c_3 \overline{\phi_1 \phi_3}$$

$$\overline{\phi_2 \phi_4} = c_1 \overline{\phi_2 \phi_1} + c_2 + c_3 \overline{\phi_2 \phi_3}$$

$$\overline{\phi_3 \phi_4} = c_1 \overline{\phi_3 \phi_1} + c_2 \overline{\phi_3 \phi_2} + c_3$$

where a, b_1, b_2, c_1, c_2, c_3 are constants to be solved in terms of $\overline{\phi_i \phi_j}$. The computation will proceed if these constants satisfy the following requirements:

$$|a| \leq 1$$
$$|b_1| + |b_2| \leq 1 \qquad \text{(E-5)}$$
$$|c_1| + |c_2| + |c_3| \leq 1$$

Otherwise, the set $\overline{\phi_i \phi_j}$ will be called inconsistent and the computation is terminated.

Take four independent random numbers ψ_i, $i = 1, 2, 3, 4$ from a set of specified probability density (e.g, Gaussian distribution) and four more independent random numbers R_i, $i = 1, 2, 3, 4$ from a set which is uniformly distributed on the interval $(0, 1)$ and define $G(R, c)$ such that:

$$G(R, c) = 1 \quad \text{for } R \leq c$$
$$= 0 \quad \text{for } R > c \qquad \text{(E-6)}$$

The flow variables ϕ_i are then calculated as follows:

$$\phi_1 = \psi_1$$

$$\phi_2 = \text{Sign}(a)G(R_1, |a|)\phi_1 + G(R_1, 1-|a|)\psi_2$$

$$\phi_3 = \text{Sign}(b_1)G(R_2, |b_1|)\phi_1 + \text{Sign}(b_2)G(R_2, |b_2|)\phi_2 \qquad \text{(E-7)}$$
$$+ G(R_2, 1-|b_1|-|b_2|)\psi_3$$

$$\phi_4 = \text{Sign}(c_1)G(R_3, |c_1|)\phi_1 + \text{Sign}(c_2)G(R_3, |c_2|)\phi_2 + \text{Sign}(c_3)G(R_3,$$

$$|c_3|)\phi_3 + G(R_3, 1-|c_1|-|c_2|-|c_3|)\phi_4 \qquad (E-7)$$

GENERATION OF THE ψ_i

The random variables ψ_i used above are generated from two basic sets: a normally distributed set with mean zero standard deviation unity and a uniformly distributed set R_i on the interval (0, 1). The former was used for obtaining the normally distributed ϕ_i and the latter was used for obtaining the normally distributed R_i and three other types of distribution of ψ_i.

$$\psi = 2\sqrt{3}(R - 0.5) \qquad (E-8)$$

$$\psi = +1 \quad \text{for } R \geq 0.5$$
$$-1 \quad \text{for } R < 0.5 \qquad (E-9)$$

$$\begin{pmatrix} \psi_a \\ \psi_b \end{pmatrix} = \sqrt{0.355773\left(\frac{1-R}{R}\right)^{-2/3} - 0.79} \qquad (E-10)$$

Equations (E-8) and (E-9) describe a uniform distribution of ψ in the range $-\sqrt{3} \leq \psi \leq \sqrt{3}$ and an equal distribution of $\psi = \pm 1$, respectively. Equation (E-10) is derived from Cauchy distribution,

$$f(\psi) = \frac{2}{\pi}(1 + \psi^2)^{-2}$$

Let

$$R = \frac{\int_{-\infty}^{\psi} f(\psi') \, d\psi}{\int_{-\infty}^{\infty} f(\psi') \, d\psi}$$

whence

$$\pi (R - 1/2) = \frac{\psi}{1+\psi^2} + \tan^{-1}\psi \ , \quad \left|\tan^{-1}\psi\right| < \frac{\pi}{2}$$

Expand the above equation for $\psi \gg 0$ and rearrange,

$$\pi (1 - R) = \frac{2}{3\psi^3}\left(1 - \frac{6}{5\psi^2}\right)$$

Solving this equation for ψ, Equation (E-10) is obtained. Equation

(E-10) is used for the tail end values of R (i.e., for $R \gg 0$). A

rejection scheme based on Equation (E-10) is described in the following

block diagram:
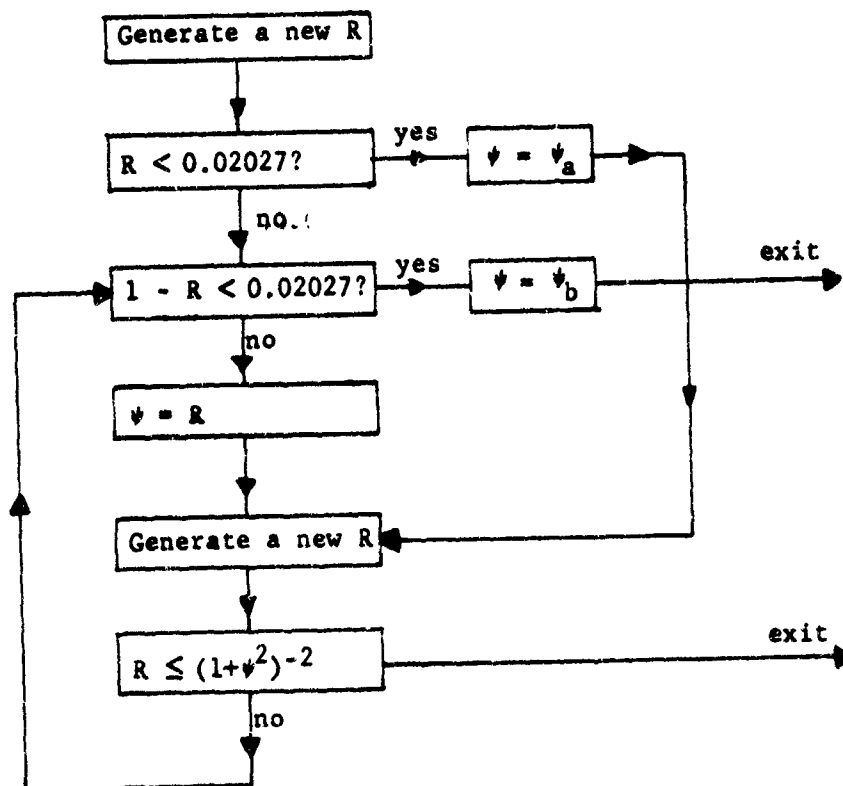
COMPUTER PROGRAM

This program is written in FORTRAN IV computer language. Three permutation schemes have been used in the main program for the purpose of parametric studies. Since there is no difficulty in programming these schemes, only one of them is included here.

Input Data

1. AW, BW, CC, CN, AL, GAM correspond to A, B, k^2, 0.5, α, γ, in Equation (5-10).

   PHIV, THEV, VM correspond to ϕ_v, θ_v, V_m in the sketch on p. 45

   ID - display index: -2 means complete display; -1 means standard display.

   NO - a number to initialize random numbers.

2. SUTI(I), SVTI(I), SWTI(I) correspond to a matrix of values of σ_u, σ_v, σ_w.

3. CKUV, CKVW, CKWU, CKUT, CKVT, CKWT correspond to the six correlation coefficients in Equation (5-9).

   STT = σ_θ

   DPHIW = $\Delta\phi_w$ (interval of ϕ_w, wire orientation)

Output Data

1. UBX, VBX, WBX, TBX are, respectively, the simulated average values of u, v, w, θ'.

2. SUTX, SVTX, SWTX, STTX are, respectively, the simulated values of σ_u, σ_v, σ_w, σ_θ.

3. CKUVX, CKVWX, CKWUX, CKUTX, CKVTX, CKWTX are, respectively, the simulated values of K_{uv}, K_{vw}, K_{wu}, $K_{u\phi}$, $K_{v\phi}$, $K_{w\phi}$.

4. EL, LOB, L1B, L2B are, respectively, the simulated values of $\overline{E}$, $\overline{W^{1/2}}$, $\overline{W}$, $\overline{W^2}$. SE, SL0, SL1, SL2 are, respectively, the standard deviation of the simulated values of E, $W^{1/2}$, W, W^2.

5. RL0, RL1, RL2 are, respectively, the values of $\overline{W^{1/2}}$, $\overline{W}$, $\overline{W^2}$ divided by their corresponding values for $\phi_w = 0^\circ$.

6. RO1 $= \overline{(W^{1/2})}^2/\overline{W}$, RO2 $= \overline{(W^{1/2})}^4/\overline{W^2}$, R12 $= \overline{W}^2/\overline{W^2}$.

```
      HOT WIRE SIMULATION PROGRAM - PARAMETER VARIATION SCHEME NUMBER 1A
      SYSTEMATIC VARIATION OF SINGLE VARIABLE DISTRIBUTION FUNCTIONS
      E=SQRT((1.0+AL*TT)*AW+(1.0+GAM*AL*TT)*BW*(SQRT(UPP2+CC*LPL2))**CN)
      REAL LOB,L1B,L2B,LOR,L1R,L2R
      LOGICAL FLAG
      DIMENSION C(4,4),B(4,4,4),SC(4),SB(4,4),CK(4,4),SUTI(100),SVTI(100
     1),SWTI(100),SUMF(20),UTT(5000),VTT(5000),WTT(5000),TTT(5000),Z(4),
     2R(3)
      COMMON AW,BW,AL,CC,CN,PHIV,THEV,PHIW,THEW,VM,SUT,SVT,SWT,STT,CKUV,
     1CKVW,CKWU,CKUT,CKVT,CKWT,NMAX,IC,ID,CK,B,SB,C,SC,FLAG,EB,SE,LOB,SL
     20,L1B,SL1,L2B,SL2,DPHIW,Z,R,SUME,UTT,VTT,WTT,TTT,GAM
      READ(5,1)AW,BW,CC,CN,AL,GAM,PHIV,THEV,VM,ID,NO
    1 FORMAT(2F8.4,4F7.4,2F8.3,F8.4/I2,I6)
      WRITE(6,2)AW,BW,CC,CN,AL,GAM,PHIV,THEV,VM,ID,NO
    2 FORMAT(1;3H1HOT WIRE SIMULATION PROGRAM - PARAMETER VARIATION SCHF
     1ME 1A- VARIATION OF DIST. FCN. INDEX IC AND NO. TRIALS N  /67H E=S
     2QRT((1.0+AL*TT)*AW+(1.0+GAM*AL*TT)*BW*(SQRT(UPP2+CC*UPL2))**CN)/4H
     30AW=F7.4,2X3HBW=F7.4,2X3  CC=F7.4,2X3HCN=F7.4,2X3HAL=F7.4,2X4HGAM=F
     47.4,2X5HPHIV=F8.3,2X5HTHEV=F8.3,2X3HVM=F7.4/4H ID=I2,2X3HNO=I6)
      RN=RNU(NO)
      RN=RNN(NO)
      I=0
    3 I=I+1
      READ(5,4)SUTI(I),SVTI(I),SWTI(I)
    4 FORMAT(6F10.5)
      IF(SUTI(I).GE.0.0)GO TO 3
      IS=I-1
    5 READ(5,4)CKUV,CKVW,CKWU,CKUT,CKVT,CKWT,STT,DPHIW
      IF(CKUV.LT.0.0)GO TO 10
      WRITE(6,6)CKUV,CKVW,CKWU,CKUT,CKVT,CKWT,STT,DPHIW
    6 FORMAT(6HOCKUV=F7.4,3X5HCKVW=F7.4,3X5HCKWU=F7.4,3X5HCKUT=F7.4,3X5H
     1CKVT=F7.4,3X5HCKWT=F7.4,3X4HSTT=F7.3,3X6HDPHIW=F8.3)
      DO 9 I=1,IS
      SUT=SUTI(I)
      SVT=SVTI(I)
      SWT=SWTI(I)
      WRITE(6,7)SUT,SVT,SWT
    7 FORMAT(5HOSUT=F9.5,5X4HSVT=F9.5,5X4HSWT=F9.5)
      DO 9 J=1,4
      IC=J-1
      DO 9 K=1,3
      IF(K.EQ.1)NMAX=100
      IF(K.EQ.2)NMAX=400
      IF(K.EQ.3)NMAX=1000
      WRITE(6,8)IC,NMAX
    8 FORMAT(4HOIC=I2,5X5HNMAX=I4)
      CALL XWIPF
      IF(.NOT.FLAG)GO TO 5
    9 CONTINUE
      GO TO 5
   10 STOP
      END
```

```
      SUBROUTINE XWIRF
      REAL LOB,L1B,L2B,LOR,L1R,L2R
      LOGICAL FLAG
      DIMENSION C(4,4),R(4,4,4),SC(4),SR(4,4),CK(4,4),SUTI(100),SVTI(100
     1),SWTI(100),SUME(20),UTT(5000),VTT(5000),WTT(5000),TTT(5000),Z(4),
     2R(3)
      COMMON AW,BW,AL,CC,CN,PHIV,THEV,PHIW,THEW,VM,SUT,SVT,SWT,STT,CKUV,
     1CKVW,CKWU,CKUT,CKVT,CKWT,NMAX,IC,ID,CK,R,SB,C,SC,FLAG,EE,SE,LOB,SL
     20,L1B,SL1,L2B,SL2,DPHIW,Z,R,SUME,UTT,VTT,WTT,TTT,GAM
      THEW=0.0
      PHIW=-DPHIW
    1 PHIW=PHIW+DPHIW
      IF(PHIW.GT.180.0)GO TO 2
      IF(PHIW.GT.90.0.AND.CKUV.EQ.0.0.AND.CKVW.EQ.0.0.AND.CKVT.EQ.0.0.AN
     1D.CKWT.EQ.0.0.AND.CKWU.EQ.0.0)GO TO 2
      CALL WIRFSP
      IF(.NOT.FLAG)GO TO 3
      GO TO 1
    2 IF(CKUV.EQ.CKWU.AND.CKVT.EQ.CKWT)GO TO 3
      THEW=90.0
      PHIW=0.0
      CALL WIRESP
    3 RETURN
      END
```

```
      SUBROUTINE WIRESP
      RFAL LOB,L1B,L2B,LOR,L1R,L2R
      LOGICAL FLAG
      DIMENSION C(4,4),B(4,4,4),SC(4),SB(4,4),CK(4,4),SUTI(100),SVTI(100
     1),SWTI(100),SUME(20),UTT(5000),VTT(5000),WTT(5000),TTT(5000),Z(4),
     2R(3),ALF(4,4),SUMA(4,4)
      COMMON AW,BW,AL,CC,CN,PHIV,THEV,PHIW,THEW,'M,SUT,SVT,SWT,STT,CKUV,
     1CKVW,CKWU,CKUT,CKVT,CKWT,NMAX,IC,ID,CK,B,SB,C,SC,FLAG,EB,SE,LOB,SL
     20,L1B,SL1,L2B,SL2,DPHIW,Z,R,SUME,UTT,VTT,WTT,TTT,ALF,SUMA,GAM
      IF(NMAX.LT.0)GO TO 10
      FLAG=.TRUE.
      CK(1,2)=CKUV
      CK(2,3)=CKVW
      CK(1,3)=CKWU
      CK(1,4)=CKUT
      CK(2,4)=CKVT
      CK(3,4)=CKWT
      DO 1 I=1,4
      DO 1 J=1,4
      IF(I.EQ.J)CK(I,J)=1.0
      IF(I.GT.J)CK(I,J)=CK(J,I)
    1 IF(ABS(CK(I,J)).GT.1.0)FLAG=.FALSE.
      DO 4 K=1,4
      SC(K)=0.0
      DO 3 I=1,4
      C(I,K)=0.0
      SB(I,K)=0.0
      DO 2 J=1,4
      B(I,J,K)=0.0
      IF(I.EQ.J.OR.J.EQ.K.OR.K.EQ.I)GO TO 2
      B(I,J,K)=(CK(I,J)-CK(J,K)*CK(K,I))/(1.0-CK(J,K)**2)
      B(I,K,J)=(CK(I,K)-CK(K,J)*CK(J,I))/(1.0-CK(K,J)**2)
      IF(ABS(B(I,J,K))+ABS(B(I,K,J)).GT.1.0)FLAG=.FALSE.
      L=10-I-J-K
      C(I,K)=(CK(I,K)*(1.0-CK(L,J)**2)-CK(L,K)*(CK(I,L)-CK(L,J)*CK(J,I))
     1-CK(J,K)*(CK(J,I)-CK(I,L)*CK(L,J)))/(1.0-CK(L,J)**2-CK(I,L)*(CK(I,
     2L)-CK(L,J)*CK(J,I))-CK(J,I)*(CK(J,I)-CK(I,L)*CK(L,J)))
    2 CONTINUE
    3 SC(K)=SC(K)+ABS(C(I,K))
      IF(SC(K).GT.1.0)FLAG=.FALSE.
    4 CONTINUE
      IF(ID.GT.-2.OR.FLAG)GO TO 6
      WRITE(6,5)((CK(I,J),J=1,4),I=1,4),(((B(I,J,K),K=1,4),J=1,4),I=1,4)
     1,((C(I,J),J=1,4),I=1,4),(SC(I),I=1,4)
    5 FORMAT(1H0,(4F12.4,5X,4F12.4))
    6 IF(FLAG)GO TO 8
      WRITE(6,7)
    7 FORMAT(37H0CORRELATION DATA INCONSISTENT - EXIT)
      RETURN
    8 IF(IC.GE.0)GO TO 80
      DO 81 I=1,4
      DO 81 J=1,4
   81 ALF(I,J)=0.0
      DO 83 N=1,20
      DO 82 I=1,4
      DO 82 J=1,4
```

```
      SUMA(I,J)=0.0
      DO 82 K=1,4
82 SUMA(I,J)=SUMA(I,J)+ALF(I,K)*ALF(K,J)
      DO 83 I=1,4
      DO 83 J=1,4
      ALF(I,J)=0.5*(-CK(I,J)+SUMA(I,J))
      IF(I.EQ.J)ALF(I,J)=ALF(I,J)+0.5
83 CONTINUE
      IF(ID.EQ.-2)WRITE(6,84)((ALF(I,J),J=1,4),I=1,4)
84 FORMAT(9H0ALF(I,J)/1H ,16F8.5)
      GO TO 10
80 A=CK(1,2)
      B1=CK(2,3)
      B2=0.0
      IF(CK(1,2)**2.LT.1.0)B1=B(3,1,2)
      IF(CK(1,2)**2.LT.1.0)B2=B(3,2,1)
      C1=CK(1,4)
      C2=0.0
      C3=0.0
      IF(CK(1,2)*CK(2,3)*CK(3,1).NE.1.0)C1=C(1,4)
      IF(CK(1,2)*CK(2,3)*CK(3,1).NE.1.0)C2=C(2,4)
      IF(CK(1,2)*CK(2,3)*CK(3,1).NE.1.0)C3=C(3,4)
      IF(ID.EQ.-2.AND.NMAX.GT.0)WRITE(6,9)A,B1,B2,C1,C2,C3
 9 FORMAT(3H A=F7.4,3X3HB1=F7.4,3X3HB2=F7.4,3X3HC2=F7.4,3X3HC2=F7.4,3
   1X3HC3=F7.4)
10 BB=PHIW/57.2958
      BETA=PHIV/57.2958
      ALA=(THEV-THFW)/57.2958
      E1=SIN(BB-BETA)+COS(BB)*SIN(BETA)*(1.0-COS(ALA))
      E2=SIN(ALA)*COS(BB)
      E3=COS(BB-BETA)-COS(BB)*COS(BETA)*(1.0-COS(ALA))
      N=0
      DO 11 I=1,6
11 SUME(I)=0.0
      IF(PHIW.NE.0.0.OR.THEW.NE.0.0)GO TO 14
      DO 12 I=7,20
12 SUME(I)=0.0
      IF(NMAX.LT.0)GO TO 14
      IF(ID.EQ.-2)WRITE(6,13)
13 FORMAT(1H0,5X2HUT,10X2HVT,10X2HWT,10X2HTT,10X2HE1,10X2HE2,10X2HE3,
   19X4HUPP2,8X4HUPL2,9X1HE)
14 DO 20 IN=1,100
      N=N+1
      IF(NMAX.LT.0)GO TO 17
      DO 16 I=1,4
      IF(IC.LE.0)Z(I)=RNN(0)
      IF(IC.GT.0)Z(I)=RNU(0)
      IF(IC.EQ.-1)GO TO 16
      IF(I.LE.3)R(I)=RNU(0)
      IF(IC.EQ.1)Z(I)=3.4641*(Z(I)-0.5)
      IF(IC.EQ.2)Z(I)=SIGN(1.0,(Z(I)-0.5))
      IF(IC.NE.3)GO TO 16
      ZA=AMIN1(Z(I),(1.0-Z(I)))
      IF(ZA.LT.0.02027)Z(I)=SIGN((SQRT(0.355773*ZA**(-2.0/3.0)-0.79)),(Z
   1(I)-0.5))
      IF(ZA.LT.0.02027)GO TO 16
```

```
   15 RZ=RNU(0)
      Z(I)=4.0*(RZ-0.5)
      RZ=RNU(0)
      IF(RZ.GT.(1.0+Z(I)**2)**(-2))GO TO 15
   16 CONTINUF
      IF(IC.GE.0)GO TO 160
      UT=(1.0-ALF(1,1))*Z(1)-ALF(1,2)*Z(2)-ALF(1,3)*Z(3)-ALF(1,4)*Z(4)
      VT=(1.0-ALF(2,2))*Z(2)-ALF(2,3)*Z(3)-ALF(2,4)*Z(4)-ALF(2,1)*Z(1)
      WT=(1.0-ALF(3,3))*Z(3)-ALF(3,4)*Z(4)-ALF(3,1)*Z(1)-ALF(3,2)*Z(2)
      TT=(1.0-ALF(4,4))*Z(4)-ALF(4,1)*Z(1)-ALF(4,2)*Z(2)-ALF(4,3)*Z(3)
      GO TO 161
  160 UT=Z(1)
      VT=Z(2)
      IF(R(1).LE.ABS(A))VT=UT*SIGN(1.0,A)
      WT=Z(3)
      IF(R(2).LE.ABS(B1))WT=UT*SIGN(1.0,B1)
      IF(R(2).LE.ABS(B1)+ABS(B2).AND.R(2).GT.ABS(B1))WT=VT*SIGN(1.0,B2)
      TT=Z(4)
      IF(R(3).LE.ABS(C1))TT=UT*SIGN(1.0,C1)
      IF(R(3).LE.ABS(C1)+ABS(C2).AND.R(3).GT.ABS(C1))TT=VT*SIGN(1.0,C2)
      IF(R(3).LE.ABS(C1)+ABS(C2)+ABS(C3).AND.R(3).GT.ABS(C1)+ABS(C2))TT=
     1WT*SIGN(1.0,C3)
  161 UTT(N)=UT
      VTT(N)=VT
      WTT(N)=WT
      TTT(N)=TT
      GO TO 18
   17 UT=UTT(N)
      VT=VTT(N)
      WT=WTT(N)
      TT=TTT(N)
   18 UT=UT*SUT
      VT=VT*SVT
      WT=WT*SWT
      TT=TT*STT
      IF(PHIW.NE.0.0.OR.THEW.NE.0.0)GO TO 19
      SUME(7)=SUME(7)+UT
      SUME(8)=SUME(8)+VT
      SUME(9)=SUME(9)+WT
      SUME(10)=SUME(10)+TT
      SUME(11)=SUME(11)+UT*VT
      SUME(12)=SUME(12)+VT*WT
      SUME(13)=SUME(13)+WT*UT
      SUME(14)=SUME(14)+UT*TT
      SUME(15)=SUME(15)+VT*TT
      SUME(16)=SUME(16)+WT*TT
      SUME(17)=SUME(17)+UT**2
      SUME(18)=SUME(18)+VT**2
      SUME(19)=SUME(19)+WT**2
      SUME(20)=SUME(20)+TT**2
   19 UPL2=((VF'+UT)*E1+VT*E2+WT*E3)**2
      UPP2=(VM+UT)**2+VT**2+WT**2-UPL2
      ESQ=(1.0+AL*TT)*AW+(1.0+GAM*AL*TT)*BW*(SQRT(UPP2+CC*UPL2))**CN
      F=0.0
      IF(ESQ.GT.0.0)E=SQRT(ESQ)
      CL=(ESQ-AW)/BW
```

```
      SUMF(1)=SUMF(1)+F
      SUMF(2)=SUMF(2)+ESQ
      SUME(3)=SUME(3)+CL
      SUMF(4)=SUMF(4)+CL**2
      SUME(5)=SUME(5)+CL**4
      SUMF(6)=SUMF(6)+CL**8
 20   IF(ID.EQ.-2.AND.NMAX.GT.0)WRITE(6,21)UT,VT,WT,TT,E1,E2,E3,UPP2,UPL
     12,E
 21   FORMAT(1H 10E12.5)
      IF(N.LT.IABS(NMAX)) GO TO 14
      FN=FLOAT(N)
      NMAX=-IABS(NMAX)
      FB=SUME(1)/FN
      E2B=SUME(2)/FN
      L0B=SUME(3)/FN
      L1B=SUME(4)/FN
      L2B=SUME(5)/FN
      IF(PHIW.NE.0.0.OR.THEW.NE.0.0)GO TO 24
      UBX=SUMF(7)/FN
      VBX=SUMF(8)/FN
      WBX=SUME(9)/FN
      TBX=SUMF(10)/FN
      UVBX=SUME(11)/FN
      VWBX=SUMF(12)/FN
      WUBX=SUMF(13)/FN
      UTBX=SUME(14)/FN
      VTBX=SUME(15)/FN
      WTBX=SUME(16)/FN
      U2BX=SUME(17)/FN
      V2BX=SUMF(18)/FN
      W2BX=SUME(19)/FN
      T2BX=SUME(20)/FN
      SUTX=-1.0
      IF(U2BX.GT.UBX**2)SUTX=SQRT(U2BX-UBX**2)
      SVTX=-1.0
      IF(V2BX.GT.VBX**2)SVTX=SORT(V2BX-VBX**2)
      SWTX=-1.0
      IF(W2BX.GT.WBX**2)SWTX=SQRT(W2BX-WBX**2)
      STTX=-1.0
      IF(T2BX.GT.TBX**2)STTX=SQRT(T2BX-TBX**2)
      CKUVX=(UVBX-UBX*VBX)/(SUTX*SVTX)
      CKVWX=(VWBX-VBX*WBX)/(SVTX*SWTX)
      CKWUX=(WUBX-WBX*UBX)/(SWTX*SUTX)
      CKUTX=(UTBX-UBX*TBX)/(SUTX*STTX)
      CKVTX=(VTBX-VBX*TBX)/(SVTX*STTX)
      CKWTX=(WTBX-WBX*TBX)/(SWTX*STTX)
      WRITE(6,22)UBX,VBX,WBX,TBX,SUTX,SVTX,SWTX,STTX,CKUVX,CKVWX,CKWUX,C
     1KUTX,CKVTX,CKWTX
 22   FORMAT(5H0UBX=F9.4,3X4HVBX=F9.4,3X4HWBX=F9.4,3X4HTBX=F9.4,3X5HSUTX
     1=F8.4,3X5HSVTX=F8.4,3X5HSWTX=F8.4,3X5HSTTX=F8.4/7H CKUVX=F7.4,3X6H
     2CKVWX=F7.4,3X6HCKWUX=F7.4,3X6HCKUTX=F7.4,3X6HCKVTX=F7.4,3X6HCKWTX=
     3F7.4)
      IF(PHIW.NE.0.0.OR.THEW.NE.0.0)GO TO 24
      WRITE(6,23)
 23   FORMAT(1H0,3X4HPHIW,3X4HTHEW,7X2HFB,5X2HSE,6X3HL0B,4X3HSL0,6X3HL1B
     1,4X3HSL1,6X3HL2B,4X3HSL2,1X7HL0B/L0R,1X7HL1B/L1R,1X7HL2B/L2R,5X3HR
```

```
  101,5X3HRO2,5X3HR12)
    LOR=LOR
    L1R=L1R
    L2R=L2B
24  SE=-1.0
    IF(E2B.GT.EB**2)SE=SQRT((E2B-EB**2)/FN)/ABS(EB)
    SLO=-1.0
    IF(L1B.GT.LOB**2)SLO=SQRT((L1B-LOB**2)/FN)/ABS(LOB)
    SL1=-1.0
    IF(L2B.GT.L1B**2)SL1=SQRT((L2B-L1B**2)/FN)/ABS(L1B)
    SL2=-1.0
    IF(SUME(6)/FN.GT.L2B**2)SL2=SQRT((SUME(6)/FN-L2B**2)/FN)/ABS(L2B)
    RLO=LOB/LOR
    RL1=L1B/L1R
    RL2=L2B/L2R
    RO1=LOB**2/L1B
    RO2=LOB**4/L2B
    R12=L1B**2/L2B
    WRITE(6,25)PHIW,THEW,EB,SE,LOB,SLO,L1B,SL1,L2B,SL2,RLO,RL1,RL2,RO1
   1,RO2,R12
25  FORMAT(1H ,2F7.2,4(F9.4,F7.4),6F8.4)
    RETURN
    END
```

Appendix F

NUMERICAL CALCULATION PROCEDURE AND COMPUTING TIME

The overall numerical calculation procedure is outlined in the following block diagram with a step by step description:

Start

1. Read basic input data and instructions

2. Decision making

3. Initialize calculations

4. Calculate repeated constants

5. Calculate Δt from stability criterion

6. Execution time limit exceeded?
   no

7. Calculate $\frac{\partial T}{\partial t}$ and then T' for all interior points

8. Calculate or specify T', on all boundary points where necessary

9. Calculate $\frac{\partial Z}{\partial t}$ and then Z' for all interior points

10. Calculate S' for all interior points

11. Calculate or specify Z' and S' on all boundary points where necessary

12. Calculate u', v'

13. Determine maximum values of u and v

14. Converged?
    no
    yes

yes

15. Output

End

The details of the above block diagram are described below:

1. The basic input data consist of the grid system, source size, Gr_T, Pr, convergence criteria, instructions for decision making, etc. A list with explanations for these input data is given in Appendix G.

2. Several decisions are made in this step:

   (a) For a starting calculation: Go directly to step 3.

   (b) For continuation of calculations: Read input data cards from intermediate results of previous calculations.

   (c) For subdividing mesh spacing: Read input data cards from results of the converged solution of the previous calculations; and set the approximate values at the added mesh points equal to the arithematic average of the known values of the neighboring points.

3. At $t = 0$, set all dependent variables equal to zero except $T_{i,1} = 1$ for $x \leqq D/2$.

4. Calculate all the repeated constants in the computer program.

5. Calculate Δt from the stability criterion (Equation 6-10).

6. If the execution time limit is exceeded, go to step 15 for card output. This card output will be used for future continuation of calculations as described in step (2b).

7. Calculate $\left(\frac{\partial T}{\partial t}\right)_{i,j}$ from Equation (6-11) for all (i,j) interior to the boundaries (hereafter these points will be referred to as the interior points as opposed to the boundary points) and then calculate $T'_{i,j}$ for all interior points as follows:

$$T'_{i,j} = T_{i,j} + \left(\frac{\partial T}{\partial t}\right)_{i,j} \cdot \Delta t$$

where $T'_{i,j}$ represents the temperature at an advanced time.[*]

8. Calculate or specify $T'_{i,j}$ for all boundary points using the applicable boundary conditions. ... e previous se tio .

9. Calculate $\left(\frac{\partial Z}{\partial t}\right)_{i,j}$ using Equation (6-12) and the $T'_{i,j}$ just obtained and then $Z'_{i,j}$ for all interior points.

10. Calculate $S'_{i,j}$ using Equation (6-13) for all interior points. A Gauss-Seidel point iterative procedure is used. The scanning is performed column by column (i.e., from $j = 2$ to jmax-1 for $i = 2$ to imax-1). In the calculations the freshly calculated values of $S_{i,j}$ are always used. The over-relaxation factor W is calculated from the following formula (51, Section 7.17):

$$W = \frac{2}{1 + \sqrt{1 - \lambda^2}} , \quad \text{where} \quad \lambda = \frac{1}{2}\left(\cos\frac{\pi}{imax-1} + \cos\frac{\pi}{jmax-1}\right).$$

The iteration is terminated as soon as the convergence criterion:

$$\left|\frac{S_{i,j}^{n+1} - S_{i,j}^{n}}{S_{i,j}^{n}}\right| \leq EPS \quad \text{for every } (i,j)$$

is satisfied. Here, the superscript n means the n-th iteration and the value of EPS used for all calculations was 0.001.

11. Calculate $Z'_{i,j}$ and $S'_{i,j}$ for all boundary points using the applicable boundary conditions discussed in Chapter VI.

---

[*]Hereafter all primed quantities refer to those at an advanced time.

12. Calculate $u'_{i,j}$ and $v'_{i,j}$ for all interior points using Equation (6-14) and the stream function just calculated.

13. Determine the maximum values of u' and v' and label them as u_{max} and v_{max}, respectively.

14. Return to step 5 and repeat the complete cycle. The complete calculation procedure is terminated when the following convergence criterion is met:

$$\left| \frac{Z'_{i,j} - Z_{i,j}}{Z_{i,j}} \right| \leqq 10^{-4} \quad \text{for all } (i,j).$$

Numerical results show that when this criterion is met, the maximum error calculated in step 10 is usually smaller than 10^{-5}, and all the other dependent variables (u,v,T,S,Z) show no appreciable changes.

15. The output consists of: partial printout for intermediate results during the calculation, card output when either the solution is converged or the execution time limit is exceeded, and complete printout for the numerical results of all the dependent variables.

The computing time depends on the combination of the array size and the source size. For the cases studied, the computer execution time required for obtaining a converged solution increases with Gr and the source size. A summary of the execution time for the cases run are given below:

No.	Grid System[*]	Time, min.	Remarks
$Gr_T = 10^4$			
1	13x15,1-4	3	
2	17x25,1-7	11	Continued from solution of No. 1.
3	17x13,1-5	6	
4	17x17,1-5	8	
5	17x21,1-5	10	
6	17x25,1-5	12	
7	15x17,1-5	5	
8	29x33,1-9	32	Continued from solution of No. 7.
$Gr_T = 10^5$			
9	15x17,1-5	8	Initialized with solution of No. 7.
10	17x33,1-9	14	Continued from solution No. 9.
11	21x33,1-17	17	Continued from solution of No. 10.

---

[*]See p.　for explanation.

Appendix G

COMPUTER PROGRAM LISTING - FLOW FIELD CALCULATION

This computer program was written in FORTRAN IV computer language.
Five primary variables (the dimensionless indraft U, updraft V, tempera-
ture T, stream function S, and vorticity function Z) are computed for an
array of mesh points of IMAX x JMAX. There are four major parts in this
computer program: reading input data, calculating all the repeated
constants, main body of the calculations, and output.

The input listing is described below:

IMAX, JMAX	maximum values of I and J
I1, J1	IMAX - 1, JMAX - 1
I2, J2	IMAX - 2, JMAX - 2
K	a register of the time steps advanced
LL	total number of iterations performed up to the K-th time step
M	size of source radius, $D/2 = (M - 1) \Delta x$
MM	$= M + 1$
N	frequency of intermediate printout, i.e., one printout after every other N time steps
IM	number of columns per line in the printout
KM	maximum allowable number of time steps to be advanced, a limit to the computer time that may be used

LM   maximum allowable number of iterations for solving the
stream function

II, JJ   array size of the card output for the presently converged
solution (This array will be used as the input for finer
mesh spacing continued calculations.)

GR   Grashof number

PR   Prandtl number

EPS   convergence criterion in the iteration procedure for
solving the stream function, usually set at 0.001

TIM   = 0.0, for initiating the dimensionless time

TI   a factor for adjusting the size of the time interval to be
advanced, usually set at 1.0

XY   the ratio $\Delta y/\Delta x$, 1.0 was used for the present calculations

UMAX, UMAX   the maximum absolute value of the component velocities u
and v

CARDS $\neq$ 0.0 means card output is desired

READS $\neq$ 0.0 means card output of previous calculations is to be
read in addition to the regular input of two cards

W   over-relaxation parameter

TEXC   maximum allowable time for execution, a time control device

DIVIDE $\neq$ 0.0 mean the data input from previous calculations is to
be interpolated to obtain the values at the new additional
points for a subdivided mesh spacing system

SKIP   skipping instruction for boundary value specifications:
                SKIP >0.0 means skipping S(IMAX, J), T(IMAX, J); SKIP =
                2.0 means skipping T(IMAX, J), S(IMAX, J), Z(IMAX, J),
                T(I, JMAX)

CO   convergence criterion (usually set at 0.0001), if met the
                complete calculation is terminated and the complete results
                are printed out

```
      DIMENSION U(43,43), V(43,43), T(43,43), Z(43,43), S(43,43), DTDT(4
     13,43), DZDT(43,43),CA(43),CB(43),CC(43),CD(43),CE(43),CF(43),CG(43)
     1),CH(43),CI(43),CJ(43)
  201 FORMAT    (/5X, 26HSTREAM FUNCTIONS -- S(I,J))
  202 FORMAT    (/5X, 25HRADIAL VELOCITY -- U(I,J))
  203 FORMAT    (//5X, 27HVERTICAL VELOCITY -- V(I,J))
  204 FORMAT    (//5X, 21HTEMPERATURE -- T(I,J))
  205 FORMAT    (//5X, 19HVORTICITY -- Z(I,J))
  206 FORMAT (1H1)
  207 FORMAT (4X,4HK = ,I4,4X,4HL = ,I3,5X,7HTIME = ,F12.5,5X,5HDT = ,
     2E10.3,5X,5HDX = ,F6.3,5X,5HDY = ,F6.3,5X,6HFPS = ,F6.3,5X,
     35HTI = ,F6.3)
  208 FORMAT (1H1,//,78H NUMERICAL SOLUTION OF NATURAL CONVECTION NEAR A
     2 CIRCULAR BOUNDARY HEAT SOURCE,4X,4HGR =, F10.3,3X,4HPR =, F4.1,
     33X,7HGRID = ,I2,1HX,I2)
  209 FORMAT (33X,1P9F11.3)
  211 FORMAT (/)
  212 FORMAT (16I5/E10.3,14F5.2)
  213 FORMAT (6H  K = ,I4,4X,4HL = ,I3,4X,6HTIME =,E11.4,4X,4HDT =,E11.4
     2,4X,7HQMAX = ,E11.4,4X,7HCONV = ,E11.4,4X,5HLL = ,I8)
  216 FORMAT (1P10E13.4)
  217 FORMAT (13X,1P7F13.4)
  219 FORMAT (1P8F10.3)
  220 FORMAT (1P12F11.3)
  221 FORMAT (3X,1P7E11.4)
  222 FORMAT (2I10, 1P4E15.7)
C
C READ DATA INPUT - FOR CALCULATIONS AND CONTROLS
  101 READ (5,212) IMAX,JMAX,I1,J1,I2,J2,K,LL,M,MM,N,IM,KM, LM,II,JJ
     2,GR,PR,EPS,TIM ,TI,XY,UMAX,VMAX,CARDS,READS,W,TEXC,DIVIDE,SKIP,CO
      TCHK1 = TIME(1.0)
      WRITE (6,212)IMAX,JMAX,I1,J1,I2,J2,K,LL,M,MM,N,IM,KM, LM,II,JJ
     2,GR,PR,EPS,TIM ,TI,XY,UMAX,VMAX,CARDS,READS,W,TEXC,DIVIDE,SKIP,CO
CALCULATE REPEATED CONSTANT TERMS IN MAIN CALCULATIONS
      XM = M-1
      XN = N
      DX = 0.5/XM
      DY = XY*DX
      DX2 = DX*DX
      DY2 = DY*DY
      C = 1.0/SQRT(GR)
      C1 = C/PR
      C2 = 2.0*(1.0/DX2+1.0/DY2)
      D = 0.5*DX2/(1.0+DX2/DY2)
      DTI = C1*C2
      DXY2 = 2.0*DX2*DY2
      CI1=I1
      CI2=I2
      C3 = CI2*DX*DY
      C4 = I(I)*DX)**2/2.0
    1 DO 2 I=2,IMAX
      CII = I-1
      COEFF = 2.0*CII*DX
      AI = 0.5/CII
      BI = 1.5/CII
```

```
      CA(I) = (1.0+AI)/DX2
      CB(I) = (1.0-AI)/DX2
      CC(I) = (1.0+BI)/DX2
      CD(I) = (1.0-BI)/DX2
      CE(I) = (CII*DX)**2
      CF(I) = COEFF*DX
      CG(I) = COEFF*DY
      CH(I) = CII**2*DXY2
      CI(I) = AI/(DX*DY)
    2 CJ(I) = AI/DX2
      IF (READS.NE.0.0)      GO TO 107
C INITIAL CONDITIONS
    5 DO 6 I = 1,IMAX
      DO 6 J = 1,JMAX
      U(I,J) = 0.0
      V(I,J) = 0.0
      T(I,J) = 0.0
      Z(I,J) = 0.0
    6 S(I,J) = 0.0
    3 DO 4 I=1,M
    4 T(I,1) = 1.0
      GO TO 82
CARD READING FOR CONTINUATION
  107 READ (5,222)      KK,LL,TIM,UMAX,VMAX,GR
      IF (DIVIDE.EQ.0.0)      GO TO 106
C INPUT DATA READING WH " SUBDIVISION OF MESH SPACING IS DESIRED
      READ (5,221) ((U(I,J),V(I,J),T(I,J),S(I,J),Z(I,J), I=1,IMAX,2),
    2     J=1,JMAX,2)
   19 DO 20     J=1,JMAX,2
      DO 20     I=2,IMAX,2
      U(I,J) = (U(I-1,J)+U(I+1,J))/2.0
      V(I,J) = (V(I-1,J)+V(I+1,J))/2.0
      T(I,J) = (T(I-1,J)+T(I+1,J))/2.0
      S(I,J) = (S(I-1,J)+S(I+1,J))/2.0
   20 Z(I,J) = (Z(I-1,J)+Z(I+1,J))/2.0
   21 DO 22     J=2,JMAX,2
      DO 22     I=1,IMAX
      U(I,J) = (U(I,J+1)+U(I,J-1))/2.0
      V(I,J) = (V(I,J+1)+V(I,J-1))/2.0
      T(I,J) = (T(I,J+1)+T(I,J-1))/2.0
      S(I,J) = (S(I,J+1)+S(I,J-1))/2.0
   22 Z(I,J) = (Z(I,J+1)+Z(I,J-1))/2.0
      T(MM,1) = 0.0
      IF (SKIP.NE.2.0)      GO TO 88
      READ (5,219)     (T(IMAX,J),  J=2,16,2)
      READ (5,219)     (T(I,JMAX),  I=2,IMAX,2)
      READ (5,219)     (S(IMAX,J),  J=2,4,2)
      READ (5,219)     (S(I,JMAX),  I=2,IMAX,2)
      READ (5,219)     (Z(IMAX,J),  J=2,6,2)
      READ (5,219)     (Z(I,JMAX),  I=2,IMAX,2)
      GO TO 88
  106 READ  (5,221) ((U(I,J),V(I,J),T(I,J),S(I,J),Z(I,J),  I=1,IMAX),
    2  J=1,JMAX)
   88 K = KK-1
      GO TO 102
```

SIZE

```
C
C MAIN CALCULATIONS
C TIME TO BE ADVANCED BASED ON STABILITY CRITERION
    82 DT =  TI/(UMAX/DX+VMAX/DY+DTI)
       TIM = TIM+DT
    80 TCHK2 = TIME(1.C)
C EXECUTION TIME CONTROL
       IF (TCHK2-TCHK1.GT.TFXC)      GO TO 100
       K = K+1
       IF (K.GT.KM)      GO TO 100
C ENERGY EQUATION
     9 DO 10       I=2,I1
       DO 10       J=2,J1
       IF (U(I,J)) 51,58,52
    51 T1 = U(I,J)*(T(I+1,J) - T(I,J))/DX
       GO TO 53
    58 T1 = 0.0
       GO TO 53
    52 T1 = U(I,J)*(T(I,J) - T(I-1,J))/DX
    53 IF (V(I,J)) 54,59,55
    54 T2 = V(I,J)*(T(I,J+1) - T(I,J))/DY
       GO TO 56
    59 T2 = 0.0
       GO TO 56
    55 T2 = V(I,J)*(T(I,J) - T(I,J-1))/DY
    56 IF (I.EQ.1)      GO TO 91
       T3 = CA(I)*T(I+1,J)+CB(I)*T(I-1,J)-C2*T(I,J)+(T(I,J+1)+T(I,J-1))/
      1DY2
       GO TO 10
    91 T3 = 4.0*(T(2,J)-T(1,J))/DX2+(T(1,J+1)-2.0*T(1,J)+T(1,J-1))/DY2
    10 DTDT(I,J) = -T1-T2+C1*T3
    11 DO 12 I=2,I1
       DO 12 J = 2,J1
    12 T(I,J) = T(I,J) + DT*DTDT(I,J)
    27 DO 28       I=MM,I1
    28 T(I,1) = (18.0*T(I,2)-9.0*T(I,3)+2.0*T(I,4))/11.0                    NO FLUX
C SKIP=2.0, VALUES ON BOTH IMAX AND JMAX ARE FIXED.  SKIP=1.0, FIXED ON IMAX ON
       IF (SKIP.EQ.2.0)      GO TO 43
    17 DO 18 I= 2,I1
    18 T(I,JMAX) = T(I,J1)
    43 DO 44       J=2,J1
       T1J = (18.0*T(2,J)-9.0*T(3,J)+2.0*T(4,J))/11.0
       IF (.NOT.(T1J.GT.0.0.AND.T1J.LT.1.0))      GO TO 45
       IF (T1J.LT.T(2,J))      GO TO 45
       T(1,J) = T1J
       GO TO 44
    45 T(1,J) = T(2,J)
    44 CONTINUE
C VORTICITY EQUATION
       DZMAX = 0.0
    13 DO 14       I=2,I1
       DO 14       J=2,J1
       IF (U(I,J)) 61,68,62
    61 Z1 = U(I,J)*(Z(I+1,J) - Z(I,J))/DX
       GO TO 63
```

```
68 Z1 = 0.0
   GO TO 63
62 Z1 = U(I,J)*(Z(I,J) - Z(I-1,J))/DX
63 IF (V(I,J)) 64,69,65
64 Z2 = V(I,J)*(Z(I,J+1) - Z(I,J))/DY
   GO TO 66
69 Z2 = 0.0
   GO TO 66
65 Z2 = V(I,J)*(Z(I,J) - Z(I,J-1))/DY
66 IF (I.EQ.1)    GO TO 92
   Z3 = CC(I)*Z(I+1,J)+CD(I)*Z(I-1,J)-C2*Z(I,J)+(Z(I,J+1)+Z(I,J-1))/
  1DY2
   Z4 = (T(I+1,J) - T(I-1,J))*CJ(I)
   GO TO 93
92 Z3 = 8.0*(Z(2,J)-Z(1,J))/DX2+(Z(1,J+1)-2.0*Z(1,J)+Z(1,J-1))/DY2
   Z4 = 2.0*(T(2,J)-T(1,J))/DX2
93 DZDT(I,J) = -Z1-Z2+C*Z3+Z4
   ZERROR = ABS(DZDT(I,J)/Z(I,J))
14 IF (ZERROR.GT.DZMAX)    DZMAX=ZERROR
15 DO 16 I = 2,I1
   DO 16 J = 2,J1
16 Z(I,J) = Z(I,J) + DT*DZDT(I,J)
46 DO 47    J=2,J1
   Z1J = (18.0*Z(2,J)-9.0*Z(3,J)+2.0*Z(4,J))/11.0
47 Z(1,J) = Z1J                                            3-PT
70 L = 0
77 L = L + 1
   IF (L.GT.LM)    GO TO 151
   RMAX = 0.0
C SOLVING FOR STREAMFUNCTION BY SUCCESSIVE OVER-RELAXATIONS
23 DO 24 I = 2,I1
   DO 24 J = 2,J1
   DS = D*(CB(I)*S(I+1,J)+CA(I)*S(I-1,J)+   (S(I,J+1)+S(I,J-1))/DY2
  1   +CF(I)*Z(I,J))
   DSSOR = W*DS+(1.0-W)*S(I,J)
   IF (ABS(S(I,J)).LT.0.1E-15)    GO TO 24
   Q = ABS(DSSOR/S(I,J))
   IF (Q.GT.RMAX)    RMAX = Q
24 S(I,J) = DSSOR
   QQ = ABS(RMAX-1.0)/DT
   IF (QQ.GT.EPS)    GO TO 77
151 QMAX = QQ
   LL = LL+L
   IF (SKIP.GT.0.0)    GO TO 31
29 DO 30 J = 2,J1
30 S(IMAX,J) = S(I1,J)
31 DO 32 I = 2,IMAX
   IF (SKIP.EQ.2.0)    GO TO 32
   S(I,JMAX) = S(I,J1)
   Z(I,JMAX) = Z(I,J1)
32 Z(I,1) = (S(I,3) - 8.0*S(I,2))/ CH(I)
C SOLVING FOR VELOCITIES
33 DO 34 I = 2,I1
   DO 34 J = 2,J1
   U(I,J) = CI(I)   *(S(I,J+1)-S(I,J-1))
```

```
   34 V(I,J) = CJ(I)*(S(I-1,J)-S(I+1,J))
  105 WRITE (6,213)   K, L, TIM , DT, QMAX, DZMAX, LL
      IF (K.LT.30)       GO TO 35
      IF (DZMAX.LT.CO)      GO TO 100
   35 DO 36     J = 2,J1
      V1J = (18.0*V(2,J)-9.0*V(3,J)+2.0*V(4,J))/11.0                    .        3-PT
   36 IF (V1J.GT.0.0)     V(1,J) = V1J
C PREPARATION FOR CALCULATIONS FOR THE NEXT TIME STEP
      UMAX = 0.0
   39 DO 40   I= 2, I1
      DO 40   J = 2, J1
      UIJ = ABS(U(I,J))
   40 IF (UIJ.GT.UMAX)    UMAX = UIJ
      VMAX = 0.0
   41 DO 42   I = 1, I1
      DO 42   J = 2, J1
      VIJ = ABS(V(I,J))
   42 IF (VIJ.GT.VMAX)    VMAX = VIJ
C
C OUTPUT
  112 IF (FLOAT(K)/XN.NE.FLOAT(K/N))      GO TO 82
  102 WRITE (6,208)      GR,PR,IMAX,JMAX
      WRITE (6,207)      K,L,TIM ,DT,DX,DY,EPS,TI
      WRITE (6,202)
      WRITE (6,220)      ((U(I,J), I=1,IM),   J=1,JMAX)
      WRITE (6,203)
      WRITE (6,220)      ((V(I,J), I=1,IM),   J=1,JMAX)
      WRITE (6,204)
      WRITE (6,220)      ((T(I,J), I=1,IM),   J=1,JMAX)
      WRITE (6,201)
      WRITE (6,220)      ((S(I,J), I=1,IM),   J=1,JMAX)
      WRITE (6,205)
      WRITE (6,220)      ((Z(I,J), I=1,IM),   J=1,JMAX)
   81 GO TO 82
  100 IF (IMAX.EQ.IM)       GO TO 104
      WRITE (6,208)      GR,PR,IMAX,JMAX
      WRITE (6,207)      K,L,TIM ,DT,DX,DY,EPS,TI
      WRITE (6,202)
      IF (IMAX.GT.20)       GO TO 110
      WRITE (6,216)      ((U(I,J), I=1,10),   J=1,JMAX)
      WRITE (6,211)
      WRITE (6,217)      ((U(I,J), I=11,IMAX),  J=1,JMAX)
      WRITE (6,203)
      WRITE (6,216)      ((V(I,J), I=1,10),   J=1,JMAX)
      WRITE (6,211)
      WRITE (6,217)      ((V(I,J), I=11,IMAX),  J=1,JMAX)
      WRITE (6,204)
      WRITE (6,216)      ((T(I,J), I=1,10),   J=1,JMAX)
      WRITE (6,211)
      WRITE (6,217)      ((T(I,J), I=11,IMAX),  J=1,JMAX)
      WRITE (6,201)
      WRITE (6,216)      ((S(I,J), I=1,10),   J=1,JMAX)
      WRITE (6,211)
      WRITE (6,217)      ((S(I,J), I=11,IMAX),  J=1,JMAX)
      WRITE (6,205)
```

```
      WRITE (6,216)      ((Z(I,J), I=1,10),    J=1,JMAX)
      WRITE (6,211)
      WRITE (6,217)      ((Z(I,J), I=11,IMAX),  J=1,JMAX)
      GO TO 104
110   WRITE (6,220)      ((U(I,J), I=1,12), J=1,JMAX)
      WRITE (6,211)
      WRITE (6,209)      ((U(I,J), I=13,IMAX), J=1,JMAX)
      WRITE (6,203)
      WRITE (6,220)      ((V(I,J), I=1,12), J=1,JMAX)
      WRITE (6,211)
      WRITE (6,209)      ((V(I,J), I=13,IMAX), J=1,JMAX)
      WRITE (6,204)
      WRITE (6,220)      ((T(I,J), I=1,12), J=1,JMAX)
      WRITE (6,211)
      WRITE (6,209)      ((T(I,J), I=13,IMAX), J=1,JMAX)
      WRITE (6,201)
      WRITE (6,220)      ((S(I,J), I=1,12), J=1,JMAX)
      WRITE (6,211)
      WRITE (6,209)      ((S(I,J), I=13,IMAX), J=1,JMAX)
      WRITE (6,205)
      WRITE (6,220)      ((Z(I,J), I=1,12), J=1,JMAX)
      WRITE (6,211)
      WRITE (6,209)      ((Z(I,J), I=13,IMAX), J=1,JMAX)
104   IF (CARDS.EQ.0.0)      GO TO 103
      WRITE (7,222)      K,LL,TIM,UMAX,VMAX,GR
      IF (DZMAX.LT.C0)      GO TO 108
      WRITE (7,221) ((U(I,J),V(I,J),T(I,J),S(I,J),Z(I,J),  I=1,IMAX),
     2  J=1,JMAX)
      GO TO 103
108   WRITE (7,221) ((U(I,J),V(I,J),T(I,J),S(I,J),Z(I,J),I=1,II),J=1,JJ)
103   GO TO 101
```

DOCUMENT CONTROL DATA - R & D

(Security classification of title, body of abstract and indexing annotation must be entered when the overall report is classified)

1 ORIGINATING ACTIVITY *(Corporate author)*	2a. REPORT SECURITY CLASSIFICATION
Naval Civil Engineering Laboratory	UNCLASSIFIED
Port Hueneme, California 93041	2b. GROUP

3 REPORT TITLE

THE TURBULENT FREE CONVECTION FLOW ABOVE A HEATED HORIZONTAL CIRCULAR PLATE

4 DESCRIPTIVE NOTES *(Type of report and inclusive dates)*

5 AUTHOR(S) *(First name, middle initial, last name)*

Tim Tse-Min Fu

6 REPORT DATE	7a. TOTAL NO OF PAGES	7b. NO OF REFS
May 1970	196	59

8a. CONTRACT OR GRANT NO	9a. ORIGINATOR'S REPORT NUMBER(S)
b. PROJECT NO ZF 38.512.001.014	TN-1079
c.	9b. OTHER REPORT NO(S) *(Any other numbers that may be assigned this report)*
d.	

10 DISTRIBUTION STATEMENT

This document has been approved for public release and sale; its distribution is unlimited.

11 SUPPLEMENTARY NOTES	12 SPONSORING MILITARY ACTIVITY
	Director of Navy Laboratories
	Main Navy Building
	Washington, D. C. 20360

13 ABSTRACT

The turbulent free convection of air above a 2-foot diameter, heated horizontal plate has been studied experimentally and numerically. The mean temperature fields and the indraft profiles for two mean plate temperatures were measured using a thermocouple and a constant temperature hot-wire anemometer. Also, the turbulence and mean velocity were measured for the higher plate temperature using the hot-wire method. The flow field was visualized by shadow photograph technique. From visualization and measurements, it was found that the region of significant deviation from ambient temperature and velocity was restricted to a region near the plate centerline (the primary flow region). The indraft velocity was found to be relatively large near the ground level (within approximately 1" of the ground).

The major temperature drop took place in the region very near the plate. Within 0.02" of the plate the temperature distribution in the air could be calculated based on conduction only. This region was therefore, called the "conduction layer." At a given mean plate temperature, the temperature gradient was found to increase with the radius. Data obtained from heat-transfer measurements were consistent with the one-third power correlation reported in the literature.

The turbulence in the flow field was found to consist of low frequency and high amplitude fluctuations (on the order of 10 Hz and 1 ft/sec). Because of the limitation of the hot-wire technique for large turbulence measurements, flow velocities could not be deduced directly from hot-wire data. To remove this difficulty, a numerical data simulation scheme has been developed in which the parameters describing the turbulence flow (r.m.s. fluctuations and correlation coefficients) were used as

Continued

input. By inferring from the simulated data of known parameters, experimental hot-wire data reduction was then possible. Data reduction model was validated by numerical experiments.

The eddy diffusivity in the region away from the conduction layer was estimated based on temperature, velocity and turbulence data using two independent methods. The agreement was good. The spatial variations of the eddy diffusivity in most of the primary flow region was found to be gradual with rapid drops occurring in the region between the primary flow and the cold ambient.

A numerical flow calculation was made. The mathematical formulation was based on Boussinesq approximations using a constant eddy diffusivity model. A turbulent Grashof number Gr_T (the governing parameter) was defined through the definition of a characteristic plate temperature rise $\Delta\theta_T$, the plate mean heat flux and the eddy diffusivity. Gr_T and $\Delta\theta_T$ were obtained based on the best fit of experimental and numerical centerline temperatures.

By the specification of $\Delta\theta_T$ at the plate surface, the effect of the intense variation of eddy diffusivity in the conduction layer region could be avoided in the numerical calculations. Numerical results based on a constant eddy diffusivity model were obtained and compared with the experimental data. Due apparently to the non-constancy of the eddy diffusivity, the calculated temperature and velocity profiles exhibit less constriction than the experimental data. Therefore a more general turbulent transport model will be required to provide a good theoretical description of the phenomena.

14 KEY WORDS	LINK A		LINK B		LINK C	
	ROLE	WT	ROLE	WT	ROLE	WT
Turbulent flow						
Convection						
Heat distributing units						
Temperature						
Variations						
Hot-wire anemometers						
Draft (gas flow)						